

5-2011

A Quantitative, Technology Independent, Fidelity Metric for Evaluating Bioprinted Patterned Co-cultures

Matthew Pepper

Clemson University, matthewpepper@gmail.com

Follow this and additional works at: https://tigerprints.clemson.edu/all_theses

 Part of the [Electrical and Computer Engineering Commons](#)

Recommended Citation

Pepper, Matthew, "A Quantitative, Technology Independent, Fidelity Metric for Evaluating Bioprinted Patterned Co-cultures" (2011). *All Theses*. 1124.

https://tigerprints.clemson.edu/all_theses/1124

This Thesis is brought to you for free and open access by the Theses at TigerPrints. It has been accepted for inclusion in All Theses by an authorized administrator of TigerPrints. For more information, please contact kokeefe@clemson.edu.

A QUANTITATIVE, TECHNOLOGY INDEPENDENT, FIDELITY METRIC
FOR EVALUATING BIOPRINTED PATTERNED CO-CULTURES

A Thesis
Presented to
the Graduate School of
Clemson University

In Partial Fulfillment
of the Requirements for the Degree
Masters of Science
Electrical Engineering

by
Matthew E. Pepper
May 2011

Accepted by:
Dr. Richard E. Groff, Committee Chair
Dr. Timothy C. Burg
Dr. Karen J.L. Burg

ABSTRACT

The study of cell-cell interactions is crucial in the understanding of cell behaviors such as tumor genesis, proliferation, migration, metastasis, and apoptosis. To break down the complex web of signals *in vivo*, researchers must replicate some parts of this environment with *in vitro* tissue test systems, composed of multiple cell types arranged close enough to communicate with their neighbors, i.e. high-resolution co-culture patterns. The field of bioprinting is specifically focused on creating co-culture patterns for the purposes of cell studies, but the sample resolutions of most bioprinting systems are still too coarse to permit cell communication. No way currently exists to compare the sample fidelity between the technologies that have succeeded in creating high-resolution co-culture patterns..

This work introduces a quantitative metric for measuring co-culture patterning fidelity for use in comparing systems or tracking changes in fidelity with experiment conditions. The “biopatterning fidelity index” (BFI) measures the performance of a system by fitting a scaled mask of the sample pattern over an image of the printed pattern and classifying the cells as correctly or incorrectly placed. A simple model is also introduced to provide a theoretical upper bound on the expected fidelity. The BFI and model were used to assess the performance of a custom bioprinter system. The performance of the system varied between the different cell types. The results indicate that the post-processing procedures were disturbing the fidelity of the patterns. New procedures should be developed that would not disturb the initial pattern fidelity. The best samples came very close to the model’s predicted upper bound. As the number of capable technologies increases, the BFI will provide a quantitative, technology-independent method to assess the fidelity of patterned co-cultures.

The last section of this work examines the ability of the bioprinting system to create multiple slides of samples with similar cell distributions. It was shown that cartridges which had been exposed to less usage and cleaning had a more consistent cell output, enabling the bioprinting system to create biological comparable samples.

DEDICATION

I would like to dedicate this thesis to my God and Savior Jesus Christ, who guided me through my years after college and saw that I ended up exactly where He wanted me. He has matured me and provided for me through these years of graduate school. I would like to thank my parents and grandparents for the many encouraging conversations we had and their continuous prayer support.

ACKNOWLEDGMENTS

I would like to thank my advisors, Dr. Richard Groff, Dr. Timothy Burg, and Dr. Karen Burg. Thanks to them, I have had the opportunity over the past three years to sharpen my skills designing experiments, troubleshooting software/hardware issues, applying my own solutions, writing manuscripts, and attending conferences both here and abroad. Over the course of this project, our many meetings and talks have fundamentally changed the way that I approach problems and organize my thoughts.

TABLE OF CONTENTS

	Page
Title Page.....	i
Abstract	ii
Dedications	iii
Acknowledgments	iv
List of Tables.....	vii
List of Figures	viii
Preface	xi
1 Introduction	1
1.1 Co-culture patterns with microscale resolution.....	1
1.2 Co-culture patterning technologies	2
1.2.1 Ink jetting technologies.....	5
1.2.2 Pneumatic Microvalves	7
1.2.3 Laser-based Transfer	8
1.2.4 High fidelity Patterned Co-cultures	9
2 System Architecture	12
2.1 Hardware.....	13
2.1.1 Cell Delivery Station	13
2.1.2 Microscope Station	18
2.1.3 Motion System.....	18
2.2 Software	21
2.2.1 Simulink Model/ Matlab Scripts.....	22
2.2.2 Calibration	24
3 The Bioprinting Fidelity Index	26
3.1 Materials and Methods.....	26
3.1.1 Computing the Bioprinting Fidelity Index.....	26
3.1.2 Drop Distribution Study	27
3.1.3 Fidelity of Patterned Co-culture	28
3.2 Results and Discussion.....	31
3.2.1 Drop Distribution Study	31

3.2.2	Fidelity of Patterned Co-cultures.....	33
4	Cell Settling Effects on Uniform Pattern Reproduction	41
4.1	Cell Settling Model.....	42
4.2	Materials and Methods.....	43
4.2.1	Cell Settling Study.....	44
4.2.2	Latex Bead versus Cell Output in New Cartridges	47
4.3	Results & Discussion	47
4.4	Conclusion	51
5	Conclusions	53
5.1	Bioprinter performance vs. BFI prediction	53
5.2	Cell Settling Study	54
5.3	Future work.....	55
6	Recommendations.....	57
A	Appendix	59
A.1	BFI Model Derivation.....	59
A.1.1	Numerical Studies.....	59
A.1.2	Modeling the drop center offset.....	60
A.1.3	Using the model to predict the maximum BFI.....	62
A.2	H/W Section.....	64
A.2.1	Driver Board Details.....	64
A.2.2	HP26A diagrams.....	72
A.2.3	Board pinout to HP26 nozzle table	72
A.2.4	Power supply	74
A.2.5	Data Cable/Connector diagrams	75
A.2.6	Q8 Terminal Board Connections	77
A.2.7	Chart comparing different aspects of different technologies	78
A.3	S/W Section	78
A.3.1	Bioprinter Struct Walkthrough	78
A.3.2	Bioprinter Simulink Model (bpXPCv204a.mdl).....	81
A.3.3	Function Dependency Diagrams.....	90
A.3.4	Print fxn code walk through	94
A.3.5	Cell Counting Algorithm	101
A.4	Bioprinter Operational notes	102

A.4.1	Applying the BFI to bioprinted patterned co-cultures	102
A.4.2	New Cartridge modification for bioprinting	102
A.4.3	EtOH Cleaning	102
A.4.4	Cartridge validation	102
A.4.5	Hardware/Software Anomaly Reporting	103
A.4.6	Hardware/Consumables Logs	103
A.4.7	Setting up/Running an experiment	103
References	106

LIST OF TABLES

Page

Table I – various performance characteristics and experiment results from the four bioprinting technologies.	11
Table II - Drop Center Distribution Statistics.....	32
Table III - Statistics showing the fidelity of the bioprinting system when producing the two patterns, A and B	37
Table IV – experiment plan and previous usage of each cartridge	46
Table V – model parameters used for the cell and bead settling output models	48

LIST OF FIGURES

Page

Figure 1- Separate cell-type patterns and how they are merged to form a patterned co-culture	2
Figure 2- Lock-and-key seeded substrates [11]	3
Figure 3 – (a) Schematic diagram of a pneumatic microvalve mechanism (b) Layout of the system used to drive a PMV [42]	7
Figure 4- the major components of the laser-based transfer system [3]	8
Figure 5 – co-culture pattern demonstrating the ability of the laser-based transfer technology to simultaneously pattern human endothelial cells (Eahy926) at cell-signaling range resolution, 200 – 300 um. [55].....	10
Figure 6 – The major components of the bioprinter	12
Figure 7 – adapted from [18]. (a) shows the construction of the printhead, (b) shows the major components of the HP26 cartridge.	14
Figure 8 – major components and layout of the HP26 cartridge.	15
Figure 9 – schematic of the custom driver board [69]	16
Figure 10 –(a) Magnification table showing the pixel-size relationship for the Microscope Station (b) the Microscope Station with labeled components.....	17
Figure 11- Sample image illustrating the effects of uncompensated backlash in our Motion System	19
Figure 12- Data flow between the different components of the bioprinter system.....	21
Figure 13 - Q8 Digital Input/Output ports	22
Figure 14 – Illustration of the calibration algorithm used to align the patterns of multiple cartridges for the bioprinter	24
Figure 15 –(a) co-culture pattern after printing (b) co-culture pattern with mask overlaid.....	27
Figure 16 – Patterns A and B used to print the D1(gray areas) and 4T07 cells (white areas)	29

Figure 17 – concept and distribution data used to create the statistical model and an example of the error stencil.	34
Figure 18 – two images demonstrating the loss of cells caused by the application of medium (left column vs. right column)	39
Figure 19 – a diagram of the inkjet cartridge reservoir and printhead used in the cell settling study.	42
Figure 20 – concentration profile of the settling model, seen in (5)	43
Figure 21 – Top) a sample slide showing the 9 patterns, each composed of 6 squares, 3 pixels by 3 pixels. Bottom) later experiments produced sample slides containing 6 patterns.	44
Figure 22 - Cell output results of the heavily used (A and B), moderately used (C D E), and new cartridges (F and G).	48
Figure 23- Bead output results of the new cartridges (F and G) to the bead settling output model. The output of both cartridges increased over the entire experiment, in contrast to F and G when printing cells.	49
Figure 24 – Cells per sample profiles for the cartridges used in the cell settling studies.	50
Figure 25 - Two dimensional Gaussian distribution.....	61
Figure 26 – Left) Quadrant schematic, quadrants 2-4 similar. I – External inputs. II – Custom driver board. III – Flex cable. IV – HP26 cartridge. Right) individual nozzle transistor model.....	65
Figure 27 – a) Voltage drop across a nozzle resistor during firing, comparison of the custom driver board and the HP Deskjet 540 shown.	66
Figure 28 - Custom driver board.	68

Preface

The thesis is organized as follows:

Chapter 1 presents the use of patterned co-cultures to study cell-cell interactions. Different methods used to create patterned co-cultures, lithography and bioprinting, are overviewed. The three key criteria that a bioprinter must fulfill in order to create high fidelity co-culture patterns are presented.

Chapter 2 gives a general overview of a typical printing experiment, presents the hardware components of the system, and then explains how these components are controlled by the software to create high-fidelity patterned co-cultures.

Chapter 3 presents a metric for measuring the fidelity of a bioprinted co-culture pattern, “bioprinting fidelity index,” (BFI). A simple theoretical model is described which predicts cell placement accuracy based on the system parameters. Studies were performed to find the system parameters for this model. The first study obtained the drop center offset distribution as a function of solution type and cartridge height, as well as an estimate of the drop gain. In the final study, high-fidelity co-culture samples were printed using two different patterns and the BFI was used to compare to the fidelity of the system’s samples to fidelity predicted by the model.

Chapter 4 presents studies with the bioprinter meant to confirm its ability to rapidly create high fidelity co-culture patterns. The output of multiple previously used cartridges while printing fluorescent tagged cells was examined. This was compared to the output of new cartridges. The new cartridges were also used to print latex beads similar in size to the cells. Comparison of the quantity of beads/cells deposited by the different cartridges will insight into performance questions revolving around settling/clumping processes of cells occurring in the cartridges over time.

Chapter 5 presents the conclusions of these studies and how the bioprinter can be utilized for creating high-fidelity patterned co-cultures for bioengineering research.

1 INTRODUCTION

1.1 *Co-culture patterns with microscale resolution*

Inside the body, cells lie in contact or in close proximity to other cell types in a microenvironment that is tightly regulated by interactions with surrounding cells, soluble factors, and ECM molecules [1]. To study cell-cell interactions; involved for example in cancer induction, proliferation, migration, metastasis, apoptosis or stem cell differentiation and function, the interactions should be controlled both spatially and temporally [1], [2]. Studying cell-cell interactions using spatial control, i.e. controlling cell placement location and cellular proximity, is the central motivator for in work covered in this thesis.

Researchers use *in vitro* co-cultures rather than monocultures to better simulate the *in vivo* environment. Co-cultures preserve native cell-cell interactions, which otherwise might cease due to tissue isolation, digestion, and the purification process of a cell population [3]. Homogeneous co-cultures, in which two cell-types are blended in the same dish, represent the coarsest spatial control. Better cell placement techniques would provide more spatial control, e.g. local cell seeding density and cell-cell contact, which in addition to choosing the cell types, would allow for detailed study of “cellular behavior, gene expression and subsequent intercellular signaling and cell function” [2], [3].

The most straightforward way to mimic *in vivo* environments in the two dimensional (2D) case is to start with 2D tissue samples and attempt to reproduce them using patterned co-cultures. The first step of this process involves imaging the tissue sample and identifying the cell types, cell spacing, and cell placement. A series of pattern images are made, each containing all the locations of a particular cell type. These pattern images are later combined to form the patterned co-culture, a discrete representation of the cell pattern found in the tissue sample. Studies of cell-cell interactions do not have to involve co-culture patterns as varied and complex as a tissue sample, but constructing simpler patterns involves the same basic process (Figure 1).

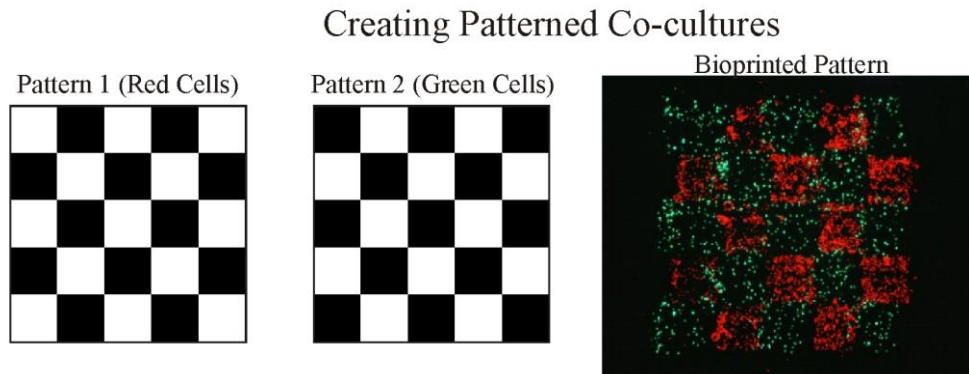


Figure 1- Separate cell-type patterns and how they are merged to form a patterned co-culture

1.2 Co-culture patterning technologies

Once co-culture pattern images are created, it is important to focus on how to accurately reproduce them onto a substrate. Technologies and techniques from the field of printing and rapid prototyping have been adapted for the purposes of cell placement by applying cells and proteins to a substrate through direct contact (i.e. lithography) or deposition (i.e. jetting methods).

Lithography involves the application of a patterned stamp or mask directly onto a substrate to control the transfer of media. The advantage of lithographic methods is that the samples are very accurate, i.e. high fidelity, reproductions of the intended pattern. The pattern will usually contain a similar level of detail, i.e. resolution, similar to that which is present in the mask or stamp.

Several lithographic techniques for patterning cells/proteins are:

- 1) *substrate adhesion modification*, using photolithography [4], soft lithography (using proteins) [5], electrically activated surface proteins, and thermally responsive surfaces [6]
- 2) *soft lithography*, depositing cells using poly(dimethylsiloxane) (PDMS) stamps or stencils, and microfluidic channels [5], [7]-[9]
- 3) *Dielectrophoresis* [10]
- 4) *lock-and-key seeded silicon substrates* [11] (see Figure 2).

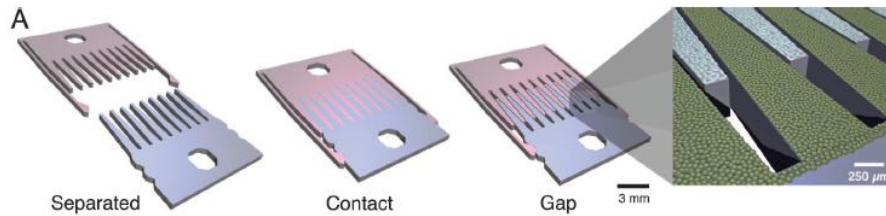


Figure 2- Micromechanical substrates enable micrometer-resolution cell positioning. Microfabricated silicon parts can be fully separated (Left), locked together with comb fingers in contact (Center), or slightly separated (Right). Cells are cultured on the top surfaces; manual scraping can be used to restrict cells to the comb fingers only (Inset). The slope of the tapered comb fingers results in a 20:1 mechanical transmission ratio; that is, sliding the parts 1.6 mm changes the gap between the fingers by only 80 μm . Together with the integrated snap-lock mechanism, it is thereby possible to control separation with repeatable micrometer-scale precision by using unassisted manual actuation. [11]

The resolutions for these techniques range from a single micron to tens of microns with soft lithographic techniques [7], [9], [11] to hundreds of microns with some of the other techniques [5], [6], [10]. With the resolutions for some of these techniques on the order of one cell diameter, the smallest feature of a tissue sample should be able to be reproduced. Lithographic techniques are effective at producing high fidelity patterned co-cultures, however, the amount of preparation and synthesis required to perform these experiments means each experiment is highly customized.

Deposition techniques involve an automated process in which the pattern is reproduced onto a substrate using small volumes of material transferred by some physical process. The advantage of using deposition techniques is that less setup and customization is required for each pattern, allowing faster experiment transition. The disadvantage is that the resolution of the co-culture patterns is usually lower than the best lithographic methods. When the deposited material contains cells or is biological, the process is referred to as bioprinting, defined by the International Conference on Bioprinting and Biofabrication in Bordeaux (3B'09) as: "the use of computer-aided transfer processes for patterning and assembling living and non-living materials with a prescribed 2D or 3D organization in order to produce bio-engineered structures serving in regenerative medicine, pharmacokinetic and basic cell biology studies" [12].

If using deposition techniques (i.e. bioprinting) over lithographic techniques means a possible loss in pattern resolution and fidelity, the important question is 'how much control over cell placement (i.e.

resolution) does a patterned co-culture need to have to be used to study cell-cell interactions?', or similarly 'how close do cells need to be to interact?'. These questions are answered by examining the length scale of intercellular signaling. Cells communicate using chemical messengers (signaling proteins) that fall into two basic signaling types: autocrine (self-signaling) and paracrine (neighbor-signaling). Theoretical studies of the range of autocrine signaling and paracrine signaling have estimated that the effective range for cell signals fall in the range of 50 μm to 250 μm (around 25 cell diameters) [13], [14]. Conservative estimates of 100 μm [7] fall in this range, while experimental results vary between 150 μm [15] and 325 μm [11]. Taking an average of these results, to create close proximity conditions *in vitro*, patterned co-cultures should use technologies capable of cell placement resolution of 200 μm or less.

Determining the sample resolution (i.e. minimum feature size) of a bioprinting technology requires explanation of two terms: drop gain and system resolution. Drop gain is defined as the substrate area taken up by a specific drop volume. It depends on the drop volume and the properties of the receiving substrate. Since the drop volume and substrate are usually constant in an experiment, drop gain remains constant as well. The system resolution or addressability refers to the minimum movement possible between depositing drops. It should be apparent that increasing the addressability of a system will not decrease the minimum feature size of its samples if the drop gain remains constant. The sample resolution therefore is better defined by the drop gain provided that it is larger than the addressability. This means that when designing a co-culture pattern, the drop gain will define the size of the smallest feature. It is important to use a bioprinting system with a sample resolution below the relevant cell-signaling range of 200 μm . While a large drop may contain multiple cells, it is important to remember when combining drops to form the pattern, a cell's location in a drop is random and the cell may be situated too far from cells in neighboring drops.

Besides having high resolution, a tool creating patterned co-cultures needs them to have high fidelity. It is important when performing cell signaling studies that the bioprinted cells end up in their intended locations. To achieve high fidelity patterned co-cultures, it is important to choose the pattern pixel size to correspond with the cell placement resolution of the system. The sample fidelity is also affected by the drop center offset. Different combinations of technologies\printing solutions have shown

that a deposited drop may not always land in the center of its intended pixel location (drop center offset), meaning the cells inside the drop may be located outside of the pixel boundaries.

In addition to high resolution and fidelity, a suitable tool to study cell–microenvironment interactions *in vitro* [1] should be capable of performing high-throughput experimentation, which enables the creation of larger datasets for more accurate conclusions and faster experimentation. Producing samples with similar cell populations is especially important for comparing results in cell-cell signaling studies. It has been shown that population ratios have influenced extracellular cues which regulated adult stem cell and embryonic stem cell fate decisions [1], [16], [17]. Maintaining the desired cell populations between all samples over the course of an experiment is very important.

The next three sections will review the implementation and capabilities of four main bioprinting technologies: thermal inkjet (TIJ), piezoelectric inkjet (PEIJ), pneumatic microvalve (PMV), and laser-based transfer (LBT). Currently, only thermal inkjet and laser-based transfer technologies have created high fidelity patterned co-cultures, but the capacity exists with piezoelectric inkjet and pneumatic microvalve, which are covered for completeness.

1.2.1 Ink jetting technologies

As early as 2000, inkjet technology was used to create bioprinted samples, in which a HP500C printer deposited DNA [18], and later in 2003, endothelial cells [19]. The principle of inkjet technology, whether thermal or piezoelectric, is to force the formation and ejection of drop from a nozzle due to the quick displacement of the liquid using some computer controlled process. With thermal inkjet, heat from a resistor causes the formation and expansion of a gas bubble creates and propels the drop. In a piezoelectric inkjet, a piezoelectric material is electrically stimulated to compress a volume of liquid.

Thermal inkjet technology in bioprinting has primarily been implemented using technology sourced from the HP 500 and 600 series of printers. TIJ technology is used for bioprinting by the research labs at Clemson University using the commercially available Hewlett-Packard (Hewlett-Packard Company, Palo Alto, CA) (HP) 26 or 21 cartridges and modifying them for bioprinting use. The vertical resolution for these experiments is restricted to the native resolution of 85 μm (300 dpi) due to nozzle arrangement.

The nozzle size of 50 μm is a large enough diameter for printing cells 20 μm or less. Most of the patterns printed using the HP26A cartridge have a drop gain of approximately 100 μm to 120 μm , which is within the cartridge's intended operating range of 75 – 100 (\pm 50 – 75) μm [20]. The native resolution, high throughput, and commercial availability are the main advantages for using this system; the HP26A ink cartridge was designed to dispense hundreds of thousands of drops per second. The disadvantages for using this system are that the nozzle size is fixed and not suitable for larger cells [19] and additional cartridges must be added and registered to simultaneously deposit multiple cell types.

At Clemson University, work has been done using the HP26A cartridge to print thrombin into fibrinogen [21], [22] or sodium alginate into CaCl_2 solution [23] to create scaffolds, as well as considerable work in probing viability [22], [24], [25] and examining the aftereffects of printing on cells [22], [24]. In later work at Clemson, the HP26A cartridge was used not with a commercial printer but with the custom bioprinter system described later in this paper. This printer has been used to investigate advancements in additives to cell solutions to make them more bioprinter friendly as well as to create high fidelity co-cultures with features approximately 160 μm in size [26], [27].

Piezoelectric inkjet (PEIJ) technology has had a diverse implementation in the field of bioprinting. It has been implemented in syringe pumps, single-nozzle single-source print heads, multi-nozzle single-source print heads, and single-nozzle multi-source configurations. The advantage for using PE-IJ technology is that each different implementation has different nozzle diameters and nozzle separation, thus allowing for a wide range of viscosities of liquid to be deposited. Each liquid/nozzle diameter combination will yield a different drop volume, changing the drop gain and overall sample resolution for a pattern. Parameters such as frequency, pulse length, and voltage must be tuned for proper printing of different materials [28], [29]. Piezoelectric syringe pumps were used to print cells in hydrogels [19], [30], [31]. Single-nozzle single-source piezoelectric print heads were used by researchers at Carnegie Mellon and Manchester Universities, both using the Microfab (Microfab Inc., Plano, TX) Microjet system. At Carnegie Mellon, their system is outfitted with a 30 μm nozzle and used to print hormone and protein gradient patterns to promote attachment and direct differentiation [28], [32]-[35]. At Manchester University, the Microfab system is used to test post-printing viability of cells and find optimum system parameters (30 μm

nozzle in [36], 60 μm nozzle in [37]), mentioned above. The Microjet is gravity fed, with the solution held in a glass capillary tube and pulsed by the piezo material [37]. At the Kanagawa Academy of Science and Technology in Japan, a lab uses their single-source multi-nozzle Epson (Seiko Epson Corp., Long Beach, CA) Seajet (508 μm , 50 dpi vertical resolution) to print cells in sodium alginate / CaCl_2 and fibrinogen/thrombin solutions as gel precursors/gel reactant combinations [38]-[40]. Additionally, they used their multi-source single-nozzle system to print sodium alginate / CaCl_2 with different colorings to show 3D gel layering ability [41].

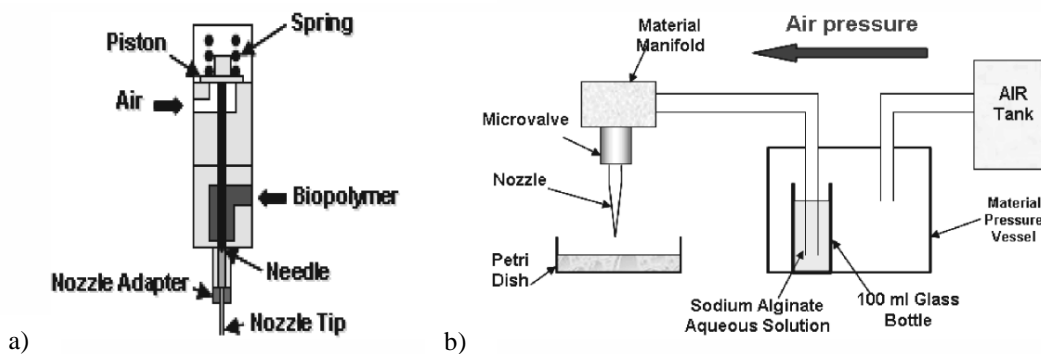


Figure 3 – (a) Schematic diagram of a pneumatic microvalve mechanism (b) Layout of the system used to drive a PMV [42]

1.2.2 Pneumatic Microvalves

The use of pneumatic microvalves (PMV) is also prevalent in printing biological material. A PMV is a pneumatically actuated mechanical valve which opens and closes to control the flow of material through a pressurized line (Figure 3). An extrusion mode is possible with a PMV if the valve is held open for a longer duration [42]. The advantages of a PMV are that it has a wide viscosity range for printable materials and the nozzle size can be mixed and matched to suit the experiment [43]. Similar to the PEIJ technology, each liquid/nozzle diameter combination will yield a different drop volume, changing the drop gain and overall sample resolution for a pattern. The disadvantages of a PMV are that parameters like nozzle size and line pressure need to be properly adjusted based on the solution or else cell viability may be affected [43]-[45].

At Drexel University, a PMV was used for almost all their experiments, though they have other types of dispensing technologies. They mostly perform cell-embedded gel extrusion, in which they can change the tip diameter to any one of 100, 150, 200, 250, 330, and 410 μm diameters, thus far achieving a drop gain of 200 μm [42], [44]-[47]. At a joint MIT/Harvard Medical School lab, a bioprinter with 4 PMVs is used to create multiple cell type samples in the following order: crosslinker (aerosol spray), hydrogel precursor (PMV), cells (PMV), crosslinker. Their experiments have exhibited drop a gain of 200 – 300 μm .

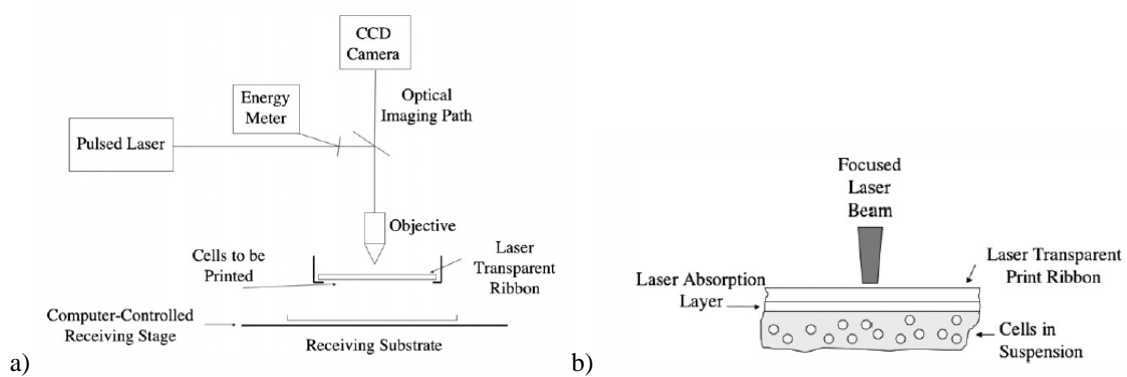


Figure 4- (a) shows the major components of the laser-based transfer system (b) side view of the layers of ribbon used by the laser-based transfer technology [3]

1.2.3 Laser-based Transfer

In 2000, laser-based transfer or laser-induced forward transfer (LIFT) technology was used by researchers at the Naval Research Laboratory to successfully print viable E.coli in 100 μm wide lines. The earliest LIFT process was referred to as matrix assisted pulsed laser evaporation direct write (MAPLE DW). In MAPLE-DW, a laser is focused on the interface of a UV-transparent disc and attached down-facing substrate containing the material to be printed (Figure 4). As a result of the laser pulse, the target area is superheated and the surrounding substrate material is ejected [48]. The timescale for the laser shot is in the picosecond to femtosecond [49] range; this short time scale results in high energy transfer efficiency and low heat transfer to the surrounding substrate [49]. The advantage of this type of system is that the area on which the laser is focused can be changed to yield ejected drops of differing size and volume, 50 μm (30

pL) [50] to 100 μm (100 pL) [51]. In addition, high viability has been shown in printing studies with mammalian cells [49], [52]-[54] as well as multicell capability [49], [55]. Since the substrates are spin coated to evenly distribute the substrate/biomaterial solution [50], it is easy to customize parameters, such as cell concentration, to enable single cell resolution [51], [53].

The technology improved in 2004, dubbed biological laser printing (BioLP), with the addition of a laser absorbing interlayer which removes the interaction between laser and biological material as well as improving the reproducibility of the process [56], [57]. As research continued, the need for a hydrogel receiving layer was shown due to the high jetting velocities (50 to 1000 m/s) of the drops and subsequent lower viability of certain samples [57]. The spacing between the donating and receiving substrate does not affect precision if the laser energy is modulated correctly for the particular substrate [50]; spacing has ranged from 0.01 to 10 mm [15], [50], [57], [58]. Once the effects of varying the laser fluence on viability were studied [59], BioLP was used to create multiple cell type patterns, both simultaneously [56] or the next day [15]. In France in 2009, researchers at the National Institute of Health and Medical Research took the BioLP system and added a laser capable of pulse rates up to 100 kHz, a high speed scanning mirror to position the laser, and a five position carousel in which substrate discs of varying cell type could be loaded [60]. Initial studies have been run to confirm cell viability and examine printing dynamics [55], [60]-[62]. In 2010, using an alginate/cell substrate and operating at 5 kHz, monoculture patterns were created with feature sizes of approximately 100 μm using 51 ± 4 μm drops and simultaneous co-culture patterns were created with feature sizes of approximately 200 μm using (see Figure 5) [60].

1.2.4 High fidelity Patterned Co-cultures

Only two technologies have demonstrated the ability to simultaneously pattern multiple cell types at relevant cell-cell signaling resolutions (<200 μm); the laser-based transfer technology, [49], [55], [56] (Figure 5) and TIJ technology in [27]. The other technologies have either not shown samples with resolutions in the cell-cell signaling range or produced samples with multiple cell types. The LBT and TIJ systems are similar in that they each require testing and parameter optimization when new solutions/materials are used. The laser-based technology does have a wider range of cell sizes/biomaterials

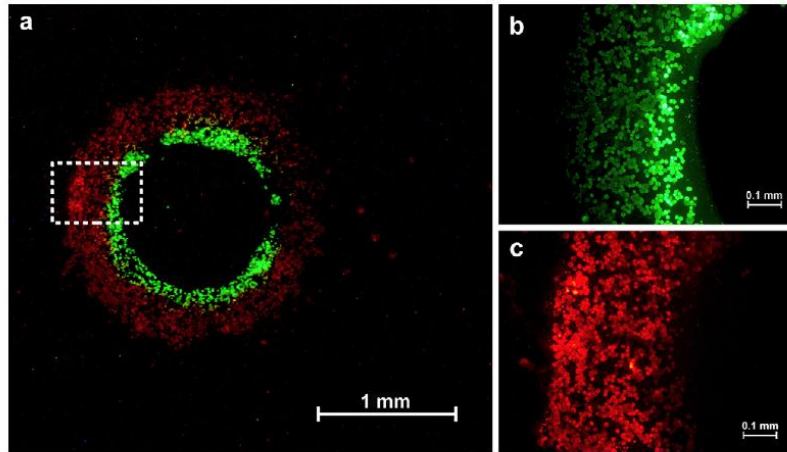


Fig. 4. Sequential two color cell printing in 2D. Human endothelial cell line (Eahy926) was loaded with $4 \mu\text{M}$ of green fluorescent Calcein-AM, or with $2 \mu\text{g/ml}$ of red fluorescent Dil-LDL prior to the experiment. (a) The two cell suspensions ($6 \cdot 10^7$ cells/ml in DMEM, supplemented with 1% (w/v) alginate) were then printed according to a pattern of concentric circles). The two cell suspensions were each blade coated onto two separate ribbons. Both ribbons were placed onto the wheel distributor of the LAB. Calcein loaded cell suspension was used to print the inner circle (1.2 mm diameter). Dil-LDL loaded cell suspension was used to print the outer circle (1.6 mm diameter). (b) Green Calcein stained cells within the region of interest as defined in 4a (dashed rectangle). (c) Red fluorescent Dil-LDL stained cells within the same region of interest. The overlay of Fig. 4b and c shows the two circles partially overlap due to the coalescence of their interface.

Figure 5 – co-culture pattern demonstrating the ability of the laser-based transfer technology to simultaneously pattern human endothelial cells (Eahy926) at cell-signaling range resolution, 200 – 300 μm . [55]

possible for deposition and drop volume adjustability, but the COTS TIJ technology only slightly lags the laser-based systems in terms of deposition speed and total number of cell types/biomaterials possible for simultaneous deposition (5 vs. 4). One of the advantages for TIJ technology is its presumably lower overall cost of implementation due to its lower complexity and widely available components. The limitations as compared to laser-based technology, such as nozzle size and biomaterial viscosity, do not prevent TIJ technology from being used in experiments with dozens of smaller cell types and compatible biomaterials.

For a bioprinting system, the ability to create high fidelity co-culture patterns is governed by three key criteria: 1) a system's capability to place drops of biomaterial containing cells in user specified locations, a.k.a manage their drop center offset and 2) the drop gain, and 3) the assumed pixel size of the system (system resolution). Only a few papers on P-IJT [29], PMV [63], and LIFT [2] have characterized their system's drop center offset. In [63], the observation was made that if the average drop-on-substrate diameter in that experiment was orders of magnitude larger than the drop center deviation, then its affects on the pattern fidelity could be negated [2]. None of the papers drew a relation between the pixel size, the drop gain, and the drop center offset to pattern fidelity. To accurately create high resolution co-culture patterns, the drop gain must be close to the assumed pixel size; both must also be within relevant cell-cell signaling range. The drop center offset must be minimized to achieve high fidelity (cells of specified type

in their intended regions). Since no metric for pattern fidelity based on these or any other criteria existed, a metric was created based on these three criteria.

Table I – various performance characteristics and experiment results from the four bioprinting technologies.

technology	University	Nozzle Size (um)	Number of Nozzles	Drop Volume	Drop Gain (um)	Sample Substrate	Drop Accuracy (x,y) (um)	Operating Frequency (Hz)	Experiment Op. Freq. (Hz)	Print Height (mm)	Stage Resolution (um)	Stage Repeatability	Multiple Cell Shown	Multiple Cell Capable	References
TIJ	CU	50	50	130 pL	120	collagen	(15,15)	2800	2800	1-3	5	10	Y	Y	27
	CU	50	50	95 pL	250	soy agar		3600	3600	1			N	N	64
PEIJ	CU	159	9	15 nL		collagen					50		N	Y	19
	CMU	30	1	18 pL	75		(4,4) ± 3	1/2 - 300	1/2 - 2		0.3		N	N	29
	M	30, 60	1			well plate		13k					N	N	36,37
	UT		12	8-160 pL	85	PET		2000	1000		0.2	4	N	N	65, 40
	UT		4		10-60	fibrinogen		1000	800				N	Y	38
PMV	D	200	1		250	alginate		0.01-14				10	N	N	44, 47
	MIT/H	150	4	9 nL	200-300	collagen	(0.5±4.9, 18±7)	1000	160		0.4	5	Y	Y	66, 63
LBT	NRL	var	1	30 pL	50	Matrigel		1-20	1,10,100	25-2000			N	Y	48,56,59,58
	NRL	var	1	30 pL	50	Matrigel	(5,5)	1-100	50,100	25-2000			Y	Y	56, 15
	INSERM	var	1		50	glass		1-100k	5k, 10k	400-700	1		Y	Y	60,55
<u>Acronyms</u>															
CU - Clemson University															
CMU - Carnegie Mellon University															
M - University of Manchester															
UT - University of Toyama															
D - Drexel University															
MIT/H - Massachusetts Institute of Technology/ Harvard Medical School															
NRL/RPI - Naval Research Laboratory															
INSERM - National Institute for Medical Research (France)															
PET - Polyethylene terephthalate															
TIJ - Thermal Inkjet															
PEIJ - Piezo Electric Inkjet															
PMV - Pneumatic MicroValve															
LBT - Laser Based Transfer															

In this paper, a metric and corresponding theoretical model are introduced to assess the success of a bioprinting system, based on established thermal inkjet technology [19], [25], [67], [68], in creating high-fidelity co-culture patterns, i.e. patterning cells at length scales relevant to intercellular signaling for the purpose of studying cell behaviors. Additionally, it will be shown that after characterization of the printing performance, the system has the ability to create multiple sets of high fidelity co-culture patterns, which will enable larger datasets and increase the effectiveness of future experiments.

2 SYSTEM ARCHITECTURE

The bioprinter is a custom built system capable of depositing multiple cell types according to specified bitmap patterns fed from a host computer. Each cell type is deposited from a separate modified TIJ (thermal inkjet) cartridge. Co-culture patterns are created by printing aligned using separate cartridges. Alignment is achieved by calibration using a mounted microscope camera.

A general overview of the steps of a bioprinting experiment is presented to give context to this section: Before printing, the user must prepare the cell solution, sample slides, and cartridges. The system is initialized and the cartridges inserted into the bioprinter. After each cartridge location is registered using a mounted camera, a sample slide is inserted and the printing script initiated. New pairs of cartridges must be inserted and calibrated every 10 to 12 minutes to ensure uniform pattern creation.

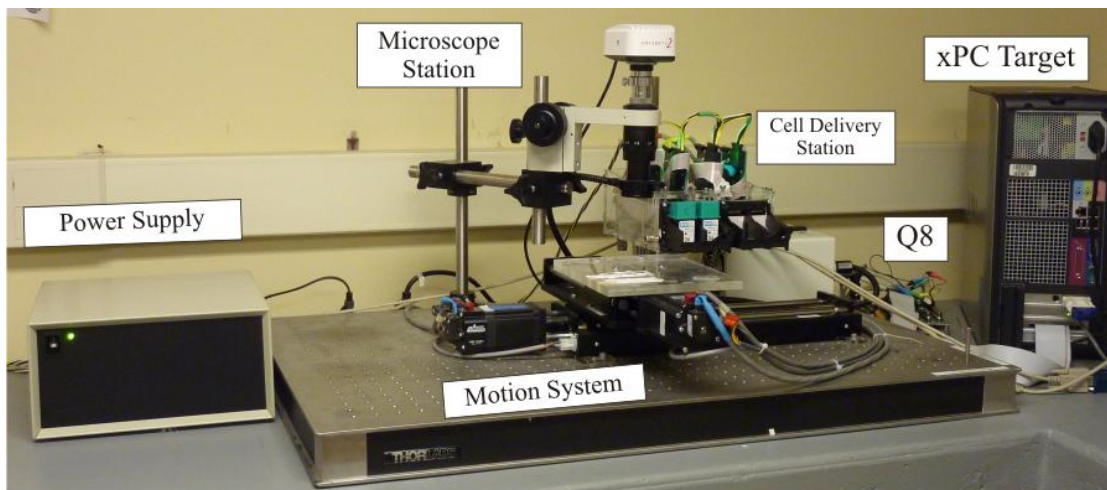


Figure 6 – The major components of the bioprinter

The bioprinter is composed of a Cell Delivery Station, Microscope Station, and a 2-axis Motion System coordinated by custom software executed in the Matlab environment and run on a host/target configuration using Matlab 2009b/xPC Target 4.2 (Mathworks Inc, Natick, MA) (Figure 12). The following sections will outline the components that comprise these stations and how the software coordinates them to create high fidelity patterned co-cultures.

2.1 *Hardware*

The following three subsections describe the main physical components of the bioprinter: the Cell Delivery Station, Microscope Station, and the Motion System (Figure 6).

2.1.1 *Cell Delivery Station*

The Cell Delivery Station prints the cell solution on the sample slides below. The solutions containing cell or biological material are placed into modified Hewlett-Packard (Hewlett-Packard Company, Palo Alto, CA) (HP) 26 thermal ink-jet cartridges which are fired using custom driver boards. These custom driver boards receive data from a Quanser (Quanser Corp. Ottawa, ON, Canada) Q8 data acquisition board (described later). The cartridges and driver boards are held in place while the Motion System moves the samples below. A stationary Cell Delivery Station simplifies the electrical connections and facilitates the extension of the bioprinter system into a mini-factory in which the sample moves from one workstation to another. Workstations could be added to deposit additional biological materials.

2.1.1.1 *Cartridge*

The HP26 thermal inkjet cartridge was chosen for this bioprinter because it can deposit biological material precisely, non-destructively, and with high-throughput. The HP26 cartridge was designed in the late 1980's and increased the resolution of Hewlett-Packard's thermal inkjet cartridges from 180 dots-per-inch (dpi) to 300 dpi. The printhead was designed to "produce image features on the order of 75 to 100 μm with a tolerance on the order of 50 to 75 μm " [20]. This resolution is on par with the desired feature size for high fidelity patterned co-cultures.

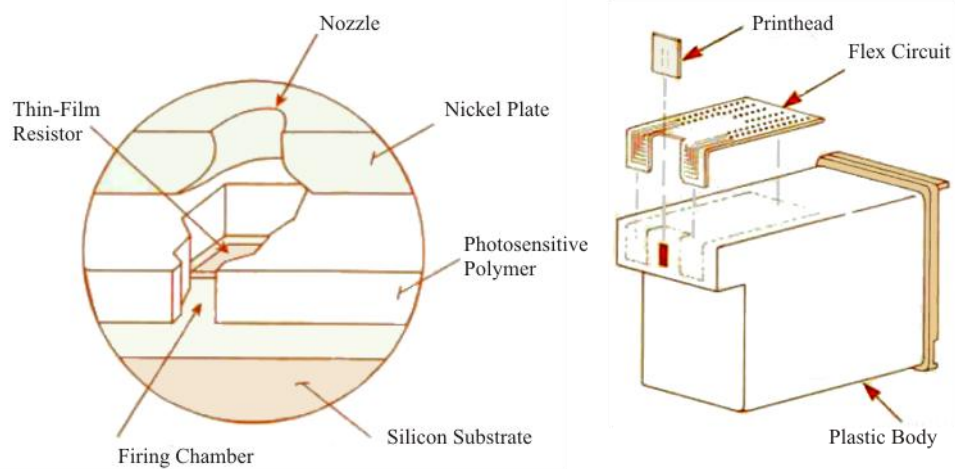


Figure 7 – adapted from [18]. (a) shows the construction of the printhead, (b) shows the major components of the HP26 cartridge.

The printhead of the HP26 cartridge is composed of three layers: a silicon substrate, a polymer adhesive layer, and a nickel plate (Figure 7a). The silicon substrate has 50 thin film resistors embedded in it, arranged in two columns of 25 (Figure 8a). The polymer layer, around 26 μm thick, is present to form the firing chamber for each resistor and to adhere the nickel plate to the silicon substrate. The nickel plate contains each of the 50 μm wide nozzles, which are aligned opposite the thin film resistors. Each individual nozzle is separated from other nozzles in the same column by 169 μm . The two columns are horizontally offset by 847 μm and vertically offset by 84.7 μm . These measurements confirm the specifications of a vertical resolution of 300 dpi (84.7 μm) between nozzles.

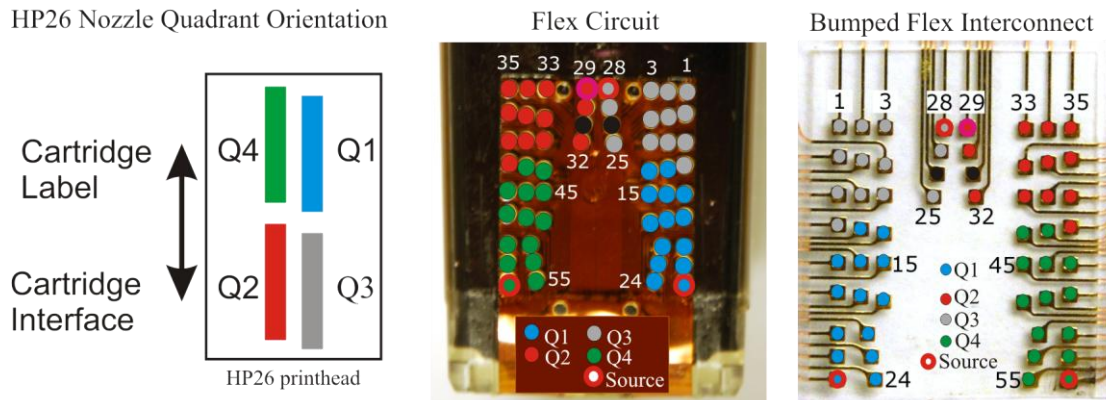


Figure 8 – (a) the quadrant arrangement of the printhead of the HP26 cartridge. (b) the flex circuit showing the arrangement of the contacts for each quadrant on the back of the HP26 cartridge. (c) the bumped flex interconnect that resides in the carriage assembly.

The TIJ process is driven within a nozzle by the heating of a thin-film resistor with a short burst of electrical current, this heats the liquid in the firing chamber, forcing a small volume of liquid to be ejected through the nozzle (~130pL for ink [20]). The current is brought to each of the 50 thin-film resistors in the printhead via a flex circuit which wraps around the back side of the cartridge (Figure 7b, Figure 8b). This flex circuit terminates in 56 contacts. Of these, 50 contacts directly address each nozzle and are arranged into four quadrants (Figure 8b). The quadrant arrangement is reflected on the printhead with each of the two columns of 25 nozzles further subdivided into 2 quadrants (composed of 12 and 13 nozzles each)

(Figure 8a). In each of the four quadrants of contacts on the flex circuit, there is contact to supply DC power to that quadrant of resistors. Supplying each quadrant of nozzles with their own common supply minimizes delivered nozzle energy variance [69], [70]. The two remaining contacts are present for cartridge identification purposes for the original HP 500 DeskJet and DeskWriter printers and are unused in this printer.

The contacts on the back of the cartridge are pressed against a corresponding set of contacts on ribbon cables, providing electrical connections through a bumped flex interconnect (Figure 8c). The bumped flex interconnect is found inside of the cartridge carriage assembly, which provides mechanical seating for two cartridges. The cartridge carriage assemblies were removed from HP 600 series printers.

The Cell Delivery Station holds two of these carriage assemblies, each one connecting two HP26 cartridges with two driver boards, allowing the bioprinter to print with up to four cartridges at once.

The Cell Delivery Station is constructed of 5.75mm thick acrylic and measures 184mm x 182mm x 196mm (Length x Width x Height). The cartridge carriage assemblies are mechanically attached to the front of the Cell Delivery Station via a rod at the bottom and set screw at the top. Each of the four cartridge positions is labeled above the carriage assemblies, *cartridge 0* to *cartridge 3*, going from left to right. Cables carrying power and data come in through the rear of the Cell Delivery Station and connect to the 4 cartridge driver boards.

2.1.1.2 Drive electronics*

Inside the Cell Delivery Station are 4 cartridge driver boards. The cartridge driver board was designed: 1) to provide an interface that can easily be used with a general computing resource such as a microcontroller, and 2) to reproduce the driving characteristics of the original HP printer while providing the versatility to completely control the cartridge. The original HP design drives the cartridge using Application-Specific Integrated Circuits (ASICs) that are not commercially available; the function of these ASICs is replicated using commercial-off-the-shelf (COTS) components.

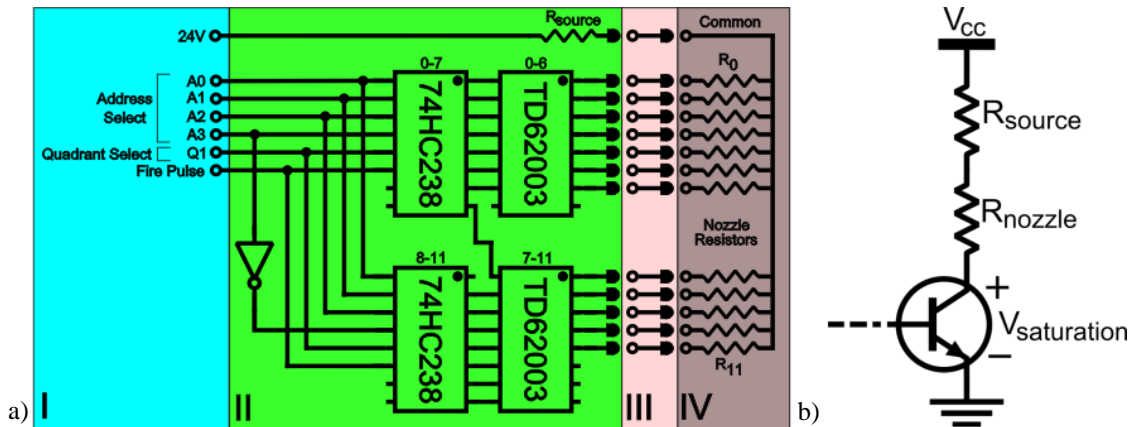


Figure 9 –(a) Simplified layout of Quadrant 1 (or 2-4): I – External inputs. II – Custom driver board. III – Flex cable. IV – HP26 cartridge. (b) Simplified circuit model for one nozzle. [69]

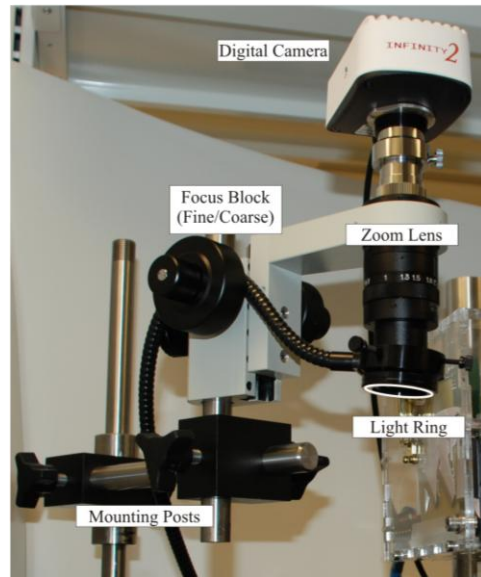
* this section was adapted from [69], it represents collaborative work with Justin Mattimore

The organization of the driver board is shown in Figure 9a and general function explained below. In section I, signals from the Q8 board are input to the board in the form of a 4-bit TTL level addresses (0 or 5V signal), a firing pulse, and quadrant select. In section II, representing the actual driver board, the address is decoded (74HC238 Decoder) and used to energize the power transistor (TD62003 Darlington) which energizes the selected nozzle in section IV. Section III represents the ribbon cables and bump flex interconnect that deliver the firing signals.

Figure 9a only represents one out of four quadrants on the cartridge board. The cartridge driver board interface actually receives nine TTL level logic inputs. The four data bits A0-A3 (high ENABLE) specify which nozzle 0-11(12, depending on quadrant) will be fired while the four data bits Q1-Q4 (low ENABLE) specify in which quadrants that particular nozzle will be fired. The remaining data line, Fire Pulse, provides a high ENABLE to allow firing. The amount of time the Fire Pulse line is high specifies the length of time the nozzle resistor is energized. Since each nozzle is assigned an address from 0 to (11)12 that identifies its position within a quadrant, a simplified interface is used where the same nozzle address

Lumenera 2-3C (3.2MP, 1536 x 2080 pixels)		Field of View			
Magnification	Pixel Size (µm)	X (mm)	Y (mm)	X (in)	Y (in)
0.4	8.625	17.94	13.25	0.7063	0.5216
0.5	6.900	14.35	10.60	0.5650	0.4173
0.7	4.929	10.25	7.57	0.4036	0.2980
1.0	3.450	7.18	5.30	0.2825	0.2086
1.3	2.654	5.52	4.08	0.2173	0.1605
1.5	2.300	4.78	3.53	0.1883	0.1391
1.8	1.917	3.99	2.94	0.1570	0.1159
2.0	1.725	3.59	2.65	0.1413	0.1043
2.3	1.500	3.12	2.30	0.1228	0.0907
2.6	1.327	2.76	2.04	0.1087	0.0802

a)



b)

Figure 10 –(a) Magnification table showing the pixel-size relationship for the Microscope Station (b) the Microscope Station with labeled components

(0-12) is addressed simultaneously in the four quadrants. The quadrant select signals (Q1-Q4) determine whether the addressed nozzle in a given quadrant will fire. The Fire Pulse simultaneously excites the addressed nozzle in each selected quadrant, firing up to four nozzles at once. While it is possible to address any single nozzle in any quadrant and fire each quadrant independently, it would lead to little performance improvements on most patterns and was impractical to design for such functionality in terms of requisite hardware and data lines.

2.1.2 *Microscope Station*

In order to align the output of each cartridge to print high fidelity co-cultures, the locations of the cartridges must be precisely known with respect to each other. In order to perform this calibration, a Microscope Station that was fixed to the base of the bioprinter was needed. This station, comprised of a digital camera, zoom lens, and mounting apparatus, provides us with a reference point around which to calibrate our system as well as a vision system useful for quickly capturing high-resolution images (Figure 10b).

The camera used in our Microscope Station is a Lumenera Infinity 2-3C (Lumenera Corp., Ottawa, ON, Canada) microscope camera with a 3.2 megapixel resolution attached to a Meiji MS-45D (Meiji Techno America, Santa Clara, CA) lens with adjustable 0.41-2.6X magnification. At 1X magnification, images have a 3.45 $\mu\text{m}/\text{pixel}$ resolution. The various pixel resolutions as well as working area dimensions at different zoom settings can be found in Figure 10a. The camera receives power and routes data through a USB cable. The camera and lens are mounted to the base of the bioprinter using a series of rods and connecting blocks. This setup allows the position of the camera to be changed, if required, with respect to the Cell Delivery Station and then held using a series of set screws. Care must still be taken around the Microscope Station as it can be slightly moved by a careless arm movement.

2.1.3 *Motion System*

The Motion System moves our sample platform beneath the Cell Delivery Station to create our patterned co-cultures as well as back and forth between the Cell Delivery Station and the Microscope Station. The Motion System was built by Anaheim Automation (Anaheim Automation Inc., Anaheim, CA)

and is composed of 2 linear stages turned by stepper motors (23MD206D) with attached 1000 count/revolution quadrature encoders (US Digital, Vancouver, WA) controlled by 2 PCL-601 motor controllers (Anaheim Automation). The X-axis (LS100-12-A-B-4O-C) and Y-axis (LS100-06-A-B-4O-C) have a linear travel of 12”(304.8 mm) and 6”(152.4 mm) respectively. The screw pitch of the linear stages is 0.0625”(1.5875 mm) per revolution.

The PCL-601 controllers handle all of the low level motor control functions such as acceleration/deceleration, maximum travel speed, and stepper motor step size. Communication is achieved with the host computer and these controllers through one RS485 connection or two RS232 connections. Once the appropriate interface setting is adjusted on the controllers, a set of preprogrammed serial commands is used to move the sample platform.

The stepper motors attached to our stage have the ability to subdivide steps down to 1/8th of a step, known as a microstep. The resolution of each microstep is 0.992 μ m. The maximum stated speed for each of these stages is 10 mm/s, but we limit the maximum velocity for stage motions to 9.5 mm/sec. Though these two axes may accept voltages from 12V to 24V, the motors/motor controllers are driven at 24V to achieve maximum performance. When running the operating the Motion System at lower voltages, significantly lower maximum velocities as well as more frequent jamming was observed.

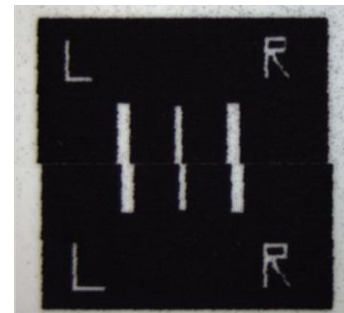


Figure 11- Sample image illustrating the effects of uncompensated backlash in our Motion System

Considering the relative affordability of these linear stages, they perform very well and enable the creation of high fidelity patterned co-cultures. However, some negative characteristics have been found, namely backlash, screw nonlinearity, and miscalibrated stage speed. The magnitude of the backlash error is on the order of 150 μ m (Figure 11). Backlash can be accounted for by moving the sample platform back and forth to set the sample platform in a known state then only moving the platform in one direction while printing. The second characteristic, screw nonlinearity, was discovered when the same net movement from different places on the sample platform resulted in different lengths traveled. This was compensated for by

insuring that the calibration location (to be explained later) and the print location are in similar places on the X-axis. The third characteristic, incorrect stage speed, is a result of the faulty commands being sent from the PCL-601 motor controllers. The velocity of the stage and frequency of our firing pulse is what determines the resolution of our system. Since the nozzles are spread in a vertical resolution of 84.7 μm , it is important to control the stage speed to achieve a horizontal resolution of 84.7 μm as well. This command error is compensated for using a function known as **verifySpeed**. This function commands a specific speed and then counts the encoder values over a certain length of time. It then does a polynomial fit to find the actual speed the stage was traveling. Once this is performed for a large number of different speeds, future speed commands can be corrected using interpolation based on this data set. The adjusted speed should yield the desired speed and distance of the sample platform.

The sample platform is composed of three layers of acrylic measuring 193 mm x 178 mm x 13 mm (Length x Width x Height). The sample platform is composed of 3 regions, the calibration, sample, and flush regions. The calibration region is where the slide used during the calibration algorithm is located. Co-located with the calibration region, the sample region is where the sample slide goes after the calibration slide has been removed before we begin printing. The flush region is located on the right side of the sample platform and is where a slide is located onto which a priming pattern will be printed before each cartridge is used to print the sample. Currently, laboratory tape is used to affix the slides in their locations and keep them from moving during the printing process.

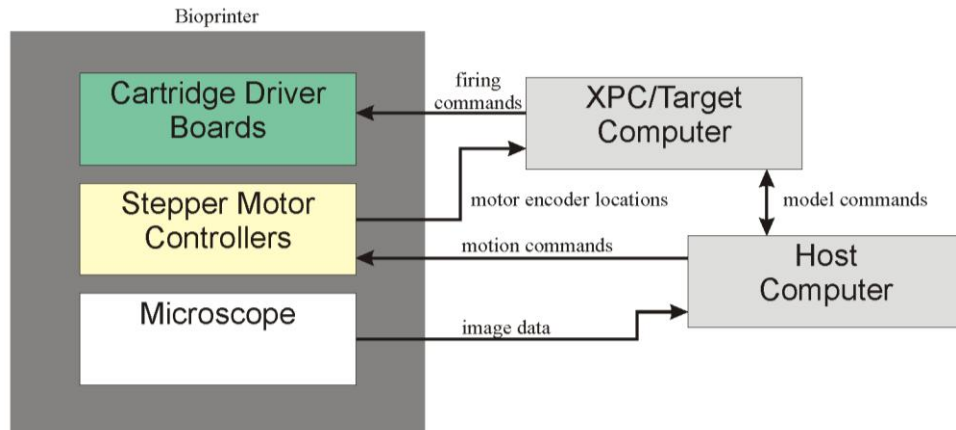


Figure 12- Data flow between the different components of the bioprinter system

2.2 Software

All the software that controls the bioprinter is written in Matlab or C (Microsoft Visual Studio 9, Microsoft Corp., Redmond, WA). The computers running the bioprinter are arranged in a host/target configuration using Matlab R2009b/xPC Target 4.2. The host PC acts as the user interface and issues commands to the motor controllers and to the target PC, while the target PC, running a compiled Simulink model, is responsible for low-level activities such as interacting with the cartridge drive electronics to fire the appropriate nozzles. The two PCs are connected with a crossover cable which allows Matlab to command and control the target xPC kernel [69]. The target PC is equipped with a Quanser Q8 Hardware in the Loop Board which sends all the signals to the driver boards and reads the position of the motor encoders, allowing the target PC to implement real-time control (Figure 12). The real-time system and cartridge drive electronics are capable of sampling rates well over 20 kHz, but the current system operates and fires the cartridges at 2.8 kHz. The operating speed of the system is constrained by the ability of the target machine to run the Simulink (Mathworks Inc, Natick, MA) model without producing runtime errors. The Simulink model, combined with custom Matlab scripts moving the stages, reading in patterns, processing the microscope images, and accepting user input, comprise the bioprinter software.

2.2.1 Simulink Model/ Matlab Scripts

The Simulink model resides on the xPC target machine and uses the Q8 board to send commands through the Cntr Out and 32 Digital Outs while reading the encoder positions through the Encoder I/O ports (Figure 13). The Cntr Out pin sends the Fire Pulse that is routed to all 4 driver boards. The Digital Outs, numbered 0-31, are split accordingly: 0-7 (to *cartridge0* driver board), 8-15 (to *cartridge1* driver board), 16-23 (to *cartridge2* driver board), and 24-31 (to *cartridge3*

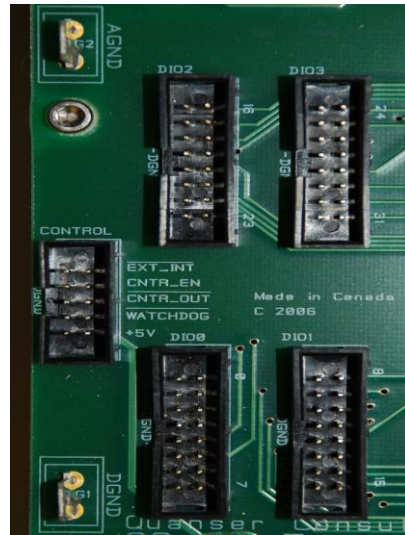


Figure 13 - Q8 Digital Input/Output ports

driver board). Each of these sets of 8 signals delivers the A0-A3 addresses and Q1-Q4 quadrant enables to each board. The Simulink model is always running while the bioprinter is being used to keep track of the encoder positions at all times.

The bioprinter software operates the bioprinter in two distinct modes, discrete and patterning. Discrete mode is useful for debugging software and hardware, e.g. cartridge test/driver board validation, characterizing the printability of materials, and optimizing print parameters. This printing mode was previously used to study nozzle clogging, which led to the recommendation to include EDTA in cell solutions in order to prevent nozzle clogging [26], which greatly improves printing performance. Patterning mode is used for creating patterned co-cultures. In order to use either of these modes, the model has to be set to Discrete or Print mode using the command, **setPrintMode**.

In discrete mode, stage motion and cell deposition are uncoupled and may be directly controlled by the user from the host PC, either through the Matlab command line or automated scripts. A user typically places a slide on the sample platform and moves it underneath a HP26 cartridge. The **setPrintMode** command allows one or all of the cartridges to be set to fire. The discrete mode commands, **fireNozzle**

and **fireAllNozzle**, allow the user to fire individual nozzles or whole quadrants at once for a desired number of repetitions.

In patterning mode, the host PC coordinates stage motion and cell deposition in order to generate a pattern, specified by a bitmap image. With multiple cartridges, a separate bitmap is provided for each cartridge. The software accepts either a binary image, specifying the presence or absence of a drop at each location, or a 16 level gray-scale image, specifying the number of drops to deposit at each location. Using the **print** command, the user designates a specific location on the sample platform to begin printing the image. To achieve horizontal resolution of 300 dpi, the **print** command uses the Fire Pulse frequency to determine the correct speed to move the X axis and also calculates the required acceleration/deceleration distances. The bioprinter can begin to print from either side of required image location, however that would negate the compensation for backlash. It is important then to insure that the sample platform is always to the left of the Cell Delivery Station, on the same side as the Microscope Station. When printing begins, the sample platform will offset itself from the print location by the calculated acceleration distance and begin to move. Once the encoders indicate that the sample platform is in the correct location (because the model is always reading the encoder locations), the model will command the cartridges to fire.

During printing, the bitmap image is automatically divided into subimages of 50 rows each. Note that each row corresponds to one of the fifty nozzles on the cartridge and thus a subimage is printed during each horizontal pass of the stage underneath the cartridges. The host PC transfers the subimage data to the target PC and commands the motor controller to start moving the x-axis at a constant velocity over the desired print area. The target PC translates the image data into a corresponding nozzle firing pattern, taking into account the offset between the two columns of nozzles. If the desired pattern contains more than 50 rows, then, after printing the current sub-image, the host PC moves the second axis, the y-direction, by the height of 50 rows (4.235 mm). The process repeats with the next sub-image in the reverse direction. This cycle continues until the entire image is printed. Until the backlash issue is corrected, images taller than 50 pixels must be subdivided to insure proper alignment (Figure 11).

2.2.2 Calibration

When multiple cartridges are placed into the system, the relative positions of the cartridge printheads are not known precisely due to small variations in mechanical seating and cartridge manufacture. In order to print an image using multiple cartridges, or even a single cartridge that is removed and refilled, the relative locations of the printheads must be calibrated. The calibration is performed by using the microscope workstation to find the position of each cartridge relative to a common reference point, specifically the center of the field-of-view of the microscope in the Microscope Station. Figure 14 illustrates the basic calibration procedure. The sample platform is moved under each cartridge, pausing long enough for the cartridge to deposit one drop on a glass slide and record the sample platform location (locations **A**, **B**, and **C**). Each drop is in close proximity to the drops deposited by other cartridges. The stage is moved to Location **M**, so that the drops can be seen underneath the microscope. Image processing techniques are used to find the drop offset vector, \mathbf{V}_{MO} , which represents the length from the center of each drop to the center of the field-of-view of the microscope, \mathbf{O} .

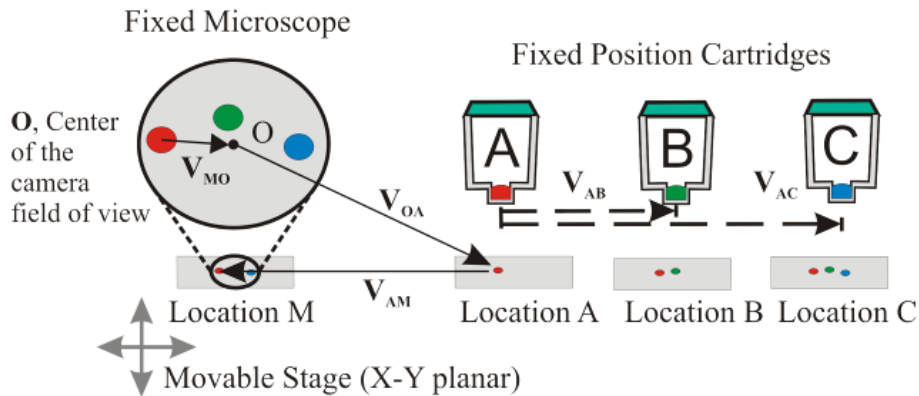


Figure 14 – Illustration of the calibration algorithm used to align the patterns of multiple cartridges for the bioprinter

Using Cartridge A as an example, the calibrated cartridge offset, \mathbf{V}_{OA} , is computed as the vector sum of the sample platform offset vector, \mathbf{V}_{AM} , plus the drop offset vector, \mathbf{V}_{MO} . The relative offsets between cartridges (\mathbf{V}_{AB} and \mathbf{V}_{AC}) may be found by subtracting the calibrated cartridge offsets, \mathbf{V}_{OB} and \mathbf{V}_{OC} , from

the first calibrated cartridge offset, \mathbf{V}_{OA} . These offsets are used to properly align the printed patterns. As implemented, the calibration procedure determines the cartridge offset, i.e. the vector distance from a specific nozzle to the camera center, to within 8 μm . The control software performs this alignment task semi-automatically for any number of cartridge substitutions and for the four cartridge holder locations.

The **calibrate** command uses different variations of the image processing technique of thresholding to find the drop offset vector, \mathbf{V}_{MO} . The choice depends on the cartridge solution, either ink or a cell solution. Thresholding works on the assumption that the brightest areas in the image are the ones of the most value. To begin thresholding, a typical image, which is composed of 3 layers of values for Red, Green, and Blue, is converted into a grayscale image where each pixel has an intensity value from 0 (black) to 255 (white). Matlab uses a weighted sum of the 3 layers to convert images from RGB to grayscale. To threshold the grayscale image, the user chooses an intensity value and all intensity values below are changed to 0 and all above to 255. This new binary image should contain the desired features. When performing the calibration algorithm using ink on paper, the act of thresholding is straightforward due to the high contrast. Most often however, the user will be printing with a cell solution. In this case, the drops of the cell solution will be printed on a glass slide set atop a dark opaque background (spray painted slide). This background provides the contrast needed since the individual cells reflect the light of the microscope illuminator (Light Ring, Figure 10b). The locations of the cells in each of the drops are not as important as the overall locations of the drops that contain those cells. Therefore, the focal plane is raised slightly to image the top of the drop, slightly blurring the cells, and allowing for a better approximation of the center of the deposited drop. If the default threshold does not yield the appropriate thresholded areas, the user is prompted to enter another value and the algorithm will reanalyze the image. Once the thresholded image is an approximation of the drop shapes, the user selects the areas and the cartridge-to-camera vectors are calculated.

3 THE BIOPRINTING FIDELITY INDEX

As noted in chapter 1, there are many different technologies that satisfy the definition of bioprinting [12]. As technologies proliferate, users will need a quantitative means to compare the output of a specific system in order to optimize system performance or to compare the output of different systems. The “bioprinting fidelity index “ (BFI) is proposed as a metric for these purposes. A statistical model is presented in conjunction with the BFI. based on parameters found in all bioprinting systems. The model takes into account the parameters and a desired pattern to estimate the maximum fidelity, e.g. highest BFI value, that can be achieved.

This chapter presents two studies. The first study attempts to estimate the parameter values for the bioprinter presented in chapter 2. Specifically, we estimate the drop distribution parameter as a function of solution type and height above the substrate. Analyzing the drop distribution helps characterize the drop center offset, mentioned in Chapter 1, which could affect pattern fidelity. The system specific parameters found in the first experiment enabled the second study, in which the BFI was applied to samples produced by the bioprinting system and the bioprinter’s pattern fidelity compared to the predicted BFI fidelity estimated from the proposed model. A detailed description of the BFI is described below and its underlying model described in Section 3.2.2, with the model derivation found in the Appendix, section A.1.

3.1 *Materials and Methods*

3.1.1 *Computing the Bioprinting Fidelity Index*

To compute the BFI for a specific pattern on a specific system, a scaled mask is superimposed on the image of a patterned co-culture and used to classify the number of cells not in their intended position (see Figure 15b). Proper scaling takes into account the intended size of the pattern (based on system resolution), the camera resolution, and microscope magnification. In this work, the mask was used to classify the number of correctly and incorrectly placed 4T07 (labeled red) and D1 (labeled green) cells (described later) (Figure 15a). Placement accuracy was quantified by cell type. Any 4T07 cells located inside areas designated for D1 cells were counted as incorrectly placed, and vice versa. All cells located outside the

mask boundaries were counted as incorrectly placed. The BFI takes these statistics and combines them into a composite score to indicate the accuracy at which the pattern was faithfully recreated by the system, e.g. pattern fidelity.

The BFI was used to quantify how well the printed pattern matched the pattern

specification. The BFI depends on both the number and types of incorrectly placed cells and the number and types of pixels in the specified pattern. Specifically, the BFI for a printed sample is defined as

$$(1) \quad BFI = \sum_{i=1}^m w_i (1 - e_i),$$

with $w_i = (p_{tot} - p_i) / ((m-1)p_{tot})$ and $e_i = \tilde{n}_i / n_i$, where m is the number of cell types, p_{tot} is the total number of pixels in the specified pattern, p_i is the number of pixels of cell type i , \tilde{n}_i is the number of incorrectly placed cells of type i , and n_i is the total number of printed cells of type i . The values for m , \tilde{n}_i , and n_i were obtained from analyzing the samples using the mask images. Note that e_i is the fraction of incorrectly placed cells of type i , while $(1 - e_i)$ is the fraction of correctly placed cells of type i . From the second expression in (1), the BFI can be interpreted as a weighted average of the fractions of correctly placed cells of each type, each weighted by the fraction of pixels of all other cell types. The closer the BFI is to 1.0, the higher the number of cells that were correctly placed.

3.1.2 Drop Distribution Study

Since this work is not comparing the patterns of different systems using the BFI, the output of the bioprinter will be compared to a proposed statistical model (described in section 3.2.2). This model is based on three main parameters: system resolution, drop gain, and drop center offset. With the system

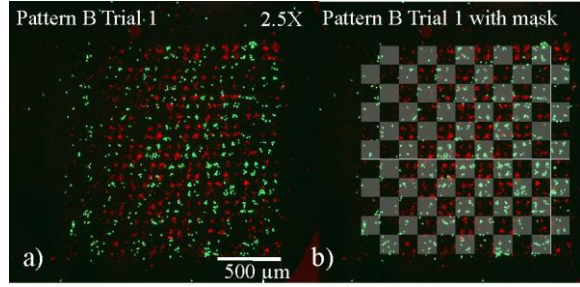


Figure 15 –(a) co-culture pattern after printing (b) co-culture pattern with mask overlaid

resolution and drop gain known, the purpose of this first study is to estimate the value of the drop center offset parameter for use in the model.

When a drop is printed onto a surface from a printhead nozzle, the center of the resulting drop is randomly distributed over some area below the nozzle. This study examined how the standard deviation of the distribution of drop centers varied (i) with the height of the printhead above the surface and (ii) with the type of solution printed. The three types of printed solutions were (1) OEM ink extracted from HP26A cartridges, (2) a solution of 4T07 cells, and (3) a solution of D1 cells. The ink from HP was printed as a baseline to determine how the performance of the nozzles changes when printing a media solution with cells. The cell solutions were prepared as described in section 3.1.3.1 below.

Single drops of solution were printed onto glass microscope slides (VWR Int'l, Westchester, PA) using the bioprinting system, and then moved underneath the camera of the vision system. Each experiment consisted of 15 sets of three printed drops. The stage positions were recorded in motor encoder counts when the stage was under the cartridge and under the camera. The camera captured an image and computer vision techniques were used to determine the location of centers of the drops. Similar to the calibration algorithm concept, the drop position vector was taken to be the difference between the printed location and the resulting location of each drop in reference to the camera center. Ground truth was considered to be the average of all the drop vector lengths in a trial. The drop offset was then determined to be the difference between length of the vectors of each of the three drops and the ground truth. Sets of drops with less than three drops were not averaged and were not included. Data points using ink were collected for each height: 1 mm, 2 mm, and 3 mm. The study was repeated at the same heights using a 4T07 cell solution and a D1 cell solution.

3.1.3 *Fidelity of Patterned Co-culture** (collaboration with Cheryl A.P. Cass)

This experiment produced patterned co-cultures for analysis by the BFI. The overall fidelity of the samples would measure the capability of our bioprinting system and effectiveness of the current post-processing procedures. Two different patterns were examined (Figure 16) and the fidelity was measured with the bioprinting fidelity index (BFI), described in section 3.1.1.

3.1.3.1 Cell Culture

D1 murine mesenchymal stem cells (American Type Culture Collection (ATCC), Manassas, VA) were cultured according to the manufacturer's suggested protocol. Briefly, cells were maintained in Dulbecco's Modified Eagle's Medium (DMEM, Invitrogen, Carlsbad, CA) containing 4 mM L-

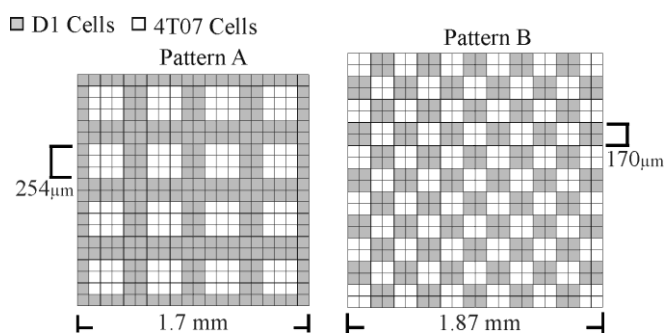


Figure 16 – Patterns A and B used to print the D1 (gray areas) and 4T07 cells (white areas)

glutamine, 1.5 g/L sodium bicarbonate, and 4.5 g/L glucose (ATCC), and every 500 mL was supplemented with 10% fetal bovine serum (FBS; Mediatech, Herndon, VA), 1% antibiotic/antimycotic, and 1% fungizone (Invitrogen). The culture medium was replaced every 48-72 hours as required, and cells were maintained in an incubator at 37°C and 5% CO₂. Cells from a non-metastatic murine mammary cancer cell line, 4T07 (ATCC), were maintained in the culture conditions described above for D1 cells.

To prepare cell solutions for printing, D1 and 4T07 cells were suspended in serum-free DMEM (SF-DMEM) at a density two times the desired final concentration. All cell suspensions were filtered using a 40 μm sterile cell strainer (Becton Dickinson, Franklin Lakes, NJ). Just prior to printing, 75 μL of the cell suspension was combined with 75 μL of Hank's Balanced Salt Solution (HBSS; Invitrogen, Grand Island, NY) containing 1.06 mM ethylene diamine tetraacetic acid (EDTA; Invitrogen), and was subsequently deposited into the HP26 cartridge well [26]. Thus, the resulting 150 μL of cell solution consisted of D1 or 4T07 cells suspended in 50% SF-DMEM and 50% HBSS, with a final EDTA concentration of 0.53 mM.

3.1.3.2 Preparation of Collagen Substrates

All samples were printed onto a collagen substrate layered on a Cell Vu (Millennium Sciences Inc., NY, NY) gridded coverslip. The grid was used to register the printed patterns to a specific location on the coverslip. The coverslips were autoclaved before use. The collagen substrate was created using aseptic techniques. Specifically, a 1.98 mg/mL collagen solution was prepared by combining 1.5 mL collagen

stock solution (3.0 mg/mL - PureCol™) with 167 μ L 10X Dulbecco's phosphate buffered saline (DPBS; Sigma, St. Louis, MO), 225 μ L fetal bovine serum (FBS), and 358 μ L DMEM; a small volume (approximately 20 μ L) of 1N NaOH (Sigma) was added to neutralize the solution. To create the collagen substrate, a 1" square was cut out of a 1/2 mm thick sheet of silicone and punch was used in the center to create a silicone ring with a 1/2" inner diameter. These silicone rings were laid on top of the coverslips to contain the collagen solution. The rings were cleaned in 70% ethanol for 30 minutes prior to use. The collagen solution was pipetted into the center of each silicone ring at 200 μ L per coverslip, and the collagen gels were polymerized in an incubator at 37 °C and 5% CO₂ for at least 4 hours. The collagen gels were then placed into a laminar flow biological safety hood and allowed to dry [71]. Once dry, gel coatings were rinsed in sterile distilled water until clear and then allowed to dry in the biological safety hood. After drying, the coverslips with collagen coatings were soaked overnight in a 1:1 solution of DMEM to FBS [71]. Excess culture medium was aspirated prior to printing, and the collagen coatings were allowed to partially dry in a laminar flow hood for 3 minutes.

3.1.3.3 *Fluorescent Labeling*

In order to differentiate between cell types in a printed pattern, D1 and 4T07 cells were labeled prior to printing, using green (Excitation 450 nm, Emission 517 nm) and red (Excitation 550 nm, Emission 602 nm) CellTracker™ probes (Invitrogen), respectively. The CellTracker™ green stock solution was prepared by adding 10.76 μ L dimethyl sulfoxide (DMSO; Sigma) to the lyophilized product diluted in 10 mL of SF-DMEM. The CellTracker™ red working solution was prepared by adding 7.29 μ L DMSO to the lyophilized product and then subsequently diluting the solution with 10 mL SF-DMEM. Cells grown to confluence in a T-75 tissue culture flask were washed with 1X DPBS and incubated for 45 minutes in their respective fluorescent tag solutions.

3.1.3.4 *Dual Cell Patterning: Co-culture*

Separate solutions of D1 cells and 4T07 cells were prepared as above, consisting of 50% SF-DMEM and 50% HBSS, containing 7.7×10^6 cells/mL and 0.53 mM EDTA. The D1 cell solution and 4T07 cell

solution were each pipetted into separate sterilized cartridges that had been previously inserted into the cartridge holder. The cartridges were calibrated for printing using the alignment algorithm described in section 2.2.2. The coverslip grid was brought into the field of view of the camera. The grid location was registered using computer vision and a set of stage coordinates was calculated so that the pattern would be printed at a known location relative to the grid. Before printing the pattern, each nozzle was fired 100 times in order to clear any cell aggregates that may have settled into the nozzles. A new pair of cartridges was inserted, filled, and calibrated every 15 minutes in order to maintain consistent printing conditions.

After printing, the samples were placed in an incubator for either 25 or 60 minutes to promote attachment. After the attachment period, all samples were covered with 10% serum-inclusive DMEM. All samples that maintained sufficient pattern definition, for proper alignment of the pattern mask (described below), after being covered with medium were photographed using a Zeiss Axiovert 40 CFL microscope (Carl Zeiss AG Oberkochen, Germany) equipped with a 50 W Xenon lamp. The images were captured using an AxioCam MRC 5, processed with Zeiss AxioVision LE 4.6, and combined using the GNU Image Manipulation Program (GIMP).

3.2 *Results and Discussion*

3.2.1 *Drop Distribution Study*

Table II provides statistics of the drop center distribution for each height and each printed solution. The observed distributions are not quite radially symmetric, i.e. they have different standard deviations, σ_1 and σ_2 , along the major and minor axes of the distribution. The distributions are compared on the basis of $\bar{\sigma} = \sqrt{\sigma_1\sigma_2}$, which is the standard deviation of the radially symmetric Gaussian distribution that has the same determinant of the covariance matrix as the original asymmetric distribution.

Initially, it was hypothesized that the distribution of drop centers was caused by small random angles of departure as drops left the nozzle. In that case, the standard deviation of the drop distribution should vary linearly with height. Examining the data, the results for ink did not agree with this hypothesis. The 4T07 solution appeared to vary linearly with height, while the D1 solution stayed fairly consistent, albeit with a large standard deviation, for all heights. This disparity was unexpected as the 4T07 cells are similar in size to the D1 cells in solution

and cell size was anticipated to be the major factor in spray distribution. Thus, a second experiment was performed in

which the height and cartridge were kept constant in order to remove the effects of individual nozzle variations (see Table II, Cartridge H).
 Altogether, the results show that there appears to be an upper limit on the standard deviation of the drop distribution for cell solutions, performing similarly enough to ink that patterns can be reproduced with similar fidelity. The drop offset parameter for a HP26 cartridge printing a cell solution consisting of 50% SF-DMEM and 50% HBSS, containing 7.7×10^6 cells/mL and 0.53 mM EDTA was estimated to be $\sigma = 15$ μm . Previous experiments have used a printhead height of 1mm, mimicking the HP500 printer, but this new data suggests that similar patterning accuracy could be achieved with the printhead farther from the surface, allowing patterning in a wider variety of containers.

Table II - Drop Center Distribution Statistics

Solution	Height (mm)	Drop Distribution (μm)			Cartridge
		σ_1	σ_2	$\bar{\sigma}$	
ink	1	8.95	6.75	7.77	A
ink	2	9.77	7.61	8.62	B
ink	3	7.03	5.77	6.37	B
D1	1	33.51	17.30	24.08	C
D1	2	36.72	16.44	24.57	D
D1	3	26.45	16.51	20.90	E
4T07	1	7.16	4.90	5.92	F
4T07	2	15.61	7.08	10.51	G
4T07	3	18.51	13.36	15.73	F
Ink	1	10.65	5.22	7.46	H
ink	1	15.18	6.88	10.22	H
Ink	1	13.56	8.88	10.97	H
D1	1	12.03	9.12	10.47	H
D1	1	18.56	11.77	14.78	H

Results for the drop distribution study showing the distributions of drop centers while printing three different solutions from three different heights. The colored rows in the table correspond to trials performed using the same cartridge.

3.2.2 Fidelity of Patterned Co-cultures

In order to interpret the results of the patterned co-culture study and analyze the causes of loss of pattern fidelity, a very simple model of cell placement was introduced that helps to highlight some fundamental tradeoffs in bioprinting and to interpret the patterning experiments. The model predicts the probability that a drop printed in one pixel will place a cell in a neighboring pixel, given system resolution (size of a printed pattern pixel), drop gain, and drop center offset distribution. The model (see Figure 17a) assumes that (i) a circular drop with radius r is placed in each pattern pixel, (ii) the drop is randomly placed within the pixel such that its center is distributed about the pixel center as a radially-symmetric Gaussian random variable with standard deviation $\bar{\sigma}$, representing drop center offset, and (iii) cells are uniformly distributed within the drop. The model can be used to estimate the probability of misplacing a cell. When a misplaced cell is located in an area designated for another cell type then it is incorrectly placed and contributes to loss of fidelity for a specific printed pattern in terms of the BFI. The model is derived using dimensionless parameters, which makes the model easier to apply to other bioprinting systems, using the plots provided here, Figure 17.

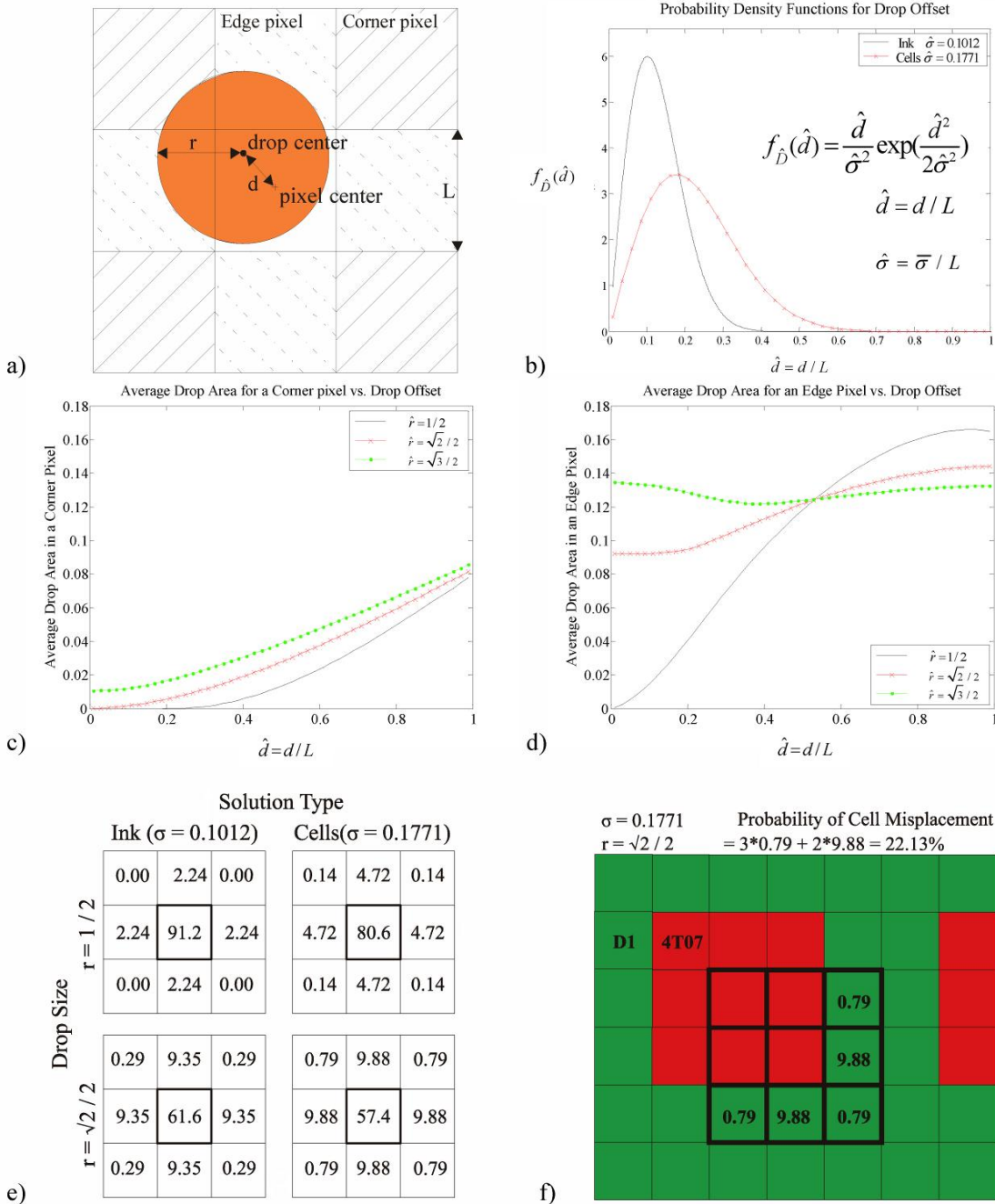


Figure 17 - (a) A drop offset by a distance d from the center of the intended pixel. Portions of the drop lie in neighboring “corner” and “edge” pixels. (b) The probability density function (pdf) for dimensionless drop offset distance $\hat{d} = d / L$. Each printed solution has a unique pdf. (c),(d) The conditional probability that a drop of dimensionless radius \hat{r} will place a cell in (c) a “corner” pixel or (d) an “edge” pixel, given that the drop is dimensionless distance \hat{d} from the pixel center. (e) For a specific drop size and pdf, the probabilities that a cell will be placed in each of the neighboring pixels can be represented as a stencil. The bold square highlights the center pixel. (f) The appropriately chosen stencil is used to predict the probability of misplacing cells while printing each pixel in the pattern.

In printing, the pixel size (system resolution) and drop sizes (drop gain) are chosen such that a printed drop completely covers the corresponding pixel. This permits total coverage of the surface without leaving gaps between drops, which is required in traditional printing applications in order to produce solid colors. In bioprinting however, if a drop completely covers a pixel, then even if the drop is placed precisely at the center of the pixel, an area at the edge of the drop will overlap neighboring pixels, guaranteeing that cells will be misplaced. The probability of misplacement increases as the drop radius r increases relative to the pixel size L , or equivalently as the dimensionless parameter $\hat{r} = r / L$ increases. The drop size that permits complete area coverage with the lowest probability of misplacement is $r = \sqrt{2}L/2$, or equivalently $\hat{r} = \sqrt{2}/2$.

If the drop center is uniformly distributed around a circle at distance d from the pixel center (See Figure 17a), then more of the drop will lie in neighboring pixels and hence the probability for cell misplacement is increased. If drop centers are distributed around the pixel center as a radially-symmetric Gaussian random variable with standard deviation $\bar{\sigma}$, then the probability distribution function for a drop center being distance d from the pixel center is

$$(2) \quad f_{\hat{d}}(\hat{d}) = \frac{\hat{d}}{\hat{\sigma}^2} \exp\left(-\frac{\hat{d}^2}{2\hat{\sigma}^2}\right), \text{ where } \hat{d} = d/L \text{ and } \hat{\sigma} = \bar{\sigma}/L$$

This distribution (2) is plotted in Figure 17b. Numerical methods are used to find the probability that a cell will be placed in each of the eight neighboring pixels given that the drop center is distributed uniformly on a circle at dimensionless distance \hat{d} from the pixel center (Figure 17c-d). The conditional cell placement probabilities and the drop center distribution are combined using the law of total probability to determine the probability that a cell will be placed in one of the eight neighboring pixels. Due to symmetry, only three distinct neighbor probabilities need to be calculated, one for the center pixel, one for edge neighbor pixels, and one for corner neighbor pixels.

$$(3) \quad P(\text{misplaced cell in neighbor } i) = \int_0^{\infty} P(\text{misplaced cell in neighbor } i | \hat{D} = \hat{d}) f_{\hat{d}} \hat{d} \, d\hat{d}.$$

A stencil may be used to visualize the placement probabilities (see Figure 17e), where each entry is the probability of a cell being placed in the corresponding pixel, given that a drop is printed to the center pixel. By laying the stencil over a pattern to be printed, one can predict the probability that a misplaced cell is actually incorrectly placed and will cause a loss in fidelity, i.e. that a cell of one type will be placed in a pixel of another type (Figure 17f). The stencil is moved to each pixel in the pattern to compute the probability for incorrectly-placing a cell from that pixel. The error probability of all pixels of a specific cell type is averaged to predict the error for that cell type in the pattern, e_i , which is used in the BFI.

Several observations arise immediately. First, if the resolution of the Motion System is much finer than the drop size, then the drop size is the dominant source of placement error. Similarly, as stated above, the effective resolution, i.e. the pixel size, should be chosen to be similar to the drop gain in order to achieve high fidelity. Third, the drop center offset, \hat{d} , needs to be characterized to determine if its magnitude is negligible when compared to the drop gain and system resolution. Lastly, the expected fidelity of a pattern depends on the complexity of the pattern, specifically on how finely pixels of different cell types are interspersed. The highest complexity pattern would be a checkerboard in which every pixel has four edge neighbors of the opposite type.

The following parameters were used with the model to simulate the pattern fidelity of the bioprinting system. The pixel size is the native resolution for the HP26 cartridge, $L = 84.7 \mu\text{m}$. The drop center standard deviations for 4T07 and D1 cell solutions were both chosen to be $\bar{\sigma} = 15 \mu\text{m}$ ($\hat{\sigma} = 0.1771$), which was found to be representative of typical performance of cell solutions in the drop distribution study. The drop radius was taken to be $r = 60 \mu\text{m}$ ($\hat{r} = \sqrt{2}/2$), which corresponds to the smallest size drop that can completely cover a pixel. This value is a reasonable estimate based on typically observed drop sizes. The stencils created using these model parameters are shown in the bottom row of Figure 17e.

<i>Pattern Statistics</i>	<i>Correctly Placed D1 Cells (%)</i>	<i>Correctly Placed 4T07 Cells (%)</i>	<i>Bioprinting Fidelity Index</i>	<i>Incorrect / Total # of 4T07 Cells</i>	<i>Incorrect / Total # of D1 Cells</i>	<i># of D1 cells/pixel</i>	<i># of 4T07 cells/pixel</i>
<i>Pattern A</i>						<i># D1 pixels:</i>	<i># 4T07 pixels:</i>
<i>Predicted Fidelity</i>	88.1	85.2	0.862			256	144
<i>Trial 1*</i>	83.1	66.3	0.723	165 / 489	310 / 1830	7.1	3.4
<i>Trial 2*</i>	88.1	85.3	0.863	101 / 689	79 / 656	2.6	4.8
<i>Trial 3</i>	82.3	63.0	0.699	319 / 863	137 / 777	3.0	6.0
<i>Trial 4</i>	70.4	61.9	0.650	363 / 953	267 / 902	3.7	6.6
<i>Trial 5</i>	86.9	79.2	0.820	132 / 635	71 / 543	2.1	4.4
<i>Trials 1-5 Mean</i>	82.2	71.2	0.752	209 / 726	168 / 942	3.7	5.0
<i>Pattern B</i>						<i># D1 pixels:</i>	<i># 4T07 pixels:</i>
<i>Predicted Fidelity</i>	78.6	78.6	0.786			240	244
<i>Trial 1</i>	79.9	76.5	0.782	343 / 1458	136 / 675	2.8	6.1
<i>Trial 2</i>	79.2	64.3	0.717	458 / 1284	129 / 654	2.7	5.4
<i>Trial 3</i>	73.3	63.7	0.685	351 / 966	158 / 591	2.4	4.0
<i>Trials 1-3 Mean</i>	77.4	68.2	0.728	384 / 1232	141 / 640	2.6	5.1

Table III - Statistics showing the fidelity of the bioprinting system when producing the two patterns, A and B. * It should be noted that Trials 1 and 2 for Pattern A were only incubated for 25 minutes, as per standard operating procedure at that time. It was later seen that an incubation time of 60 minutes yielded higher numbers of high fidelity samples, thus the remaining trials were incubated for the longer duration

Table III provides the model's BFI predictions for Pattern A and B as well as the experimental BFI results from the patterned co-culture fidelity study. Pattern B is more complex, since it has more shared borders between pixels of different types. Due to this higher complexity, the model predicts Pattern B will print with lower fidelity than Pattern A. The mean experimental BFI for Pattern B is lower than for Pattern A, supporting the prediction. The experimental BFI for many of the individual trials is close to the predicted value. Based on the simple assumptions of the model, significant fidelity improvement could only be achieved by changing the parameters of the modeled system, e.g. increasing pixel size, decreasing drop size, or reducing the standard deviation of the drop center distribution. The experimental results show the D1 cells printed closer to the predicted fidelity than the 4T07 cells, in which the model consistently overestimated the fidelity. This disparity suggests that there were other sources of error outside the scope of the model. Looking at the error due to miscalibrated cartridges, pattern A should be less sensitive to slight errors from calibration because of its lower complexity when compared to Pattern B. However, the calibration algorithm has been shown to be accurate to within $7(\pm 5)$ μm .

By applying the BFI to images of the same patterned co-culture at different stages of the post-processing procedure, the results suggested that the bioprinting system patterned the 4T07 cells accurately, but that post-processing steps, specifically application of medium onto the samples after the attachment period, disrupted the pattern (Figure 18). The effects of medium application may be directly observed in Pattern B Trial 3, shown in Figure 18a. For this sample, the BFI was 0.829 before the application of medium but fell to 0.685 after application. Moreover, 23% and 46% of the initial populations of D1 cells and 4T07 cells, respectively, were washed away from the pattern by the application of medium. The D1 and 4T07 cells exhibited correct placement ratios of 87.8% and 78.0% before the application of media and 73.3% and 63.7% afterwards. Similarly in Pattern B Trial 2, application of medium washed away 16% and 27% of D1 and 4T07 cells, respectively. This phenomenon helped explain why many samples displayed a near total loss of fidelity, could not be properly analyzed, and were discarded from the analysis. Of the twenty samples were created for each of the two test patterns shown in Figure 16, only 25% of samples were fully analyzed after application of medium.

When adjusting the post-processing incubation time, a careful balance must be struck between pattern fidelity and cell viability. Application of medium within a reasonable timeframe is necessary to maintain the viability of the cells, but doing so too early disturbs the cell locations in the pattern. In the first trials, the samples were allowed to incubate for an attachment period of 25 minutes

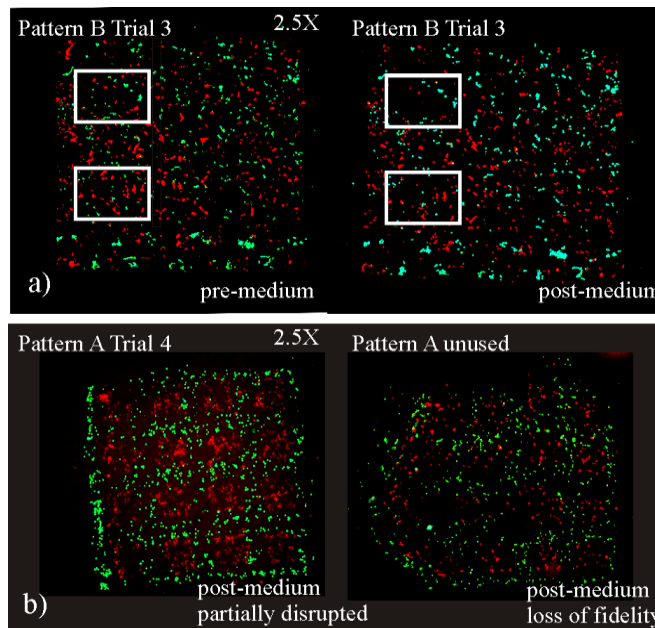


Figure 18 – two images demonstrating the loss of cells caused by the application of medium (left column vs. right column)

before applying medium. Most of these samples had low fidelity due to pattern distortion. In response, the attachment period, i.e., the incubation time before applying medium, was lengthened to one hour in the remainder of the trials. This revision allowed the cells time to more fully attach to the substrate, increasing pattern fidelity. Decreasing the amount of time it takes cells to attach will be critical to improving bioprinting fidelity. The use of a medium-saturated collagen substrate was motivated by previous experiments which yielded lower fidelity and poorer viability from patterns printed directly onto polystyrene slides. The saturated collagen substrate allows the application of bulk medium to be delayed for the full hour while maintaining good cell viability; however the low modulus 1.98 mg/mL collagen substrate may impede the rate of attachment of anchorage dependent cells [72]. The attachment disparity between the two cell types may be attributed to the difference in the amount of surface attachment proteins produced by each cell type. In order to simultaneously increase pattern fidelity and cell viability, the focus for improving the bioprinting process should be on combinations of biomaterials and post-processing methods that: (i) ensure that cells remain in their printed locations, (ii) promote quicker attachment between the cells and substrate (iii) provide a more hospitable environment before application of bulk medium. The

BFI, which characterizes a printed pattern with a single number, will permit a direct, principled comparison of the effects of alternate processing methods.

This chapter examined the validity of using the Bioprinting Fidelity Index to analyze the performance a bioprinter and optimize its sample creation. The BFI is a general fidelity metric, computed by overlaying a virtual mask on the printed co-culture sample and counting the number of incorrectly placed cells. A simple statistical model based on the technology independent parameters of system resolution, drop gain, and drop center offset distribution was introduced to provide the maximum BFI fidelity theoretically possible for the system. The experiment BFI results trended as expected with more complex patterns displaying lower BFI values. The fidelity numbers of the best samples matched very well with the BFI predicted by the model. The application of the BFI at certain stages of our post-processing procedure allowed us to determine that the fidelity of many of our samples was being destroyed by the application of media before the cells were fully attached. This finding highlights the need to characterize the attachment behavior of specific cell types over different times and on varying substrates. The bioprinter system was determined to be able to produce patterned co-cultures at biologically relevant length scales. The Bioprinting Fidelity Index was shown to provide an effective quantitative means of presenting the fidelity of a patterned co-culture pattern for the purpose of analysis and optimization. Its accompanying model was shown to provide a reasonable standard by which to compare the theoretically maximum BFI fidelity with experimental BFI values.

4 CELL SETTLING EFFECTS ON UNIFORM PATTERN REPRODUCTION

Over the last decade, bioprinting has emerged as a tool suitable for investigating cell–cell interactions. Current bioprinters are beginning to exhibit the high amount of spatial control, i.e. controlling cell placement location and cellular proximity [2] necessary to control the degree of homotypic and heterotypic cell–cell contact for *in vitro* studies [3]. These studies broaden understanding of many different types of cell-cell and cell– extracellular matrix (ECM) interactions, such as cancer proliferation, migration, metastasis, apoptosis or stem cell differentiation and function [1], [2]. Through automation, these bioprinters produce samples with precision and high throughput, enabling the creation of large datasets to support statistically significant conclusions [1].

Three of the main technologies in bioprinting, thermal inkjet (TIJ), piezoelectric inkjet (PEIJ), and pneumatic microvalve (PMV), require a cell suspension of some specific concentration to be loaded into a reservoir to supply the printing mechanism. While investigating printing performance over time, several papers have noted [43], [66] or documented [73] print failure or decreased cell output while printing over time periods greater than 10 to 20 minutes. This phenomenon has been attributed to the settling and aggregation of cells in suspension [37], [43], [66], [73]. Implementing physical workarounds such as agitating the suspensions through vibration or stirring the cell suspension with a stir bar still resulted in unusually low or unpredictable cell output characteristics past the 20 minute mark [66], [73]. The cell concentration in a suspension should remain relatively constant so that the ‘cells per drop’ is consistent in the co-culture. Maintaining a desired cell density is important to guarantee proper cell communication, growth, and spreading [66]. The dual constraints of acceptable printer and co-culture performance demand a delicate balance of the upper and lower limit for the cell concentration in suspension. This is seen directly in [43] when different cell types had to be finely tuned to the correct concentration based on the observed clogging tendencies of each cell type.

Producing samples with similar cell populations is especially important for comparing results in cell-cell signaling studies. It has been shown that extracellular cues are important in regulating adult stem cell and

embryonic stem cell fate decisions [1], [16], [17]. Desired cell populations between all samples over the course of an experiment should be monitored and maintained.

The goal of this chapter is to establish the link between cell settling and the cell concentration in a printed drop. From this understanding it is expected that the consistency of cells per printed drop can be improved through i) management of the printing process, *i.e.* establishing a window of time for a particular bioprinting system in which the samples have consistent cell populations, ii) compensation in the printing process for predictable evolution in printed drop concentrations, and iii) additional insight into the requirements of reservoir stirring or agitation systems.

4.1 Cell Settling Model

An approximate model that assumes all cells of the same type settle at a constant rate can be used to frame our expectations for the effect of cell settling on printing. The diagram in Figure 19 shows the geometry of the reservoir area above the printhead for a TIJ bioprinter based on the HP26 cartridge. Since the printer is drawing fixed volumes from the bottom of the reservoir it would be expected that the concentration of cells in a printed drop would reflect the concentration of cells near the printhead. The volume of liquid above the printhead is labeled V_2 and has associated height h_2 and the volume of liquid located directly above the

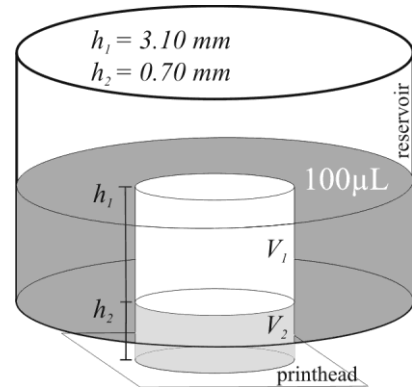


Figure 19 – a diagram of the inkjet cartridge reservoir and printhead shows the volumes of liquid in the reservoir (V_1) and above the print head (V_2). The total of these volumes is $100 \mu\text{L}$. This ratio of these volumes estimates the final cell output concentration after settling.

printhead in the reservoir, V_1 , has associated height h_1 . First, Stokes' law can be used to estimate the cell settling velocity of each cell by assuming the cells are small particles in a slow velocity fluid flow. Stokes' law is defined as

$$(4) \quad v = \frac{(\rho_p - \rho_f) g D_p^2}{18\mu}$$

where ρ_p is the density of the particles, ρ_f is the density of the fluid, μ is the fluid's viscosity, g is gravitational acceleration, and D_p is the average diameter of the particles.

The settling velocity can be used with the initial concentration, C_0 , to model the concentration in the printhead as

$$(5) \quad C_2(t) = \begin{cases} C_0 \left(1 + \frac{vt}{h_2} \right) & \text{for } t < \frac{h_1}{v} \\ C_0 \left(1 + \frac{h_1}{h_2} \right) & \text{for } t \geq \frac{h_1}{v} \end{cases}$$

The model in (5) predicts that the concentration in the print area will linearly increase until it reaches a constant steady state value after time t , when all cells from V_1 have completely settled into V_2 , see Figure 20.

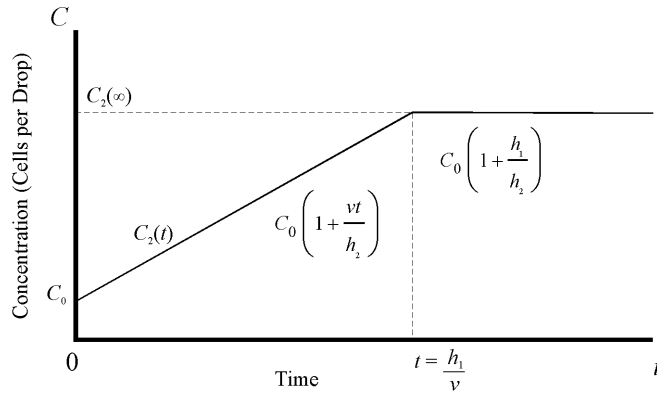


Figure 20 – concentration profile of the settling model, seen in (5)

4.2 Materials and Methods

The bioprinting system used in this paper uses TIJ technology. The bioprinting system, described in detail in [69], uses modified Hewlett-Packard (HP; Hewlett-Packard Company, Palo Alto, CA) 26A inkjet cartridges with 50 nozzles. Previous work done in [26] found the anti-scalant ethylene diamine tetraacetic

acid (EDTA; Invitrogen, Carlsbad, CA) to be a cell suspension additive which significantly decreased the probability of nozzle failure over a span of 25 minutes.

4.2.1 Cell Settling Study

The cell output characteristics of the bioprinting system were examined by tracking the change in number of cells per pattern (which is used to calculate the number of cells per drop) over a time span of fourteen minutes. Sample slides were produced starting immediately after loading cells into the cartridge and every two minutes thereafter. Each slide has six or nine printed samples, each sample was composed of a simple pattern of six squares, 3 pixels x 3 pixels each, 54 pixels total (Figure 21). The two minute interval between slides was chosen to correspond to the typical time required by the TIJ bioprinter to produce one slide of patterned co-cultures, and the fourteen minute experiment duration was based on previous observations of bioprinter performance using a 8.0×10^6 cells/mL D1 cell (described below) suspension.

Five HP26 cartridges labeled A, B, C, D, and E were chosen from a set of cartridges used in previous cell printing experiments along with two new cartridges labeled F and G. These cartridges were modified from their original form and prepared for printing by removing the top, inner bladder, and reservoir filter. Prior to use in previous experiments, cartridges A, B, C, D, and E were cleaned using a set *Cleaning Method*, which consisted of a 15 minute soak in Cool Soak Stain and Rust Remover (Burnishine Products, Gurnee, IL), a 15 minute soak in Instrument Lubricant (Burnishine Products), then followed by 15 minutes of

sonication (Branson Ultrasonics Corp., Danbury, CT). Each cartridge was then prepared for an experiment using the Experiment Preparation procedure, in which each cartridge was filled with ink and a verification pattern was printed to ensure proper performance of all nozzles. After printing, each cartridge was

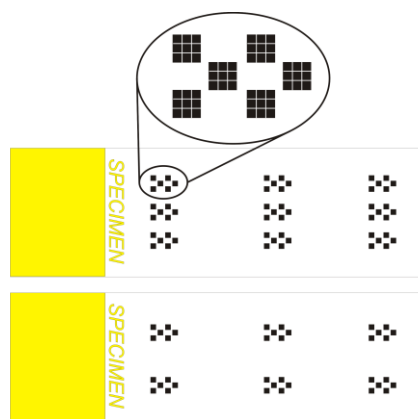


Figure 21 – Top) a sample slide showing the 9 patterns, each composed of 6 squares, 3 pixels by 3 pixels. Bottom) later experiments produced sample slides containing 6 patterns.

sonicated for 10 minutes and vacuum dried. The sonication steps in these methods was omitted when preparing Cartridges F and G.

4.2.1.1 Cell Culture

D1 murine mesenchymal stem cells (American Type Culture Collection (ATCC), Manassas, VA) were cultured according to the manufacturers suggested protocol. Briefly, cells were maintained in Dulbecco's Modified Eagle's Medium (DMEM, Invitrogen) containing 4 mM L-glutamine, 1.5 g/L sodium bicarbonate, and 4.5 g/L glucose (ATCC), 10% fetal bovine serum (FBS; Mediatech, Herndon, VA), 1% antibiotic/antimycotic, and 1% fungizone (Invitrogen). The culture medium was replaced every 48-72 hours, and cells were maintained at 37°C with 5% CO₂.

The D1 cells were labeled with Hoescht 33342 trihydrochloride trihydrate (Invitrogen). The D1 cells were suspended in 2 mL of DMEM at 16.0×10^6 cells/mL. Next, 10 μ L of the stock Hoescht solution (concentration: 1mg/mL) was added to the cell suspension resulting in a dye concentration of 5 μ g/mL. The cell suspension was incubated for 30 minutes at 37 °C and 5% CO₂. The cell suspension was centrifuged at 1000 rpm for 5 minutes. The supernatant was removed and the cell pellet resuspended in 1mL of serum free DMEM (SF-DMEM). After labeling the cells, the 16.0×10^6 cells/mL D1 cell suspension was filtered using a 40 μ m sterile cell strainer to remove any large cell clumps (Becton Dickinson, Franklin Lakes, NJ) and kept on ice. Before loading into the cartridge, 50 μ L of cell solution in SF-DMEM and 50 μ L of HBSS solution with 1.06 mM EDTA were combined to form 100 μ L of SF-DMEM/HBSS with 0.53 mM EDTA containing D1 cells at a concentration of 8.0×10^6 cells/mL.

4.2.1.2 Printing Experiments

In the first experiment (E1), the cell suspension was pipetted into the cartridge reservoir of cartridge C, D, and E, the firing chambers primed, and the cartridge inserted into the bioprinter. The first experiment slide was removed from its Petri dish and printed immediately after cartridge insertion. Seven slides were successively printed at two-minute intervals. After printing, each slide was returned to its Petri dish. When printing was complete, the cartridges were cleaned and dried according to the Cleaning Method. Each slide

was inspected with a Zeiss Axiovert 40 CFL microscope (Carl Zeiss AG Oberkochen, Germany) equipped with a 50 W Xenon lamp and the number of cells in each of the 9 samples was hand counted and recorded.

In the second experiment (E2), A and B were chosen because these cartridges had almost twice as many previous uses as C, D, and E (Table IV), allowing investigation into the possible effects of use and cleaning on cartridges. Cartridges A and B were cleaned and verified according to the Cleaning Method and Experiment Preparation method. Eleven

glass slides were prepared as above for cartridge A and eight glass slides for cartridge B. The cell suspension was prepared and labeled as above. Cartridge A was used to create 11 slides, each printed at a 1 minute interval, to investigate if the cell output per sample would change with increased printing frequency. Cartridge B printed eight slides at 2 minute intervals. Instead of hand counting all samples on each slide, each sample was imaged using the Zeiss Axiovert 40 CFL microscope, captured

Table IV – experiment plan and previous usage of each cartridge

Experiment	Cartridge	Suspension	Slides	Interval (min.)	Prior Uses
E1	C	D1 cells	8	2	6
E1	D	D1 cells	8	2	6
E1	E	D1 cells	8	2	5
E2	A	D1 cells	11	1	11
E2	B	D1 cells	8	2	9
E3	D	D1 cells	8	2	7
E3	E	D1 cells	8	2	6
E3	B	D1 cells	8	2	10
E4	F	Latex beads	8	2	0
E4	G	Latex beads	8	2	0
E5	F	D1 cells	8	2	1
E5	G	D1 cells	8	2	1

using an AxioCam MRC 5, and processed with Zeiss AxioVision LE 4.6. The cell counts of all samples for all slides of A and B were calculated using image processing techniques implemented in Matlab R2009b (Mathworks Inc, Natick, MA).

In a third experiment (E3), additional data was collected from cartridges D, E, and B in order to compare it with the first and second experiments for consistency. Cell suspension preparation and labeling was the same as above. Each cartridge generated eight slides of 9 samples each every two minutes. The samples were imaged and counted as in E2.

4.2.2 *Latex Bead versus Cell Output in New Cartridges*

Once the data from the Cell Settling study was analyzed, two new cartridges F and G were chosen and samples of 10 μm polystyrene latex beads (Beckman-Coulter Co., Miami, FL) and D1 cells were printed for comparison. These cartridges were modified for use in bioprinting experiments as described above. The same Cleaning Method and Experiment Preparation procedure was used with cartridges F and G but with the omission of the sonication step.

In a fourth experiment (E4), cartridges F and G were used to produce 16 slides each, consisting of 2 trials of 8 slides, printed at 2 minute intervals. The latex beads were suspended in the cell solution of 50% SF-DMEM and 50% HBSS solution with 0.53 mM EDTA and at a concentration of 8.0×10^6 beads/mL. The glass slides were prepared as in previous experiments. The cartridges were alternated every eight slides and the bead suspension was vortexed before being loaded into the cartridge between trials. Each cartridge was cleaned between experiments using the Cleaning Method, omitting the sonication step. Six samples per slide were printed as opposed to nine to reduce the amount of images required per slide while maintaining statistical significance (Figure 21). All samples were imaged and sample counts obtained using image processing techniques as in E2.

After cleaning, cartridges F and G were used in a fifth experiment to produce 24 slides each, consisting of 3 trials of 8 slides, printed at 2 minute intervals. The cartridges printed D1 cells and all cell suspensions and slides were prepared as in the Cell Settling Study experiments. Each cartridge was cleaned between experiment trials using the Cleaning Method, omitting the sonication step. Six samples were printed per slide and all samples were imaged and analyzed as in E2.

4.3 *Results & Discussion*

The mathematical settling model in (1) and (2) predicts that the concentration of particles in suspension in the print area will linearly increase until it reaches a constant steady state value. The measured geometry of the HP26 cartridge suggests the concentration should linearly increase until reaching a steady state concentration of $C_{2,steady\ state} = 5.4C_0$. The model parameters can be found in Table V. The D1 cell density

was estimated from literature that measured Chinese Hamster Ovary (CHO) cells [74]; it was assumed that since D1 and CHO cells are both mammalian cells and of similar size that they have similar densities. The bead density was given by the manufacturer. The viscosity of the SF-DMEM/HBSS/0.53 mM EDTA solution was measured without particles using a size 50 glass capillary viscometer by comparing its viscosity to that of distilled water at 20°C. The Wall effects and particle effects were not taken into consideration as the concentration of the suspension was below 10×10^6 cells/mL [75].

Table V – model parameters used for the cell and bead settling output models

Model Parameters	Symbol	D1 Cell	Latex Bead
Particle Density (g/cm^3)	ρ_p	1.051	1.050
Particle Diameter (μm)	D_p	13	10
Gravitational Acceleration (m/s^2)	g	9.8	
Solution Viscosity (cP)	μ	1.036 (20°C)	
Solution Density (g/cm^3)	ρ_f	0.998	

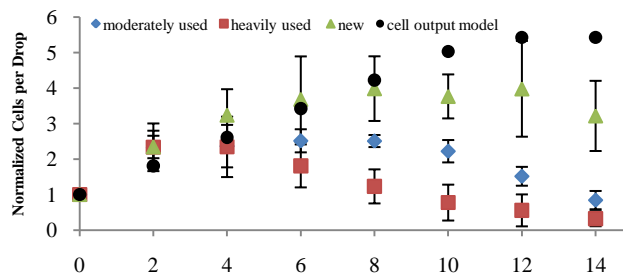


Figure 22 - Cell output results of the heavily used (A and B), moderately used (C D E), and new cartridges (F and G). Note the inverse relationship between number of uses and consistent printing performance. Each trial was normalized based on the initial ‘cells per drop’ from the slide at time 0 before being averaged ($N > 9$ for all timepoints).

Figure 22 shows how settling affected the “cells per drop” output of the cartridges over time. The number of cells per sample was normalized by the initial cells per sample to remove variation due to the initial suspension concentration, C_0 , between experiments. The normalized average cell output of all cartridges follows the predicted cell settling output closely until they begin to diverge after 4 to 8 minutes. Divergence was not due to cell depletion, as no slide contained more than 3000 cells between all of its

printed patterns and no experiment came close to depleting the approximately 100,000 cells located in the column of liquid above the printhead.

With the output profiles of A, B, C, D, and E consistent between experiments E1, E2, and E3, grouping the cell output profiles by previous usage (Table IV) rather than experiment showed three distinct output profiles for the (i) heavily used cartridges (A

and B), (ii) moderately used cartridges (C, D, and E), and (iii) new cartridges (F and G). The heavily and moderately used cartridges had performed previous experiments; they were cleaned and prepped using the Cleaning Method and Experiment Preparation method. Compared to the cell output model in Figure 22, a cartridge's cell output peaks sooner and decreases quicker the more use cycles it has.

Figure 22 shows that the new cartridges followed the settling output model four minutes longer than the other two cartridge groups. The cell settling output model predicted that the output should reach peak concentration after 11 minutes. The output of the new cartridges plateaus at the same time the output of the moderately used cartridges decreases; this suggests that another process was present, independent of the process that affected used cartridges. The output of the heavily and moderately used cartridges suggest that the first process was dependent on damage due to usage or cleaning and occurred 4 minutes after loading while output of the moderately used and new cartridges suggest the second was an aggregation process that occurred after 8 minutes. The sonication step, present in both the Cleaning Method and Experiment Preparation methods, can pit hard materials [76]; sonication could be pitting the surfaces of the cartridge printhead and firing chamber walls, promoting the process of cell attachment, leading to the decrease in cell output. The second process, believed to be cell aggregation, appears to affect bioprinter performance earlier

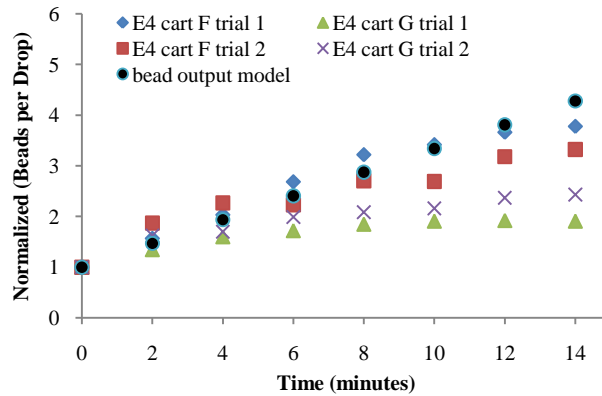


Figure 23- Bead output results of the new cartridges (F and G) to the bead settling output model. The output of both cartridges increased over the entire experiment, in contrast to F and G when printing cells.

(<10 minutes) in these experiments versus experiments using other technologies [4-6] (10 to 20 minutes) because the concentration of our cell suspension was two to three times higher.

Looking at the results of the fourth experiment in Figure 23, in which the new cartridges printed the latex beads, the output of the cartridges continued to rise over the whole experiment. The bead settling model predicted that output would rise until maximum output concentration after 18 minutes. In Figure 23, the output profiles for cartridge G follow the bead settling output model closely. Cartridge F did not conform as well to the model but continued to rise. The results of

the bead settling experiment indicate that the process that caused the output of the new cartridges to plateau around 8 minutes when they printed cells was not present.

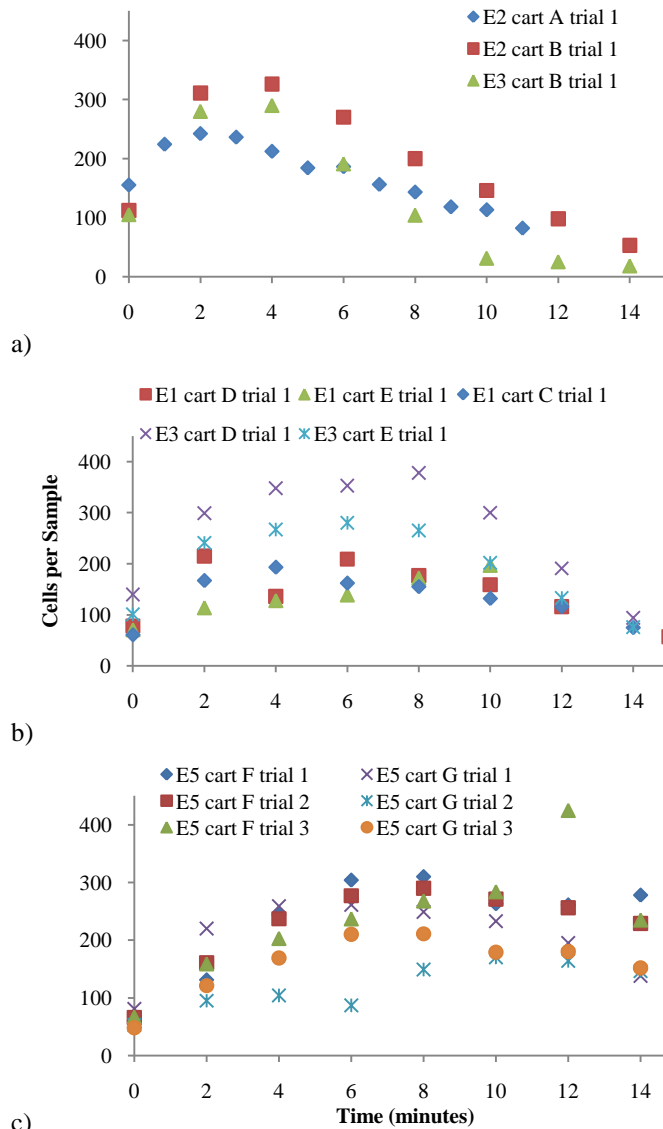


Figure 24 a) Cells per samples profiles of the 3 trials of cartridges A and B. b) cells per sample profiles for cartridges C, D, and E. c) cells per sample for cartridges F and G. The trials of cartridges F and G stayed the closest together over the experiment, i.e. more predictable, versus the other cartridges (negating E5 Cart G trial 2).

In Figure 22, the output profile for the new cartridges performed as predicted until around 8 minutes, as mentioned above. The normalized average output plateaus from six minutes until twelve minutes, during which time 3 to 4 slides of samples containing comparable cell populations could be produced. This productive window is also seen in the raw data of the trials of the new cartridges versus the others, Figure 24. The initial concentration and cell output profiles were more consistent with each other for the new cartridges than those of the heavily and moderately used cartridges.

Bioprinting protocols have been modified to require cartridges with less exposure to sonication than the moderately used cartridges (<2 hours) to attempt to maximize the number of samples with comparable cell populations. The output profiles of the moderately used and new cartridges suggest that 3 to 4 slides of samples containing comparable cell populations can be produced as long as cartridges that have seen similar amounts of moderate use and sonication are paired. Refining the cleaning and preparation methods to use less sonication (< 10 minutes per use versus 25 minutes previously) should improve cartridge performance and increase a cartridge's useful life.

The effects of cell settling and aggregation on printer performance over time should be characterized as a function of cell type and suspension concentration. Once the cell output profile has been found, many adjustments can be made over the course of the experiment to ensure optimal sample creation, e.g. desired cell populations. Consistent cell density in a sample can be maintained over time by adjusting the number of drops deposited per location. The cell output profile indicates how many acceptable samples of a specific pattern can be created. The cell output profile can be used to dictate when reservoir stirring or agitation needs to occur. Ultimately, characterizing cell suspension performance allows for cell settling to be accounted for generating large datasets of samples with comparable cell populations.

4.4 Conclusion

Generating large datasets of patterned co-cultures is an important bioprinter milestone. This work indicates that cell settling is an important factor that must be addressed to achieve this milestone. A simple

cell settling model was shown to predict the effect of particle settling over an initial printing period starting from a uniform concentration. It was also observed that other effects such as cell aggregation or attachment eventually dominated the settling effects on the “cells per drop” behavior. The model is general enough to be adapted to examine cell settling effects in other systems.

Comparing cells per drop over time between three sets of cartridges with varying usage levels showed an inverse relationship between the number of use cycles and conformity to the cell settling output model. The latex bead results showed that the performance decline in the new cartridges was most likely due to some interaction between the cells and less with the cartridge environment. New cleaning procedures minimizing sonication may increase the number of use cycles per cartridges as well as maintain output consistency. Additional discoveries included the fact that the cartridge wiping procedure tended to leave debris in the nozzles, thus the wiping material was changed to lint-free lens wipes (Uvex Safety Inc., Smithfield, RI)

By more fully characterizing the processes of bioprinting, we are now able to estimate the number of cells per drop and compensate for evolution in cell number. This knowledge is necessary to produce the largest number of comparable samples while operating within the time constraints imposed by cell settling and subsequent aggregation.

5 CONCLUSIONS

5.1 *Bioprinter performance vs. BFI prediction*

A metric was proposed to assess the capability of bioprinting technologies to create high resolution patterned co-cultures. The metric could also be used to analyze the affect of different procedures and processes on the printed output. While a number of fidelity metrics could be created, the particular form of the BFI was chosen for several reasons. First, the logic behind using the mask image to classify misplaced cells is intuitive and easy to understand. Second, the BFI is data-centric. That is, it can be computed directly from the pattern specification and an image of the printed pattern, with no further knowledge or assumptions about the printing process. Third, the BFI weights the error rate of a given cell type inversely to area coverage of that type, making the metric sensitive to fine features. Fourth, it can be coupled with a theoretical model which relies on parameters that are technology independent; the system resolution, i.e. pixel size, drop gain, and the drop center offset distribution.

In conjunction with the BFI, a statistical model was introduced that predicts the number of correctly placed cells given the system parameters. Among other insights, the model highlights a tradeoff between a bioprinting system's capability to completely cover a surface and create connected patterns with the probability of misplacing cells in neighboring pixels. This model can be applied to compare performance between or even design other bioprinting systems. The fidelity of printed co-culture samples was measured and compared to the fidelity expected from the model and the values were found to be very close in the best cases. In part, patterning fidelity was shown to depend on cell type in these experiments, with D1 cells maintaining pattern fidelity better than 4T07 cells. Application of the BFI to images of the same sample during different parts of the post-processing procedure showed that the largest source of pattern disruption appeared to occur after bioprinting, during the addition of medium. Application of medium was necessary in order to keep the cells hydrated and viable, but application of the medium washed away many cells, disrupting patterns. In order to maintain both pattern fidelity and cell viability, a set of biomaterials and post-processing techniques should be developed that provide a hospitable environment for cells before

application of bulk medium, promote rapid cell attachment, and do not disrupt the existing pattern. With such procedures in place, the initial fidelity of the samples should be preserved and raise the percentage of correctly placed 4T07 cells closer to the predicted level. While characterizing the system, the drop center distribution was studied for various heights and it was concluded that the cell solutions behaved similarly to ink and that cartridge height could be increased to several millimeters without impacting pattern fidelity.

The Bioprinting Fidelity Index was shown to provide an effective quantitative means of presenting the fidelity of a patterned co-culture pattern for the purpose of analysis and optimization. Its accompanying model was shown to provide a reasonable standard by which to compare the theoretical maximum BFI fidelity with experimental BFI values. The similarity of the D1 fidelity numbers and the model's predicted values suggest good accuracy of our experiments in estimating the model parameters of drop distribution value, σ , and drop-on-substrate diameter, d . The application of the BFI demonstrated that our system does have the capability to create high fidelity patterned co-cultures at biologically relevant length scales.

5.2 *Cell Settling Study*

The ability to create large datasets of high resolution patterned co-cultures that would contain similar numbers of cells between the samples was studied. The first three experiments examined the cell output over time of cartridges that had seen varying amounts of use and sonication. A simple settling model based on Stokes' equation was developed as a guide to predict cell output over time. When the cell output of two new cartridges was compared with the older cartridges it appeared that the cell output peaked sooner and decreased quicker the more uses and cleanings a cartridge had. Latex beads were also printed through the two new cartridges and their cell output profiles tended to increase over the duration of the experiment, suggesting that the plateau in output for the new cartridges when printing cells after eight minutes was caused by some cellular interaction inside the firing chamber.

Future experiments will only use cartridges with less use and exposure to sonication than the moderately used cartridges (<2 hours of sonication) to maximize the number of samples with comparable cell populations. The output profiles of the moderately used and new cartridges suggest that 3 to 4 slides of samples containing comparable cell populations can be produced as long as cartridges that have seen

similar amounts of moderate use and sonication are paired. These samples could be printed between four and ten minutes after cartridge loading. Refining the cleaning and preparation methods to use less sonication (< 10 minutes per use versus 25 minutes previously) will improve cartridge performance and increase a cartridge's useful life.

By more fully characterizing the processes of bioprinting, we are now able to estimate the number of cells per drop and compensate for variations. This knowledge is necessary to produce the largest number of comparable samples while operating within the time constraints imposed by cell settling and subsequent aggregation.

5.3 *Future work*

Extending the capability of the bioprinter to printing more than one sample per slide highlights the deficiencies of the current stage setup. The nonlinearity present in the screw affects the accurate placement of the different layers of a co-culture pattern. In the past, when printing one co-culture pattern per slide, if the calibration location was in approximately the same location as later pattern creation, the nonlinearities of the stage screw would not affect the placement accuracy of the pattern layers. However, by printing three patterns over a 40 millimeter span, at most only 1 of 3 patterns will be aligned. The current calibration algorithm records the distances from the microscope station to each cartridge, the difference in their lengths represents their offset from each other. If the pattern were printed at the same location on the sample platform (i.e.the stage screw), then the pattern layers should align. Assuming the stage backlash is completely compensated for, the motion system nonlinearity guarantees that different locations on the sample platform (and on the stage screw) will yield varying vector lengths (average error of 60 μm in x and y). The error will only get worse as co-cultures are created with more than two solutions. The system is currently capable of printing up to four solutions, provided they can be imaged with the calibration algorithm. The nonlinearity will not affect the printing accuracy if the solution doesn't need to be precisely placed, but administered over all or part of a pattern.

The studies in this work have sought to characterize the external and internal processes associated with the creation of high fidelity patterned co-cultures. The current bioprinting system is capable of reliably printing patterns with details on the order of 160 μm (or $2 * 84.7 \mu\text{m}$), which is sufficient for most patterns but not for very fine details. The first study demonstrated that fidelity will be most immediately increased through development of improved post-processing methods. Investigating these new post-processing methods would be one of the best ways to exploit the high throughput nature of this system demonstrated in the cell settling studies. The data analysis tools generated from the cell settling studies can be implemented to process images quicker in future characterization studies, such as those finding improved post-processing methods. As previously stated, the BFI metric will aid in the analysis of these new post-processing methods and provide a clear indication of the effects of proposed post-processing techniques on pattern reproduction. With high fidelity and high throughput, this bioprinter should be able to be used to create improved *in vitro* models of cell-cell interactions and support the study of cell-cell signaling and other cell behaviors.

6 RECOMMENDATIONS

- The motion system of the bioprinter should be upgraded to one that exhibits the backlash or screw nonlinearity below the current system. Variation below 5 μm for backlash and below 5 μm for the screw nonlinearity over a six inch distance would be desirable. Upgrading will improve calibration and pattern alignment.
- With the current Anaheim Automation motion system and its the backlash issues, all images should be printed in pieces that are 50 rows high. If the current **print** function is used, images larger than 50 pixels will need to be broken up into multiple prints. However, the **print** function should be able to be easily modified to only print from one side and preserve backlash compensation.
- The error introduced by the screw nonlinearity is going to become more prevalent as more solutions are used and the sample has to travel farther to be printed on by the other cartridges.
- A cell counting algorithm similar to that used in section 4.2.1 needs to be developed to analyze the patterned co-cultures and generate data for the BFI metric. This would save many hours and the results should be just as accurate as hand counting, but with much less time required.
- Improved post-processing methods to improve long term pattern fidelity, as in section 3.1.3, need to be developed. Their effectiveness can be measured by the BFI
- When using the BFI to compare two different bioprinting systems with a specific pattern, it is important that the ratio of drop gain to pixel size be similar.
- The standard deviation of the drop center offset distribution (section 3.1.2) and the bioprinter's output over time (section 4.2.1.2) should be characterized whenever a solution significantly different (subjective) in viscosity, cell concentration, or cell size from the solutions used in this thesis is used in the bioprinter.
- Cartridges with similar use cycles and sonication exposure should be paired to ensure the cell output profiles between the cartridges are similar.

- Cartridges that been cleaned and used in seven or more experiments should be retired to keep the cell output profiles consistent over time
- Studies should be run that more accurately characterize the effects of sonication on the cell output profile a cartridge while bioprinting. This could be done by printing latex beads (section 4.2.2) through cartridges of various use cycles

A APPENDIX

A.1 BFI Model Derivation

The ultimate goal of the bioprinter is to correctly place every cell and generate a patterned co-culture with perfect fidelity. Every misplaced cell decreases pattern fidelity. Examining the masked image results from the co-culture patterning experiment (section 3.2.2) showed many of the misplaced cells were located very close to their intended location. This led to the hypothesis that the printed drops may have been correctly placed but that the cells were misplaced because the drop gain for the system was larger than the 85 um pixel size. This means that as long as the drop gain is larger than the intended pixel size, a bioprinter will never achieve perfect fidelity and cells would always end up misplaced.

The statistical model presented in section 3.2.2 was meant to be an accompaniment to the BFI. Since there is an element of randomness present between where a drop lands and its intended pixel when every bioprinter deposits a drop on a substrate, this model attempts to estimate how that drop center offset distance, specific system resolution, and the drop gain combine to affect the overall fidelity of a pattern. The greater the drop center offset, the more area of a drop overlaps the areas of neighboring pixels. This increases the probability that the cell(s) in that drop are going to be misplaced. The model predicts the maximum achievable BFI for a specific system with a specific pattern based on these three basic criteria: system resolution (pixel size), drop gain, and the drop center offset distribution (see sections 3.2.1 & 3.2.2).

A.1.1 Numerical Studies

A MatLab program was written to find the different areas associated with varying the distance of the drop center offset; these areas correlate with differing probabilities of drop misplacement. Assuming a pixel has side length, L , a square point cloud with side length, $L\sqrt{2}/2$, was created with equally spaced points. A circular point cloud was selected from within that cloud with 3.5 million points with radius $L\sqrt{2}/2$. This radius was chosen because it was the smallest radius that completely covers the pixel area. The circular point cloud was shifted along the circumferences of a set of ever larger concentric circles with their center around the pixel center (Figure 17a). A snapshot was taken of the point cloud at various locations

around these circles and the points that fell outside the pixel boundaries and into neighboring pixels were recorded. In the context of a pattern, each pixel is surrounded by eight neighboring pixels; these neighbors can be sorted into edge neighbors or corner neighbors. For each set of snapshots associated with a particular concentric circle, the average areas that fell into the edge neighbors, the corner neighbors, and the center pixel were recorded. These areas were made into graphs (Figure 17c & d) and show how the probability of misplacing a cell increases with the increase in the drop center offset, d . This distance is contained within the set D , which is composed of a set of concentric circles whose radii is d . D represents all possible locations for the drop center. These graphs in Figure 17c & d represent

$$(6) \quad P(\text{misplaced cell in neighbor } i | D = d), \text{ with } \textit{neighbor} = \textit{edge} \text{ or } \textit{corner}.$$

A.1.2 Modeling the drop center offset

The way in which in the drop center offset, d , varies, was modeled by a 2-dimensional Gaussian random variable. Due to the symmetry of the problem (Figure 17a), the actual x y coordinates of the drop offset vector, d , were not as important as its length. This is the reason why the drops in the numerical studies were shifted along the radii of concentric circles. The following section will explain how a change of variables was performed to the general multivariate two-dimensional Gaussian equation (7) to create a radially symmetric Gaussian equation (12):

$$(7) \quad f_x(x) = \frac{1}{(2\pi)^{|K|^{1/2}}} \exp\left(-\frac{1}{2}(x-\mu)^T K^{-1}(x-\mu)\right)$$

For (7), the general multivariate two-dimensional Gaussian equation, $x = \begin{bmatrix} X \\ Y \end{bmatrix}$ and $\mu = \begin{bmatrix} \mu_x \\ \mu_y \end{bmatrix}$, with

$K = \begin{pmatrix} \sigma_{xx}^2 & \sigma_{xy} \\ \sigma_{xy} & \sigma_{yy}^2 \end{pmatrix}$. In the drop distribution study, section 3.1.2, all of the data points were reported as

offsets from the camera center, we set $\mu = \begin{bmatrix} 0 \\ 0 \end{bmatrix}$. In the data analysis, section 3.2.1, singular value

decomposition (SVD) was used to find two orthogonal vectors that point along the major and minor axes of the drop center offset distribution, whose lengths, σ_x and σ_y , represent the one standard deviations. The

observed distributions are not quite radially symmetric, i.e. they have different standard deviation lengths, so they are compared on the basis of $\bar{\sigma} = \sqrt{\sigma_x \sigma_y}$, which is the standard deviation of the radially symmetric Gaussian distribution that has the same determinant of the covariance matrix as the original asymmetric distribution. Since the major and minor axes are orthogonal to each other, their covariance is zero, making

$$K = \begin{pmatrix} \sigma_{11}^2 & 0 \\ 0 & \sigma_{22}^2 \end{pmatrix} = \begin{pmatrix} \bar{\sigma}^2 & 0 \\ 0 & \bar{\sigma}^2 \end{pmatrix} = \bar{\sigma}^2 I. \text{ Substituting } K \text{ and } \mu \text{ into (7) yields:}$$

$$(8) \quad f_x(x) = \frac{1}{(2\pi)\bar{\sigma}^2} \exp\left(-\frac{1}{2\bar{\sigma}^2} x^T x\right) \text{ substituting } K^{-1} = 1/\bar{\sigma}^2 I$$

Once again, since the probabilities of cell misplacement changes with the length of the vector d , a change of variables needed to be made, such that $f_x(x) \xrightarrow[\substack{D=\|x\| \\ d=\|x\|}]{\rightarrow} f_D(d)$. To perform this change of variables on (8),

the following properties were utilized:

$$(9) \quad f_D(d) = \frac{dF_D(d)}{dd} = \lim_{\delta d \rightarrow 0} \frac{F_D(d + \delta d) - F_D(d)}{\delta d} = \lim_{\delta d \rightarrow 0} \frac{P(D \leq d + \delta d) - P(D \leq d)}{\delta d}$$

Where $f_D(d)$ is the probability density function and $F_D(d)$ is the cumulative distribution function, $F_D(d) = P(D \leq d)$. The quantity $P(D \leq d)$ is represented by the volume of the cylinder with radius, d , underneath the surface, $f_x(x)$. The rightmost expression of $f_D(d)$ in (9) can be

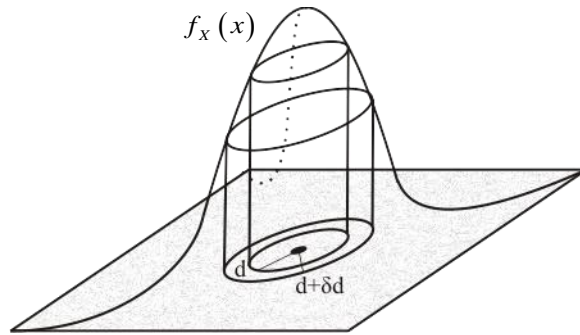


Figure 25 - Two dimensional Gaussian distribution

described as the difference in volume between two cylinders of radii, d and $d + \delta d$ (Figure 25). As the limited is evaluated in that expression in (9),

$$\begin{aligned}
(10) \quad f_D(d) &= \lim_{\delta d \rightarrow 0} \left(\frac{[2\pi(d + \delta d)^2 - 2\pi d^2]}{\delta d} f_X(d) \right) \\
&= \lim_{\delta d \rightarrow 0} \left(\frac{[2\pi(d^2 + 2\delta dd + \delta d^2 - d^2)]}{\delta d} f_X(d) \right) \\
&= \lim_{\delta d \rightarrow 0} \left(\frac{2\pi\delta dd + \delta d^2}{\delta d} f_X(d) \right)
\end{aligned}$$

$$\begin{aligned}
(11) \quad f_D(d) &= 2\pi d (f_X(d)) \\
&= 2\pi d \left(\frac{1}{2\pi\bar{\sigma}^2} \exp\left(-\frac{1}{2\bar{\sigma}^2} d^2\right) \right), \text{ substituting from (8)}
\end{aligned}$$

After simplification,

$$(12) \quad f_D(d) = \frac{d}{\bar{\sigma}^2} \exp\left(-\frac{1}{2\bar{\sigma}^2} d^2\right)$$

Dimensionless variables were used to further simplify equation (12), these were made by dividing by the side length of a pixel (system resolution), L , creating: $\hat{D} = D/L$, $\hat{d} = d/L$, and $\hat{\sigma} = \bar{\sigma}/L$, giving:

$$(13) \quad f_{\hat{D}}(\hat{d}) = \frac{\hat{d}}{\hat{\sigma}^2} \exp\left(-\frac{1}{2\hat{\sigma}^2} \hat{d}^2\right)$$

Equation (13) provides the probability that a drop offset will be a certain distance, \hat{d} , given the standard deviation of the solution, $\hat{\sigma}$.

A.1.3 Using the model to predict the maximum BFI

With the equation for the distribution of the drop center offset calculated, the probability of a misplaced cell in a certain pixel printed with a solution with a known drop offset distribution was calculated by combining (6) with (13) to yield:

$$(14) \quad P(\text{misplaced cell in neighbor } i) = \int_0^{\infty} P(\text{misplaced cell in neighbor } i | \hat{D} = \hat{d}) f_{\hat{D}} \hat{d} \, d\hat{d}$$

Equation (14) was used to create a stencil which displays the placement probabilities (Figure 17e), where each entry is the probability of a cell being placed in the corresponding pixel, given that a drop is printed to the center pixel. By laying the stencil over a pattern to be printed, one can predict the probability that a misplaced cell is actually incorrectly placed and will cause a loss in fidelity, i.e. that a cell of one type will be placed in a pixel of another cell type (Figure 17f). The stencil is moved to each pixel in the pattern to compute the probability for incorrectly-placing a cell from that pixel. The error probability of all pixels of a specific cell type were averaged to predict the error for that cell type in the pattern, e_i , used in (15). When analyzing different patterns, it is easy to see that the number and arrangement of the pixels is important in determining the error, e_i . Patterns with a larger occurrence of alternating-type pixels, i.e. a higher complexity, will have a larger probability for misplaced cells than those which have large areas of the same cell type.

Now that a theoretical error probability (BFI value) for a specific pattern printed with a certain solution can be found using the system and solution specific stencil, a comparison could be made with the actual printing performance of the bioprinting system.

An explanation of the bioprinting fidelity index (BFI) is repeated for completeness. Remember, the first step in computing the BFI is taking the original pattern and using it as a mask by stretching and scaling it according to the size of the patterned co-culture image (section A.4.1). This mask will aid in finding both the number and type of incorrectly placed cells and the number and types of pixels in the patterned co-culture image. Specifically, the BFI for a printed sample is defined as

$$(15) \quad BFI = \sum_{i=1}^m w_i (1 - e_i),$$

with $w_i = (p_{tot} - p_i) / ((m-1)p_{tot})$ and $e_i = \tilde{n}_i / n_i$, where m is the number of cell types, p_{tot} is the total number of pixels in the specified pattern, p_i is the number of pixels of cell type i , \tilde{n}_i is the number of incorrectly placed cells of type i , and n_i is the total number of printed cells of type i . Note that e_i is the fraction of incorrectly placed cells of type i , while $(1 - e_i)$ is the fraction of correctly placed cells of type i

. From the second expression in (15), the BFI can be interpreted as a weighted average of the fractions of correctly placed cells of each type, each weighted by the fraction of pixels of all other cell types. The closer the BFI is to 1.0, the higher the number of cells that were correctly placed.

A.2 *H/W Section*

A.2.1 *Driver Board Details*

The following two sections contain the design details and validation of the cartridge driver board performed by Justin Mattimore [69].

A.2.1.1 *Cartridge Driver Board Design*

The driver circuit is designed around a 24V supply. A TD62003 package consisting of seven NPN Darlington transistors is used to turn on the nozzle resistors. Specifically, the AFG model was chosen, which allows the Darlington transistors to be driven with TTL level inputs. The TD62003 is capable of sinking the necessary 0.5A of current which must flow through the nozzle resistor. Similar to Hewlett-Packard (HP; Hewlett-Packard Company, Palo Alto, CA) design, a current limiting resistor R_{source} , is placed in series with each quadrant common in order to minimize variations in energy delivered due to thermal fluctuations and manufacturing tolerance of the thin film resistors [77]. After accounting for the saturation voltage of the NPN transistor, the model (see Figure 26 Left) for the nozzle energy is

$$(16) \quad E = \frac{(V_{cc} - V_{R_{source}} - V_{sat})^2}{R_{tf}} t_{fire} .$$

Using the model in (16) and $V_{sat} = 0.7V$ a current limiting resistor R_{source} of 14.7Ω must be placed in series with the nozzle resistor to limit current and deliver $17.2\mu J$ to the nozzle.

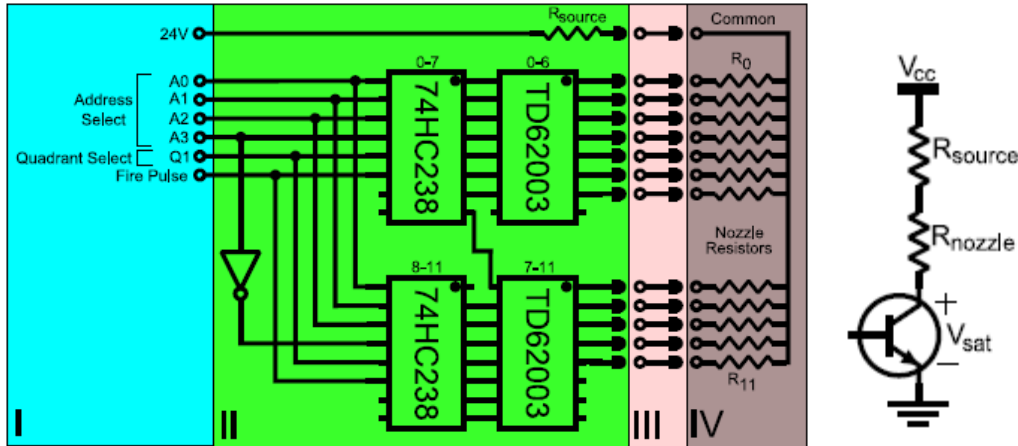


Figure 26 – Left) Quadrant schematic, quadrants 2-4 similar. I – External inputs. II – Custom driver board. III – Flex cable. IV – HP26 cartridge. Right) individual nozzle transistor model

A 4-to-16 decoder is assembled from two 3-to-8 decoders with three I/O lines (A0-A2) to select address 0-7 on each decoder and a fourth I/O (A3) line to select either low decoder or high decoder (see Figure 26a). For each decoder there are two additional chip enables, one active high and the other active low. The active low enable serves as a quadrant select (Q1-Q4) which allows any combination of the four quadrants to be selected during a fire event for a given nozzle address. The active high input is used fire the nozzles when a fire event is commanded. The length of time the active high enable (fire pulse) is enabled determines the amount of time the nozzle resistor is energized. The length of the high enable pulse should roughly be $2\ \mu s$, longer ‘on’ times will result in reduced cartridge life or damage.

In summary, this interface board design has eight input lines to select a nozzle, an appropriate short duration pulse source to control the firing of the nozzle, and power supply connection for 5V and 24V (20W). Control of the driver board can be realized through use of a microprocessor or any general purpose I/O controller attached to a PC.

The PCB is designed to ensure signal integrity. First, consideration was given to ensure that the PCB did not have to be designed considering transmission line effects. The propagation time P_t of any signal on the PCB must be less than one half the rise time of the signal t_r , $P_t < 0.5t_r$. If a trace violates this rule of thumb, then that trace is considered to be electrically long [78]. The propagation time P_t is found as $P_t = \frac{l}{v_p}$, in which v_p is the phase velocity and l is the length of the trace.

The fastest rise time on the board is the output of the 3-to-8 decoder which has a measured value of 10ns and an approximate trace length of 15mm, the resulting length to phase velocity ration is an order of magnitude smaller than half the rise time. The NPN Darlington transistor connection to the nozzle resistor through the flex cable has the longest length of 0.61m with a measured rise time of 40ns to turn the transistor on, the propagation time is much smaller than half the rise time.

Application of the test, $P_t < 0.5t_r$, indicates no traces are electrically long, and thus a high frequency PCB is not required.

The second consideration is to ensure adequate decoupling of components. First, bulk capacitors are selected to decouple the power bus from the PCB. The PCB requires 24V for a cartridge supply and 5V for on-board logic such as the 3-to-8 decoders. A noise margin of 0.25V is

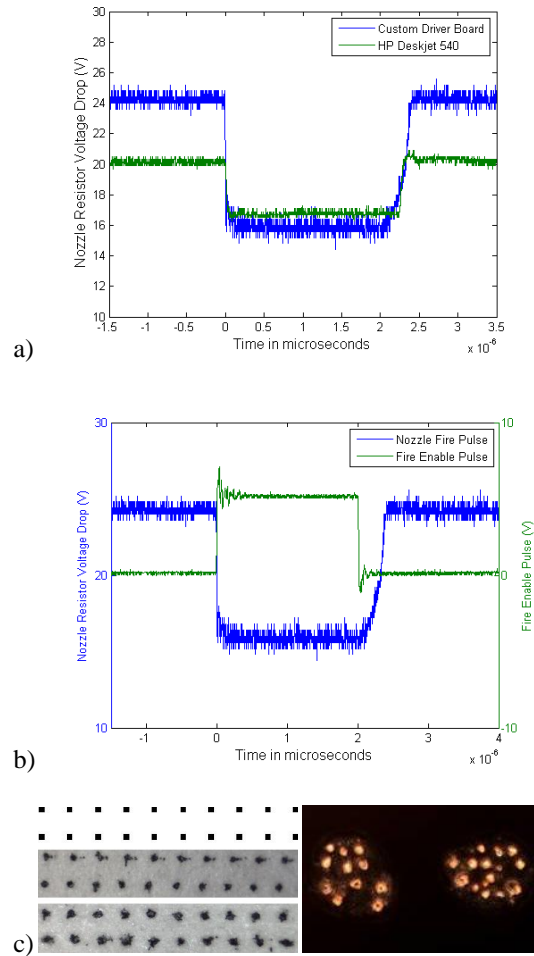


Figure 27 – a) Voltage drop across a nozzle resistor during firing, comparison of the custom driver board and the HP Deskjet 540 shown.

b) Comparison of fire pulse and drop across nozzle resistor. Note the dual ‘y’ scale

c) Left - Original image (top), HP540(middle), driver board (bottom). Right - Two drops of cellular bio-ink printed using the custom driver board (100x magnification).

allocated to the 24V supply rail. A value of $173\mu\text{F}$ is calculated [79] which is close to the $180\mu\text{F}$ decoupling capacitor found in the HP 540. A final value of $220\mu\text{F}$ is used due to availability and to ensure that the noise margin is met. Two bulk decoupling capacitors for the 5V supply rail are located at slightly different parts of the board placing them in parallel thus shifting the resonant frequency up 6dB which increases decoupling performance over the frequency band [79].

The integrated circuits require additional decoupling capacitors for high frequency events such as ground bounce. When logic gates change state both of the mosfets composing the gate are on at the same time causing ground to be pulled up and the supply to be pulled down [78]. The physical placement of the capacitors is important as long traces increases inductance and connection to power planes [78] are affected by flux around the via [80]. The custom driver board consists of four layers, the outer two layers are signal layers while the inner layer close to the top layer is a 5V power plane and the other inner layer is a return plane. The power and return planes were placed close together to maximize the interplane capacitance and to reduce inductance [78]. For any high frequency decoupling capacitor placed on the top layer, the capacitor is connected directly to the ground pin of the IC.

For capacitors that must be located on the bottom layer due to space constraints, the via which connects the decoupling capacitor to the ground plane is not directly connected to the device pin. Instead, the decoupling capacitor is connected to a via which is adjacent to the via connecting the ground pin of the device to ground. When the device needs power it begins drawing energy from the ground plane, at the same time the inductive coupling between the traces causes a current to be forced into the ground plane from the decoupling capacitor thus reducing the amount of energy actually drawn from the ground plane preventing ground bounce [81].

A.2.1.2 Validation and Performance

The performance of the driver board was confirmed in two ways. First, the firing waveform observed across the nozzle resistor generated by the custom driver board was compared to the original HP waveform. Second, the quality of the printed ink drops was compared to the original system.

Signal quality of the eight address lines (A0-A3, Q1-Q4), fire pulse and TTL signal driving the Darlington transistors was confirmed during state transition; a 1.28V bounce is observed to be damped in 118ns. The ground plane of the driver board experiences no detectable bounce with respect to both the power supplies and the Quanser (Quanser Corp., Ottawa, ON, Canada) Q8 data acquisition card.

An HP Deskjet 540 printer equipped with an HP26 cartridge was commanded to print. While printing, the voltage drop across the nozzle resistor and drive transistor was observed and the energy delivered found to be 17.2 μ J. Similarly the custom driver board was commanded to print while the drop across the nozzle resistor and drive transistor was recorded (Figure 27a). Comparing the original HP printer waveform with the waveform produced by the custom driver board reveals the firing event closely resembles the original (Figure 27b). The fire pulse delivered to the nozzle resistor has no bounce. It should be noted that the duration of the fire pulse is consistently 350ns longer than what is requested. The switching time of the transistor accounts for 110ns, however, the remainder has not been accounted for. The total energy delivered to the nozzle is 15.87 μ J which compares with the goal of recreating the original HP amount of 17.2 μ J. It should be noted that compensation for energy delivered to the nozzle may be accounted for through manipulation of the fire pulse period.

Print quality is validated by printing an image (Figure 27c, left, top) with an original HP 540 and the custom driver board. Comparing the sample printed by the HP 540 (Figure 27c, left, middle) and the custom HP26 driver (Figure 27c, left, bottom) the results are favorable and expected. Both samples contain drops with shape irregularities. The similarity of the drops indicates the custom driver board is producing a correct drive signal. Figure 27c also shows the board printing a cell solution containing D1 murine mesenchymal stems suspended in media at a concentration of 7.7e6 cells per milliliter (Figure 27c, right).

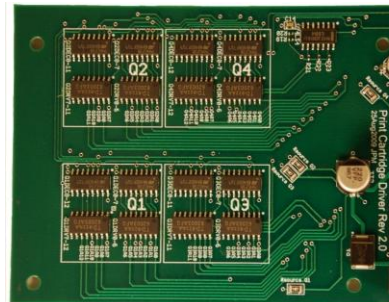


Figure 28 - Custom driver board.

A.2.1.3 Cell Delivery Station Mount

Also at the rear, the Cell Delivery Station is attached to a Newport 423 low-profile linear stage with 1" travel (Newport Corp., Irvine, CA). A Newport Rod Clamp (340-RC) suspends the station above the sample platform by clamping onto a 12" tall stainless steel rod with 1.5" diameter attached to the breadboard.

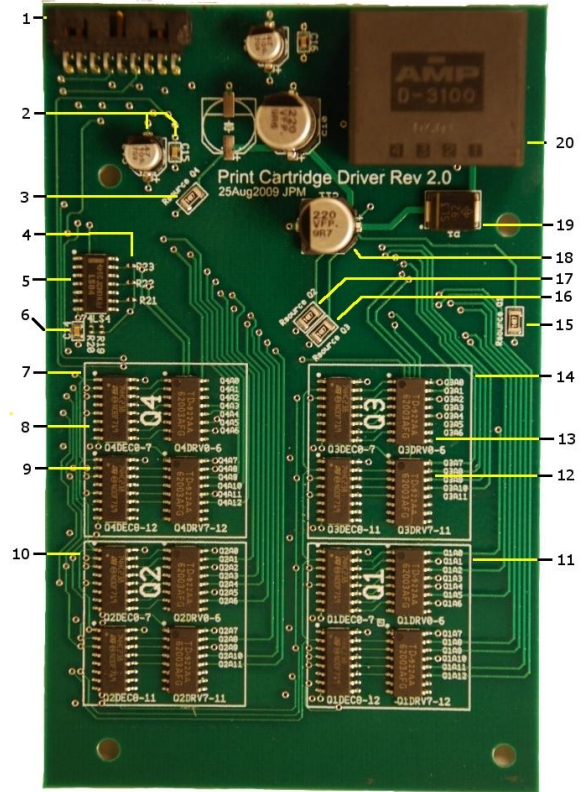
A.2.1.4 Microscope Station Mount

The camera and lens are mounted using a Meiji (Meiji Techno America, Santa Clara, CA) course/fine focus block which is mounted to a 19mm diameter post via a set screw. This 19mm post expands to $\frac{3}{4}$ " diameter and is threaded through an Edmund Optics (Edmund Optics Inc., Barrington, NJ) 90° angle mount. Another angle mount and 2 more stainless steel posts, 12" and 15" respectively, allow the entire station to be affixed to the breadboard using a $\frac{3}{4}$ " post breadboard adapter. This setup allows the position of the camera to be changed, if required, with respect to the Cell Delivery Station and then held using a series of set screws. Care must still be taken around the Microscope Station as it can be slightly moved by a careless arm movement.

A.2.1.5 Driver Board Part Identification

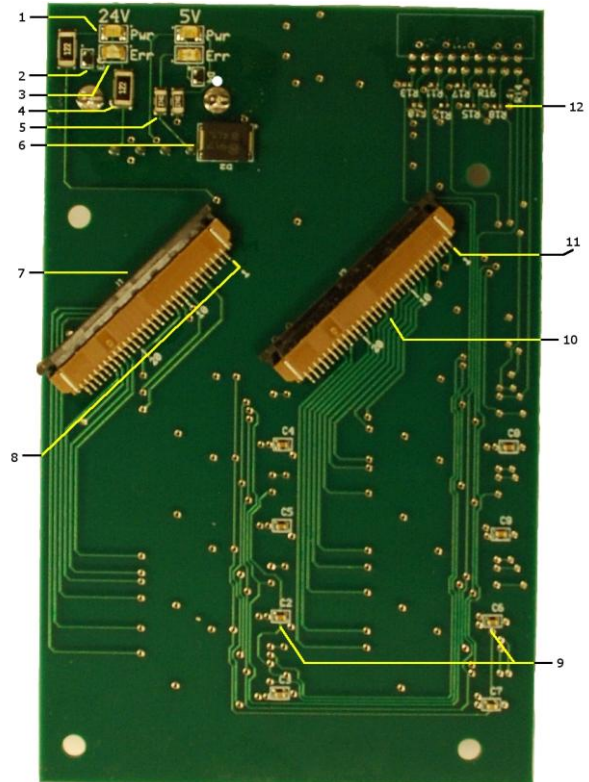
Board - Top Part Identification:

1. Data Connector
2. 5V Power bus decoupling caps:
 - 47 μ F electrolytic is for low frequency,
 - 22nF ceramic is for high frequency.
3. Quadrant 4 source resistor
4. Hex inverter unused input pull down resistor
5. Hex inverter
6. Hex inverter decoupling capacitor
7. Quadrant 4
8. Quadrant lower decoder
 - (0-7; similar for all quadrants)
9. Quadrant upper decoder
 - (8-12 for Q4, Q1; 8-11 for Q3, Q2)
10. Quadrant 2
11. Quadrant 1
12. Quadrant upper darlington driver
 - (7-12 for Q4, Q1; 7-11 for Q3, Q2)
13. Quadrant lower darlington driver
 - (0-6; similar for all quadrants)
14. Quadrant 3
15. Quadrant 1 source resistor
16. Quadrant 3 source resistor
17. Quadrant 2 source resistor
18. 24V power bus decoupling
19. 24V rail Schottky diode
20. Power connector



Board - Bottom Part Identification:

1. 0.5 Lumen LED good 24V PWR indicator
2. ERR LED series Diode
3. .5 Lumen LED
 - incorrect 24V PWR indicator
 - (polarity reversed)
4. Current limiting resistor (1.2k Ω)
5. Current limiting resistor (274 Ω)
6. 5V rail Schottky diode
7. Ribbon Cable connector (J1)
 - for data/pwr
8. Pin 1 of J1 Data connector
9. Decoupling caps (0.022uF)
10. Ribbon Cable connector (J2)
 - for data/pwr
11. Pin 1 of J2 Data connector
12. Pull up/down resistor (10k Ω)



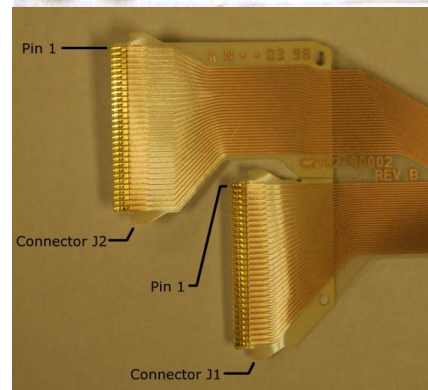
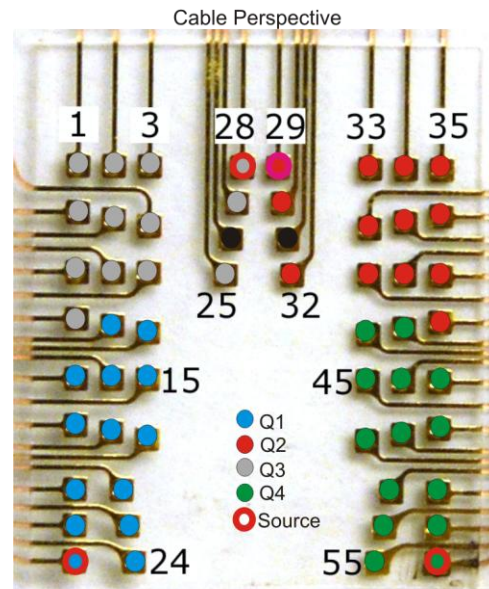
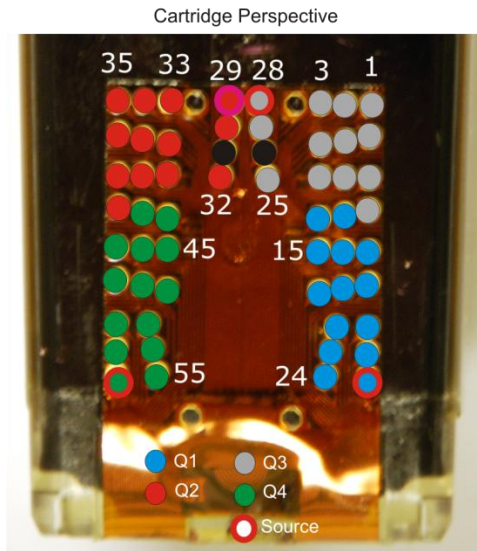
A.2.1.6 Driver Board Parts List

Driver Board Parts				
Part Name / Description	Part Description	Digikey Part#	Qty	Schematic ID
LED diode	DIODE SCHOTTKY 30V 200MA 0603	641-1008-1-ND	2	
5V Pwr Bus Decoupling	CAP ELECT 47UF 10V VS SMD	PCE3875CT-ND	2	C13, C1
24V Pwr Bus Decoupling	CAP 220UF 35V ELECT FP SMD	PCE4444CT-ND	3	C12, C10, C11
Power conn; board mount	CONN HDR 4POS R/A KEY-Y 30GOLD	A29446-ND	1	J5
data conn; board mount	CONN HEADER 18POS 2MM R/A GOLD	WM18865-ND	1	J4
				R11, R12, R14, R13, R15, R16, R17, R18, R10, R19, R20, R21,
pull up/down resistor	RES 10K OHM 1/10W 5% 0402 SMD	P10KJCT-ND	14	R22, R23
current limiting res for 5V LED	RES 274 OHM 1/4W 1% 1206 SMD	P274FCT-ND	2	R6, R5
current limiting res for 24V LED	RES 1.2K OHM 1/2W 5% 2010 SMD	541-1.2KWCT-ND	2	R7, R8
red LED	LED 3.2X1.6MM 635NM RED CLR SMD	754-1165-1-ND	2	24VRedLED, 5VRedLED
green LED	LED 3X1.5MM 525NM GN WTR CLR SMD	754-1115-1-ND	2	24VGrnLED, 5VGrnLED
				Q1DRV8, Q1DRV812, Q3DRV8, Q3DRV811, Q2DRV8, Q2DRV811,
darlington driver IC	IC DRIVER DARL SNK TTL 7CH 16SOP	TD62003AFGCT-ND	8	Q4DRV7, Q4DRV812
				C15, C16, C8, C9, C6,
decoupling capacitor	CAP .022UF 50V CERAMIC X7R 0603	399-1280-1-ND	11	C7, C4, C5, C2, C3, C14
source resistor	RES 14.7 OHM 1/4W 1% 1206 SMD	P14.7FCT-ND	4	R4, R2, R3, R1
30 pin ribbon cable connector	CONN FPC/FFC 30POS 1MM R/A SMD	609-1926-1-ND	2	J1, J2
Hex inverter	IC HEX INVERTER 14-SOIC	296-1628-5-ND	1	74LS4
				Q1DEC8, Q1DEC812, Q3DEC8, Q3DEC811, Q4DEC812, Q4DEC7,
3-8 decoder	IC DECODER 3 TO 8 LINE 16-SOIC	497-1800-1-ND	8	Q2DEC8, Q2DEC811
5v rail diode	DIODE SCHOTTKY 10V 4A SMC	MBRS410LT3GOSCT-ND	1	D2
24v rail diode	DIODE SCHOTTKY 4A 30V SMC	SL43-E3/57TGICT-ND	1	D1
Cable Parts				
Part Name / Description	Part Description	Digikey Part#	Qty	Schematic ID
Power conn; cable termination	CONN RECEPT 3.81 4POS KEY-Y	A29424-ND	1	
crimp terminals for pwr cbl termination	CONN RCPT 14-16AWG CRIMP TIN	A29303-ND	4	
data conn; cable termination	CONN HOUSING 2MM 18POS POLARIZED	WM18049-ND	1	
crimp terminals for data cbl termination	CONN TERM FEMALE 24-30AWG CRIMP	WM1128-ND	18	

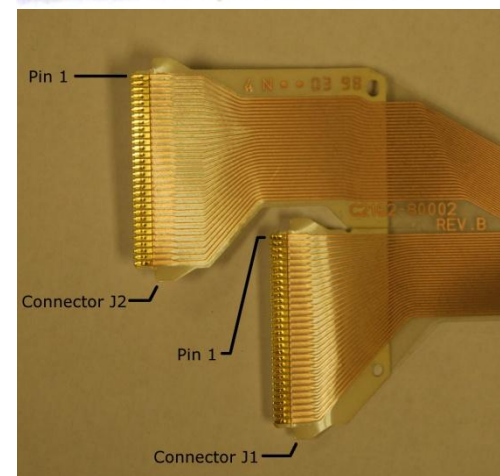
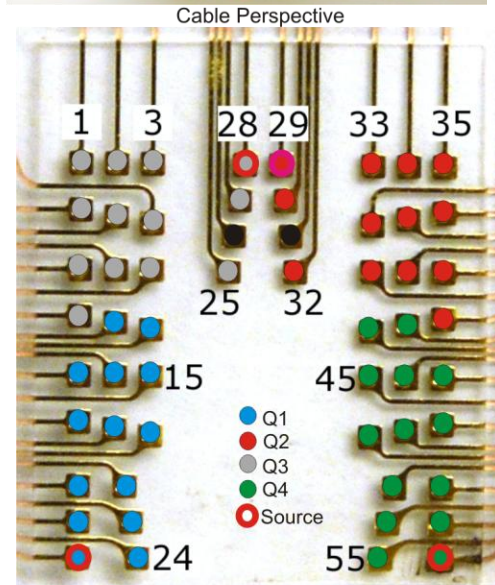
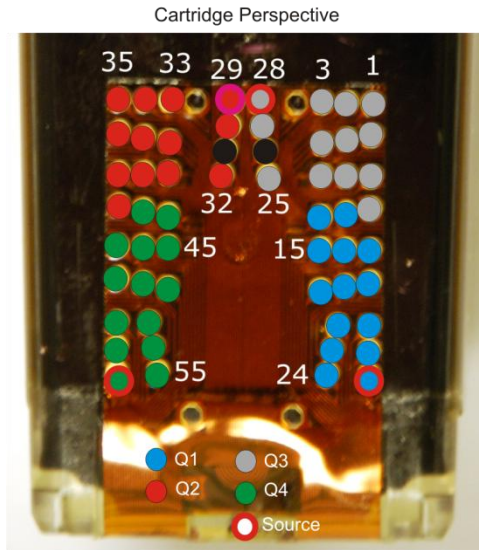
A.2.2 HP26A diagrams

A.2.3 Board pinout to HP26 nozzle table

Cartridge / Ribbon Cable / Driver Board Pinout				
Cartridge	Nozzle	Driver Board	Connector	Catridge Pin
Pin #	Address	Connector	Pin	Function
1	Q3 A7	J1	5	Group R3
2	Q3 A8	J1	4	Group R3
3	Q3 A9	J1	3	Group R3
4	Q3 A6	J1	7	Group R3
5	Q3 A5	J1	8	Group R3
6	Q3 A4	J1	6	Group R3
7	Q3 A1	J1	10	Group R3
8	Q3 A2	J1	9	Group R3
9	Q3 A3	J1	11	Group R3
10	Q3 A0	J1	12	Group R3
11	Q1 A12	J1	13	Group R1
12	Q1 A11	J1	14	Group R1
13	Q1 A8	J1	16	Group R1
14	Q1 A9	J1	15	Group R1
15	Q1 A10	J1	17	Group R1
16	Q1 A7	J1	18	Group R1
17	Q1 A6	J1	19	Group R1
18	Q1 A5	J1	20	Group R1
19	Q1 A1	J1	22	Group R1
20	Q1 A2	J1	21	Group R1
21	Q1 A0	J1	24	Group R1
22	Q1 A3	J1	23	Group R1
23	Source	J1	26	Source for R1
24	Q1 A4	J1	25	Group R1
25	Q3 A10	J1	2	Group R3
26		J1	1	Catridge ID

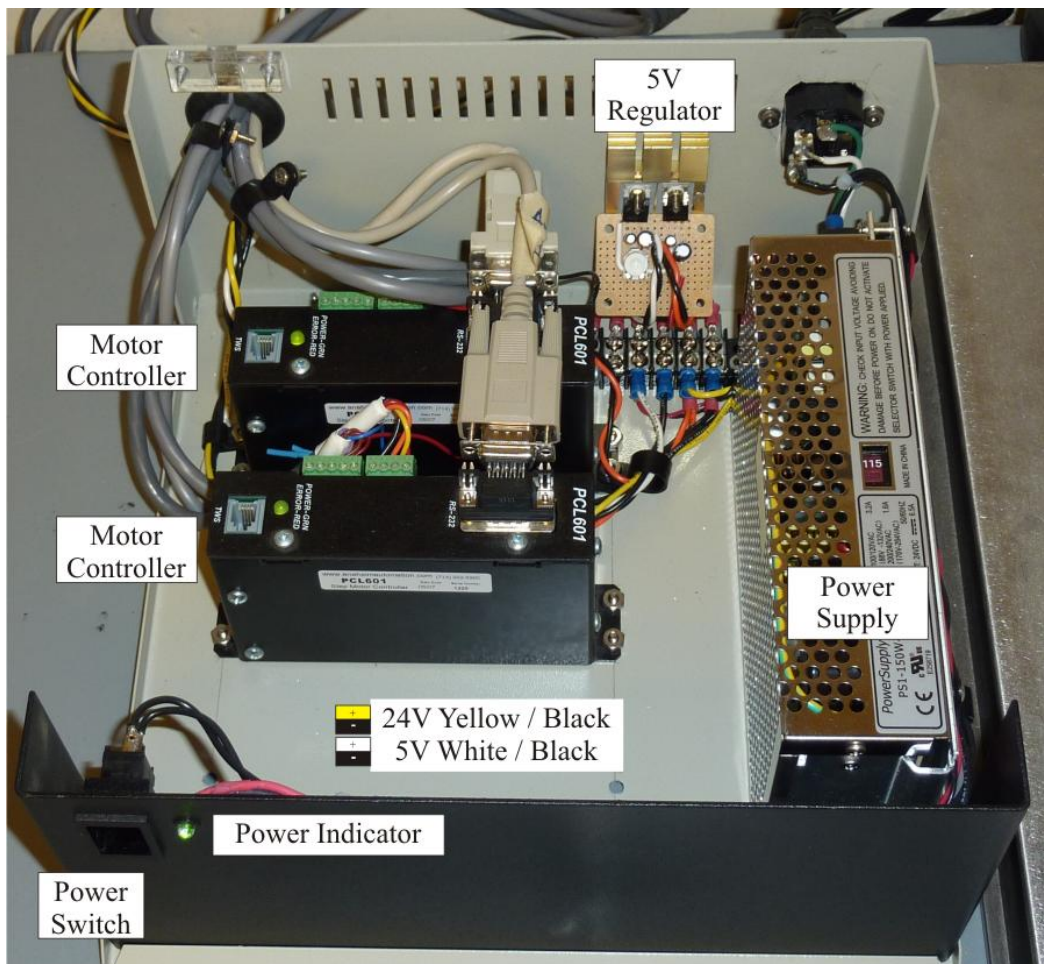


Cartridge / Ribbon Cable / Driver Board Pinout				
Cartridge	Nozzle	Driver Board	Connector	Catridge Pin
Pin #	Address	Connector	Pin	Function
27	Q3 A11	J2	30	Group R3
28	Source	J2	28	Source for R2
29	Source	J2	29	Source for R3
30	Q2 A11	J2	27	Group R2
31		J2	26	Catridge ID
32	Q2 A10	J2	25	Group R2
33	Q2 A9	J2	24	Group R2
34	Q2 A8	J2	23	Group R2
35	Q2 A7	J2	22	Group R2
36	Q2 A4	J2	21	Group R2
37	Q2 A5	J2	19	Group R2
38	Q2 A6	J2	20	Group R2
39	Q2 A3	J2	16	Group R2
40	Q2 A2	J2	18	Group R2
41	Q2 A1	J2	17	Group R2
42	Q4 A11	J2	13	Group R4
43	Q4 A12	J2	14	Group R4
44	Q2 A0	J2	15	Group R2
45	Q4 A9	J2	10	Group R4
46	Q4 A8	J2	12	Group R4
47	Q4 A10	J2	11	Group R4
48	Q4 A5	J2	7	Group R4
49	Q4 A6	J2	8	Group R4
50	Q4 A7	J2	9	Group R4
51	Q4 A0	J2	6	Group R4
52	Q4 A2	J2	5	Group R4
53	Q4 A4	J2	4	Group R4
54	Q4 A4	J2	3	Group R4
55	Q4 A1	J2	2	Group R4
56	Source	J2	1	Source for R4

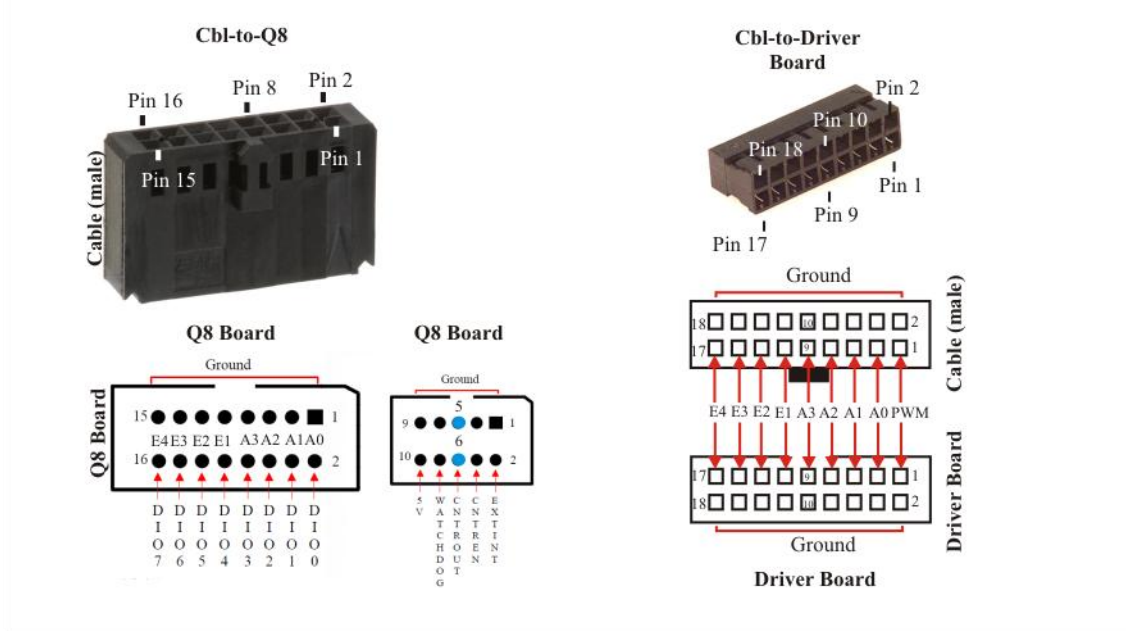


A.2.4 Power supply

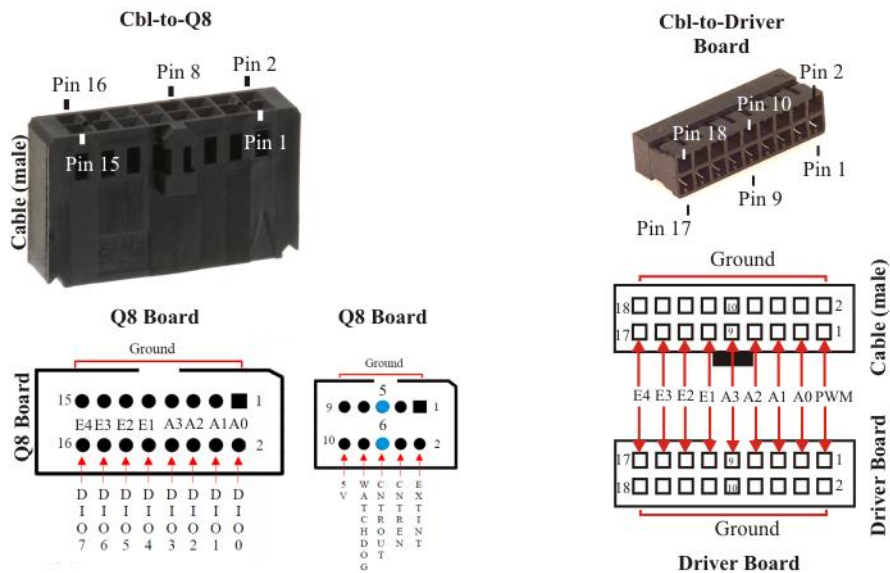
The power for the Cell Delivery Station and Motion System of the bioprinter comes from a 150W switch mode power supply (POTRANS Intl Inc, Irvine, CA). The power supply is located inside of a metal enclosure (Hammond Manufacturing, Guelph, Ontario, Canada) measuring 11.75”L x 11” W x 5.5” H. This enclosure also holds a 24V-to-5V regulator and two PCL-601 motor controllers (Anaheim Automation, Anaheim, CA). The 24V 6.5A output of the power supply is split into three lines. Two lines supply 24V (color coded: Yellow/Black) to the cartridges and to the PCL-601 motor controllers for the Motion System. The third line is fed to a 24V to 5V voltage regulator (Fairchild Semiconductor, San Jose, CA) where the outgoing 5V power (color coded: White/Black) is routed to the electronics on our driver boards.



A.2.5 Data Cable/Connector diagrams



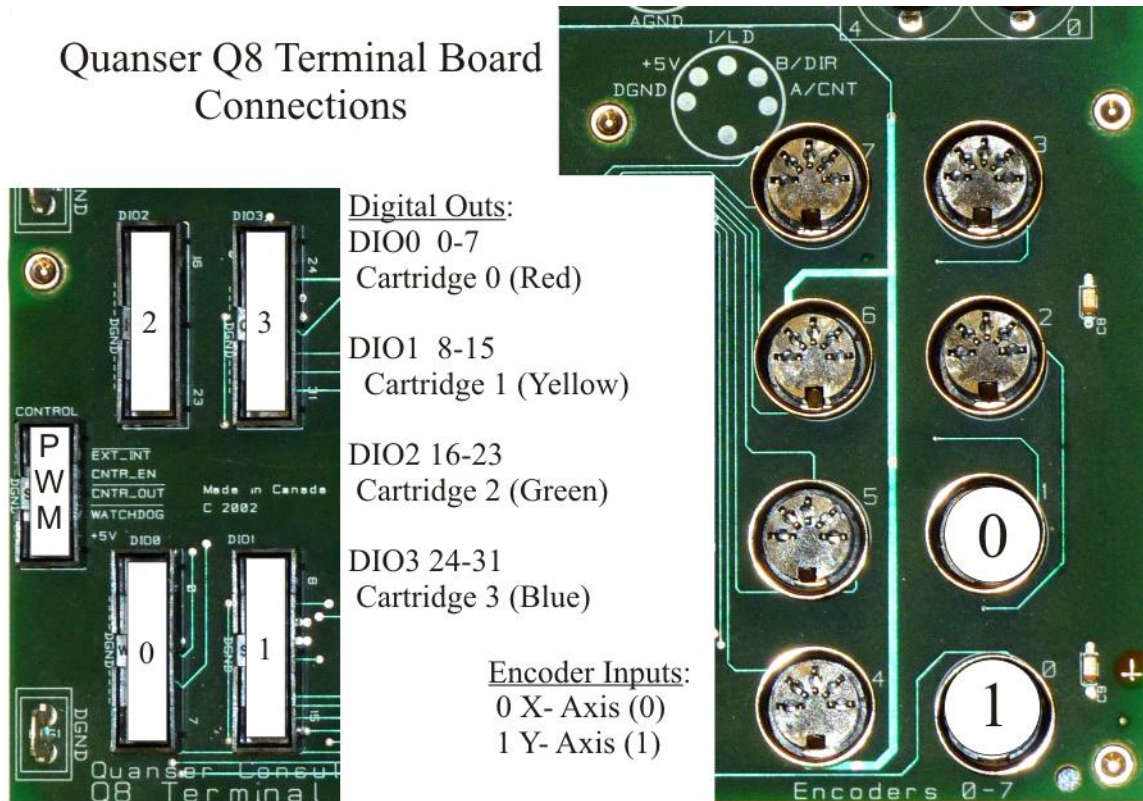
Data Cable Conductor/Pin Cross Reference						
Q8 Board Conn		Cbl Q8 Side	Cbl Driver	Driver	Data	Label
Digital Out	Control	Conn Housing	Board	Board	Cable	
1		1	4	4	4	A0 Gnd
2		2	3	3	3	A0
3		3	6	6	6	A1 Gnd
4		4	5	5	5	A1
5		5	8	8	8	A2 Gnd
6		6	7	7	7	A2
7		7	10	10	10	A3 Gnd
8		8	9	9	9	A3
9		9	12	12	12	En1 Gnd
10		10	11	11	11	En1
11		11	14	14	14	En2 Gnd
12		12	13	13	13	En2
13		13	16	16	16	En3 Gnd
14		14	15	15	15	En3
15		15	18	18	18	En4 Gnd
16		16	17	17	17	En4
	5		2	2	2	PWM Gnd
	6		1	1	1	PWM



Data Cable Pair Identification								
Pair	Conductor	1st Conductor		Label	Conductor	2nd Conductor		Label
		Solid	Band	Signal		Solid	Band	Ground
1	1	Black	Red	PWM	2	Red	Black	PWM Gnd
2	3	Black	White	A0	4	White	Black	A0 Gnd
3	5	Black	Green	A1	6	Green	Black	A1 Gnd
4	7	Black	Blue	A2	8	Blue	Black	A2 Gnd
5	9	Black	Yellow	A3	10	Yellow	Black	A3 Gnd
6	11	Black	Brown	En1	12	Brown	Black	En1 Gnd
7	13	Black	Orange	En2	14	Orange	Black	En2 Gnd
8	15	Red	White	En3	16	White	Red	En3 Gnd
9	17	Red	Green	En4	18	Green	Red	En4 Gnd
10	19	Red	Blue	N/A	20	Blue	Red	N/A

A.2.6 Q8 Terminal Board Connections

This image describes the different connections on the Q8 board that are used to communicate with the Cell Delivery Station. On the left are the Digital I/O ports that communicate with each of the cartridge driver boards (color coded) and the Control port that sends the fire pulse and sample time pulse. On the right are the two Encoder ports that read the positions of Axis 0 and Axis 1.



A.2.7 Chart comparing different aspects of different technologies

A.3 S/W Section

The following section contains sections of code from the bioprinter project. Normal comments will be colored per MatLab in green, all comments in red are for the purposes of explanation and to link to other functions. Command names are in 'Courier New' while code file names or sections are in 'Arial'.

A.3.1 Bioprinter Struct Walkthrough

The Bioprinter structure was created to give a central location to all settings and values that don't often change.

```
%%%%%%%%%%%%%%%%%%%%%%%%%%%%%%%%%%%%%%%%%%%%%%%%%%%%%%%%%%%%%%%%%%%%%%%%
%BioPrinter Struct - This structure houses all pertinent values for the
%respective BioPrinter
%%%%%%%%%%%%%%%%%%%%%%%%%%%%%%%%%%%%%%%%%%%%%%%%%%%%%%%%%%%%%%%%%%%%%%%%
global BioPrinter; % The BioPrinter struct needs to be global so that it can be accessed
by all functions

%Host Parameters
BioPrinter.Host.hostname = 'XPCBioPrinter';
BioPrinter.Host.location = 'Rhodes';
BioPrinter.Host.matlabver = '2009b';
BioPrinter.Host.basepath = 'C:\Documents and Settings\grofflab\Desktop\XPCv204a';
BioPrinter.Host.imagepath = 'C:\Documents and Settings\grofflab\Desktop\images';
BioPrinter.Host.paths = { '\Code\mfiles'...
                          '\Code\mfiles\AAStage'...
                          '\Code\mfiles\Calibration'...
                          '\Code\mfiles\CameraCommands'...
                          '\Code\mfiles\ExperimentScripts'...
                          '\Code\mfiles\ImageProcessing'...
                          '\Code\mfiles\LumeneraImaqDriver'...
                          '\Code\mfiles\ModelCommands'...
                          '\Code\mfiles\StageCommands'...
                          '\Code\mfiles\UserCommands'};

BioPrinter.Host.models = '\Code\models'; % the model directory is separated from the
other paths because it is needed explicitly for load/rtwbuild (model commands). We want
to specify this folder exactly, so as not to be sensitive to position in 'paths' array
BioPrinter.Host.logs = '\Logs'; %need this explicitly for logging

%Target Parameters
BioPrinter.Target.sim_model = 'bpXPCv204a';
BioPrinter.Target.manufacturer = 'Dell';
BioPrinter.Target.pc_model = 'Optiplex';
BioPrinter.Target.comm_type = 'TCP/IP';
BioPrinter.Target.nic = 'Intel 8154x';
BioPrinter.Target.boot_type = 'TCP/IP';

BioPrinter.Target.execution_speed = 350e-6; %calibrated 2010July9 MEP % this is where the
model speed is set. Making this number larger/smaller will cause the stage to slow
down/speed up during printing and may cause instability if set lower than 350e-6.

BioPrinter.Target.swath_length = 1200; %this is the maximum width in pixels for loading
an image into the model. This value is multiplied by 50 and a 60,000 zero vector is
loaded into the data parameter for the PrintSwath0 block in the model. %this is in pixels
- 50xSwathLength

BioPrinter.Target.pulse_length = 2; %this is in uS
BioPrinter.Target.fill_pattern = [4 1 3 2]; % designates the highest allowable density in
a pattern

BioPrinter.Target.max_density = length(BioPrinter.Target.fill_pattern); %highest density
in image, done without running PWM faster than samptime
```

```

%using the fill_pattern variable the printer subdivides the pixel into
length(BioPrinter.Target.fill_pattern) number of sections and fills them in order. For
example, if a pixel has density of 3, then the printer will print [0 1 1 1] drops of ink
in that pixel

```

```

BioPrinter.Target.cmd_density = 0;
BioPrinter.Target.image_load_ts = 0.002; % the model briefly shifts to this slower
execution time to load the data from the print function into the model.

```

```

%Stage Setup and Initialization

```

```

BioPrinter.Stage.axes_char = ['x', 'y'];
BioPrinter.Stage.axes_num = [0, 1];
BioPrinter.Stage.com_port = ['COM1'];%column vector for initializeAxis()% this value is
different in Riggs

```

```

%Axis 0 Parameters % these numbers should be the same between both systems except for the
speed_correction variable

```

```

BioPrinter.Stage.Axis0.base_speed = 300; % this value is in counts/sec
BioPrinter.Stage.Axis0.base_speed_mm = 0.29765625;
BioPrinter.Stage.Axis0.max_acceleration = 3000; % this value is in counts/sec
BioPrinter.Stage.Axis0.max_acceleration_mm = 2.9765625;
BioPrinter.Stage.Axis0.max_speed = 9500; % this value is in counts/sec
BioPrinter.Stage.Axis0.max_speed_mm = 9.4258;
BioPrinter.Stage.Axis0.ustepping = 1/8;
BioPrinter.Stage.Axis0.size= 305.1;
BioPrinter.Stage.Axis0.um_per_ustep=0.9921875;
BioPrinter.Stage.Axis0.usteps_per_rev= 1600;
BioPrinter.Stage.Axis0.enc_counts_per_rev= 4000;

```

```

BioPrinter.Stage.Axis0.speed_correction = [0.5027    1.0052    1.5078...
                                           2.0097    2.5103    3.0137...
                                           3.5123     4.0122    4.5151];%calibrated

```

```

2010July12 MEP

```

```

% found using verifySpeed.m, these numbers correct for the nonlinearity of the stage
screws

```

```

BioPrinter.Stage.Axis0.manufacturer='Anaheim Automation';
BioPrinter.Stage.Axis0.model='LS100-18-A-B-40-C';
BioPrinter.Stage.Axis0.id = 0;
BioPrinter.Stage.Axis0.address = 0;

```

```

%Axis 1 Parameters

```

```

BioPrinter.Stage.Axis1.base_speed = 300;
BioPrinter.Stage.Axis1.base_speed_mm = 0.29765625;
BioPrinter.Stage.Axis1.max_acceleration = 3000;
BioPrinter.Stage.Axis1.max_acceleration_mm = 2.9765625;
BioPrinter.Stage.Axis1.max_speed = 7500;
BioPrinter.Stage.Axis1.max_speed_mm = 7.44140625;
BioPrinter.Stage.Axis1.ustepping = 1/8;
BioPrinter.Stage.Axis1.size= 152.4; %This is in mm from AA specs, 6in.
BioPrinter.Stage.Axis1.um_per_ustep=0.9921875;
BioPrinter.Stage.Axis1.usteps_per_rev=1600;
BioPrinter.Stage.Axis1.enc_counts_per_rev=4000;

```

```

BioPrinter.Stage.Axis1.speed_correction = [0.500    1.000    1.500...
                                           2.000    2.500    3.000...
                                           3.500    4.000    4.500];

```

```

% the y axis isn't really worth running the verifySpeed.m algorithm because it's
linearity isn't imperative

```

```

BioPrinter.Stage.Axis1.manufacturer='Anaheim Automation';
BioPrinter.Stage.Axis1.model= 'LS100-6-A-B-40-C';
BioPrinter.Stage.Axis1.id= 1;
BioPrinter.Stage.Axis1.address = 1;

```

```

%Calibration Values and Sample Platform Parameters

```

```

BioPrinter.Calibration.abshome = [0 0];

```

```

BioPrinter.Calibration.ideal_position = [0 0]; %****Keep this!
BioPrinter.Calibration.home_ref_abs = [0 0];
BioPrinter.Calibration.slide_corners_ref_stage = [18.689 -38.725...%calibrated 2010Aug23
18.469 -63.805...%calibrated 2010Aug23
-56.336 -63.156...%calibrated 2010Aug23
-56.287 -37.939]; %calibrated 2010Aug23

BioPrinter.Calibration.stage_ref_abs = [];
BioPrinter.Calibration.camera_ref_abs = [49.308 55.524]; %calibrated 2010July9 MEP
BioPrinter.Calibration.cart_ref_relToCam = [63.918 0.904... %calibrated 2010July9 MEP
98.69 0.379... %calibrated 2010July12 MEP
151.126 -0.856...%calibrated 2010July12 MEP
185.842 -1.422]; %calibrated 2010July12 MEP

BioPrinter.Calibration.cart_ref_home
[BioPrinter.Calibration.cart_ref_relToCam(1)+BioPrinter.Calibration.camera_ref_abs(1)...
BioPrinter.Calibration.cart_ref_relToCam(2)+BioPrinter.Calibration.camera_ref_abs(2)...
BioPrinter.Calibration.cart_ref_relToCam(3)+BioPrinter.Calibration.camera_ref_abs(1)...
BioPrinter.Calibration.cart_ref_relToCam(4)+BioPrinter.Calibration.camera_ref_abs(2)...
BioPrinter.Calibration.cart_ref_relToCam(5)+BioPrinter.Calibration.camera_ref_abs(1)...
BioPrinter.Calibration.cart_ref_relToCam(6)+BioPrinter.Calibration.camera_ref_abs(2)...
BioPrinter.Calibration.cart_ref_relToCam(7)+BioPrinter.Calibration.camera_ref_abs(1)...
BioPrinter.Calibration.cart_ref_relToCam(8)+BioPrinter.Calibration.camera_ref_abs(2)];
% using the values found by findCartRefRelToCam.m to fill in this array

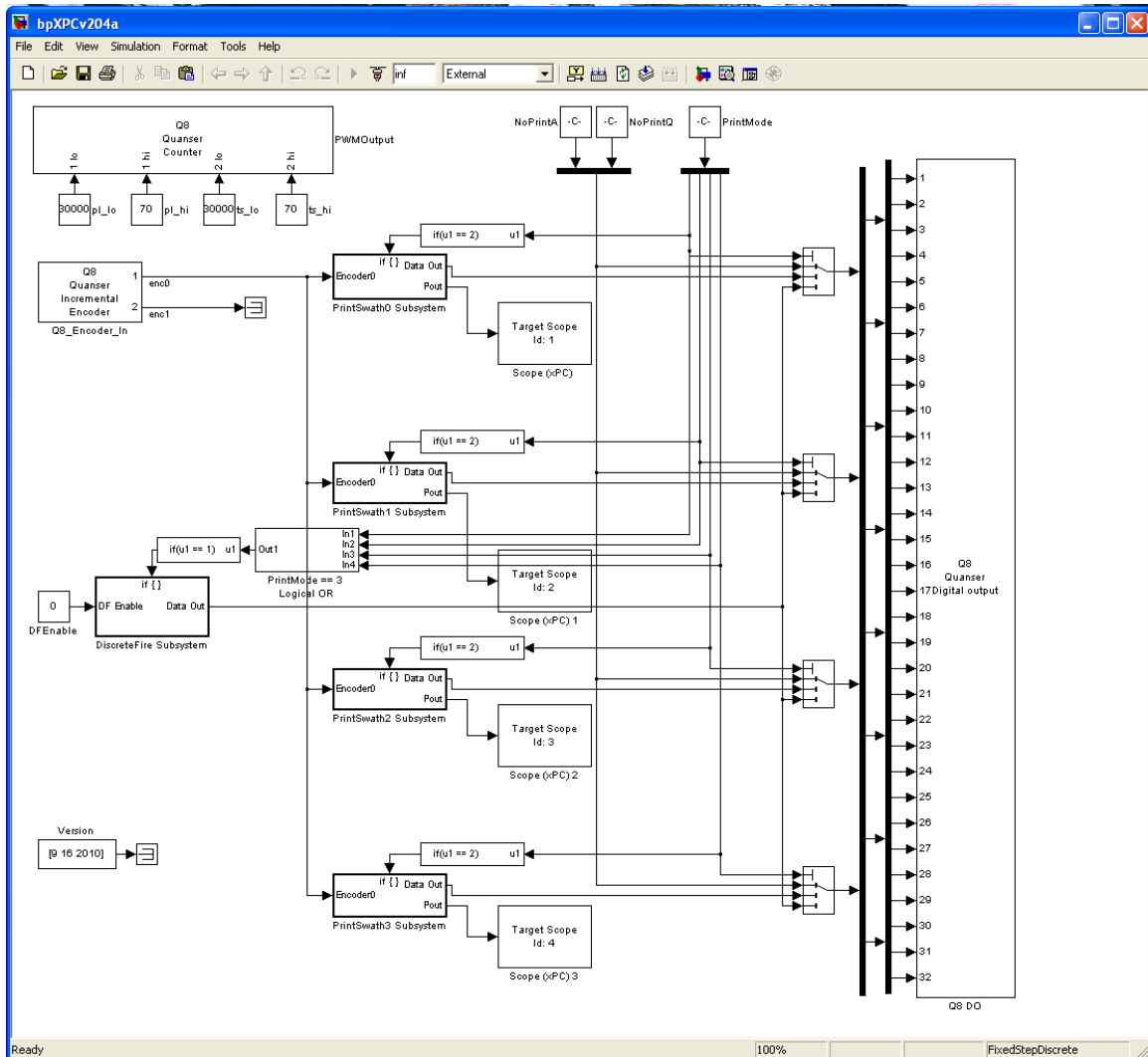
BioPrinter.Camera.manufacturer = 'Lumenera';
BioPrinter.Camera.model = '2-3C';
BioPrinter.Camera.mag_pixel_ratio = [];
BioPrinter.Camera.fps_at_res = [];
BioPrinter.Camera.cam_id = 1;
BioPrinter.Camera.binning = [1 2 4];

```

A.3.2 Bioprinter Simulink Model (bpXPCv204a.mdl)

The simulink model is the brains of the bioprinter project. Besides the simple Anaheim commands and their wrappers (like the moveAxis command), any image creation or experiment script will need to call commands that use the Simulink model. The Simulink model coordinates the firing of the cartridges at the correct time with the position of the stage.

A.3.2.1 Model Overview



The current Simulink model, bpXPCv204a.mdl, has been thoroughly tested and doesn't have any known issues outstanding.

A.3.2.2 Individual Blocks

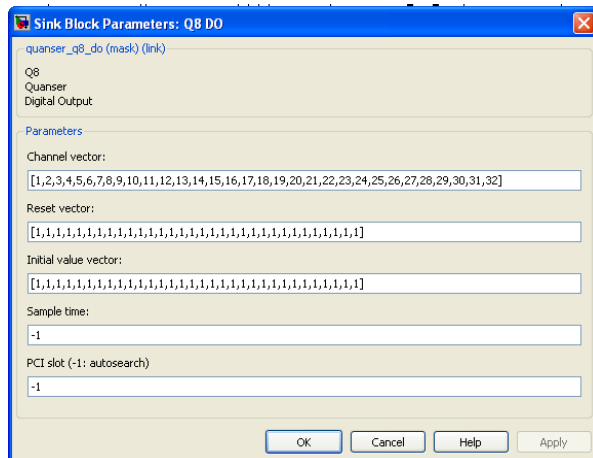
A.3.2.2.1 PWMOutput

The inputs into the PWMOutput block are set by the `setSampleTime` (`ts_hi`, `ts_lo`) and `setFirePulseParameters` (`pl_hi`, `pl_lo`). The computer clock's smallest increment is 30 ns, which means that all times are defined as multiples of that value. `setSampleTime` sets the execution time for the model while `setFirePulseParameters` sets the firing pulse length and frequency for firing the cartridges. The total length of these two vectors is the same to ensure that the model and firing of cartridges are synced.

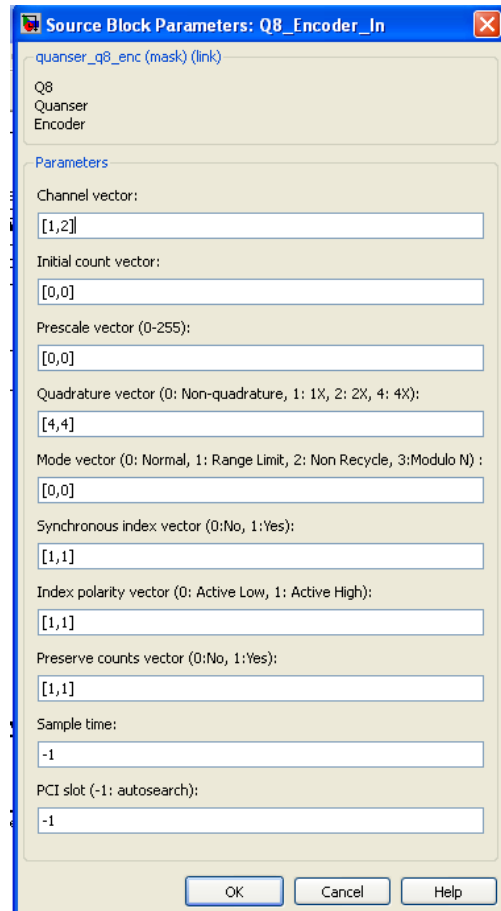
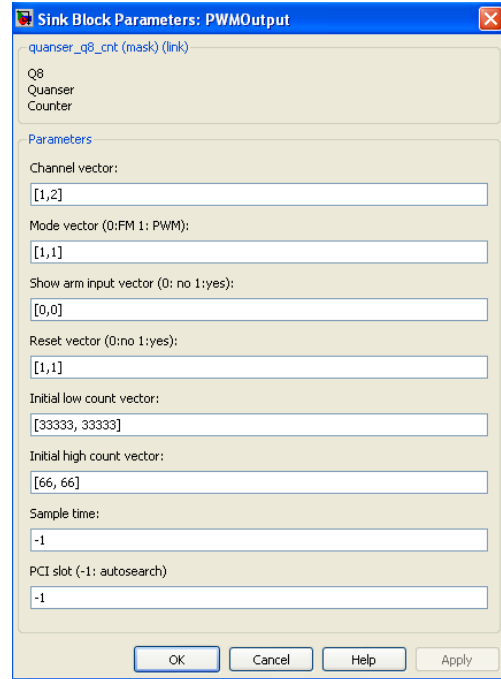
A.3.2.2.2 Q8_Encoder_In

This block dictates how the encoders are handled in our model. Notice the model is set to preserve the encoder reading even if the model is stopped. The only way the encoders get reset is by loading the `resetencoders_model` called by `resetEncoders`.

A.3.2.2.3 Q8 DO



This block takes each set of input signals given by each of the PrintSwath Subsystems (Address lines A0-A3 and Quadrant enables Q0-Q3) and delivers them to their respective cartridge, 1-8 to cart0, 9-16 to cart1, 17-24 to cart2, and 25-32 to cart3. These signals correspond to the Digital I/O lines on the Q8 board (0-7,8-15,16-23,24-31), section A.2.6.



Input Ports:

- 1) **encoder0** – the encoder value of Axis 0. It is polled every sample time to determine when to start firing the cartridge and printing the 50 row subsection of the pattern

Output Ports

- 1) **A** – a row vector with four values A0 – A3. These values go out to the various driver boards (through the Q8 DO block) and select the address on the cartridge which will fire
- 2) **Q** – a row vector with four values Q0 – Q3. These values go out to the various driver boards (through the Q8 DO block) and enable the quadrants on the driver board (energizes the decoders), allowing A0-A3 to fire particular nozzles
- 3) **printing** – this is a status bit that is output by the PrintSwath block while it is printing, this value is polled by the `print` command in order to know when to move Axis 1 and prepare to print the next 50 rows of the pattern

Parameters

- 1) **data** – this 1D vector consists of each 50 element column of the pattern transposed and concatenated together. For example, a 20 pixel wide image would have a data vector of (20*50=) 1000 elements with the requisite padding on the end. Each data row is padded by zeros due to fact that the model is expecting a vector of a certain length and thus the default value is large (`BioPrinter.Target.swath_length*50 =`), 60,000 elements, to allow for different width images to be printed without having to stop the model and reload the element length.
- 2) **width** – this value is generated by the `print` command and set to the model using the `setPrintTrigger` command. It is used to tell the code in **Outputs** when to start printing the different columns of nozzles based on which direction the printer is moving
- 3) **Np** – this value is permanently set to 13 and gets its value from the maximum number of nozzles in Q1 and Q4. It is used in the code in the **Discrete Update** tab to determine when to move to the next column of pixel values.
- 4) **direction** – value supplied by the `print` command to tell the **Outputs** code which direction the stage is moving, which helps it know when to start printing and which quadrant lags the other.
- 5) **maximgdensity** – this value is supplied by the `print` command and is set to `BioPrinter.Target.max_density`, the code in **Outputs** then cycles through each pixel that many times to print the desired density, though only a few pixels in the image may need that density (multiple drops in one location).
- 6) **im_edge_enc_counts** – these values are created in `setPrintTrigger` and tell each PrintSwath Subsystem when to start printing its cartridge (since each PrintSwath block is receiving `encoder0` values). Each PrintSwath block receives a different value based on the calibration values.
- 7) **im_width_enc_counts** – this value is also created in `setPrintTrigger` and tells **Outputs** when the cartridge should start printing when coming from **direction 1** (stage moving right to left)
- 8) **fill_pattern** – this row vector comes from `print` passing on the value found in `BioPrinter.Target.fill_pattern`. This vector tells the code in **Ouputs** in what order to

print a pixel with density greater than 1. For example, if a pixel has density of 3 (BioPrinter.Target.max_density of 4), then the printer will print [0 1 1 1] drops of ink in that pixel.

A.3.2.2.5.2 Libraries Tab

PrintSwathAuxFun.h and PrintSwathAuxFun.c were written to simplify the Outputs and Discrete Update code (commented below)

PrintSwathAuxFun.h %declares the variables used in PrintSwathAuxFun.c

```
#define QUAD1 0
#define QUAD2 1
#define QUAD3 2
#define QUAD4 3

uint16_T pixelIndex(uint16_T row, uint16_T col) ;
uint16_T rowNumber(uint16_T quad, uint16_T nozNumber);
```

PrintSwathAuxFun.c % written to remove some of the calculation steps from the Outputs code and make it easier to read and understand.

```
#if defined(MATLAB_MEX_FILE)
#include "tmwtypes.h"
#include "simstruc_types.h"
#else
#include "rtwtypes.h"
#endif

/* %%-SFUNWIZ_wrapper_includes_Changes_BEGIN --- EDIT HERE TO _END */
#include <math.h>
#include "PrintSwathAuxFun.h"

uint16_T pixelIndex(uint16_T row, uint16_T col)
// returns the array index of the pixel, computed from the row and column.
// row, col, and index are indexed from 0.
{
    return row + 50*col;
}

uint16_T rowNumber(uint16_T quad, uint16_T nozNumber)
// returns the row number (numbered 0-49) in the image corresponding to
// the quadrant (numbered 0-3) and nozzle (numbered 0-12)
// that is printing.
// Note that quadrant 1, 2 (Q2 and Q3) have nozzles 0-11 nozzles rather than
// 0-12.
// if nozzle 12 of Q2 or Q3 is requested, this function will return a row
// number
// larger than 49, which is nonsensical. The nozzle number must be checked
// by the
// calling function.
{
    //correction for incorrectly wired quadrant 4
    const int q4nozmap[13] = {1, 3, 4, 2, 0, 5, 6, 7, 10, 8, 9, 11, 12};

    switch(quad)
    {
        case QUAD1: //QUAD1
            return 2*nozNumber + 1;
        case QUAD2: //QUAD2
            return 26 + 2*nozNumber;
        case QUAD3: //QUAD3
            return 27 + 2*nozNumber;
        case QUAD4: //QUAD4
```

```

        return 2*q4nozmap[nozNumber];
    }
}

```

A.3.2.2.5.3 Outputs Tab (code walkthrough)

```

// Code for OUTPUT tab
//
// When the enable input to this block is low, all address lines A[] are 0
// and all quadrant enable lines are high Q[]=1. (Note that the quadrant
// enables are active-low, so this means the system is *not* printing)
// When enable goes high the system begins to print a 50 row high swath of the
// image (the full height of the printhead. Depending on print direction, it
// prints certain quadrants with an appropriate lag so that the printed columns
// are straight, even though the nozzles are arranged in two separate columns on
// the printhead.
// Assume quadrant arrangement is Q3 Q2; Q1 Q4 rather than Q1 Q2; Q3 Q4
// Firing order is Q4 Q1 Q2 Q3, in order to access the corresponding elements Q4
// is indexed (by 2*counter), Q1 is indexed by (2*counter + 1), Q2 is indexed by
// (2*counter + 26) {Q1 and Q4 use first 0-25 spaces for 26 nozzles}, Q3 is indexed
// by (2*counter + 26 + 1)

//Address: Q4A00 Q1A00 Q4A01 Q1A01 ... Q4A12 Q1A12 | Q2A0 Q3A0 Q2A1... Q2A11 Q3A11
//Position 0 1 2 3 24 25 | 26 27 28 48 49
//in data vector:

// Q[0] = Q1, Q[1] = Q2, Q[2] = Q3, Q[3] = Q4
// xD[0] - counter
// xD[1] - col

// PIXLAG is the number of pixels between columns on the printhead.
// Distance between pixels is 84.7um, distance between columns is ~850um,
// so PIXLAG should be 10, at least in theory.
#define PIXLAG (uint16_T) 10 // also defined in Discrete update

% the variables xD[0], xD[1], xD[2] are set in the Discrete Update code
uint16_T counter = (uint16_T) xD[0]; // counter to determine which nozzle to print
uint16_T nozNum; // address of nozzle to print
uint16_T colLead = (uint16_T) xD[1]; // image column number currently being
printed by leading quadrants
uint16_T colLag = colLead - PIXLAG; // image column number currently being
printed by lagging quadrants
uint16_T density = (uint16_T) xD[2]; // counter to determine fill level for
current pixel
% the density variable will be used as the index for the fill_pattern array, and a
check will be made to see if the current pixel's density value is >= that position
in the fill_pattern array

int row, pixInd, fillLevel; // image row to be printed, pixel index corresponding
to a row and column, number of drops to place in current pixel.
int colQ2Q4, colQ1Q3; //variables that will be assigned colLead or colLag
int i;

//correction for skew in nozzles for each quadrant, q4nozmap needs to be
eliminated first
const int noz_skew[13] = {0,1,2,3,4,5,6,7,8,9,10,11,12};

// Initialize outputs A[] and Q[]. Outputs will remain at these values unless
they are changed below.
A[0] = 0; A[1] = 0; A[2] = 0; A[3] = 0; // these are the address lines
Q[0] = 0; Q[1] = 0; Q[2] = 0; Q[3] = 0; // All Q[]'s are inverted at the
bottom of this routine, thus the default output is Q[]=1, which corresponds to not
printing a drop (the cartridge interface electronics are active low)

//check to see if on right side of encoder counts to start printing

```

```

if      (          (direction[0]==1          &&          encoder0[0]          <
im_edge_enc_counts[0]+im_width_enc_counts[0]) ||
        (direction[0]==0 && encoder0[0] > im_edge_enc_counts[0]))
{
    if (xD[0] < 13)    // only print when counter is in range 0 to 12.
    {
        // define counter
        if (direction[0] == 1)
            nozNum = noz_skew[counter];
        else
        {
            counter = 12 - (uint8_T) xD[0]; // in this direction, print from
bottom to top
            nozNum = noz_skew[counter];
        }

        // decode address lines from counter
        A[0] = (nozNum) & 0x01;
        A[1] = (nozNum>>1) & 0x01;
        A[2] = (nozNum>>2) & 0x01;
        A[3] = (nozNum>>3) & 0x01;

        // determine image columns from which the quadrants should get pixels
        if (direction[0] == 1)
        {
            colQ2Q4 = colLead; // (Q1, Q3) lag behind (Q2, Q4) by PIXLAG pixels
            colQ1Q3 = colLag;
        }
        else
        {
            colQ2Q4 = colLag; // (Q2, Q4) lag behind (Q1, Q3) by PIXLAG pixels
            colQ1Q3 = colLead;
        }

        // determine which quadrants should print
        if ( (colQ2Q4 >= 0) && (colQ2Q4 < width[0]) ) //check if colQ2Q4 is inside
the image
        {
            if ( nozNum < 12 )    // Q2 only has 12 nozzles (not 13)
            {
                row = rowNumber(QUAD2,nozNum); %calling the PrintSwathAuxFun.c
functions

                pixInd = pixelIndex(row, colQ2Q4);
                fillLevel=data[pixInd]; %checking the density value of the current
pixel

                if (fill_pattern[density] <= fillLevel)
                    Q[QUAD2] = 1;
            }
            row = rowNumber(QUAD4,nozNum);
            pixInd = pixelIndex(row, colQ2Q4);
            fillLevel=data[pixInd];
            if (fill_pattern[density] <= fillLevel)
                Q[QUAD4] = 1;
        }
        if ( (colQ1Q3 >= 0) && (colQ1Q3 < width[0]) ) // check if colQ1Q3 is
inside the image
        {
            if ( nozNum < 12 ) // Q3 only has 12 nozzles (not 13)
            {
                row = rowNumber(QUAD3,nozNum);
                pixInd = pixelIndex(row, colQ1Q3);
                fillLevel=data[pixInd];
                if (fill_pattern[density] <= fillLevel)
                    Q[QUAD3] = 1;
            }
            row = rowNumber(QUAD1,nozNum);

```

```

        pixInd = pixelIndex(row, colQ1Q3);
        fillLevel=data[pixInd];
        if (fill_pattern[density] <= fillLevel)
            Q[QUAD1] = 1;
    }
}

// invert quadrant outputs Q[]. This eliminates the need for a separate inverter
in the model
for (i=0;i<4;i++) {
    Q[i] = (Q[i]==0)?1:0;
}

if ( (direction[0]==1 && encoder0[0] > im_edge_enc_counts[0]) ||
    (direction[0]==0 && encoder0[0] <
im_edge_enc_counts[0]+im_width_enc_counts[0]) &&
    (colLag) < width[0] )
    printing[0] = 1;
else
    printing[0] = 0;

```

A.3.2.2.5.4 Discrete Update Tab (code walkthrough)

% this code is run after the Outputs code is run. Therefore, when Outputs runs the first time through, the values for xD[0], xD[1], and xD[2] are all 0.

```

// xD[0] - counter
// xD[1] - col
// xD[2] - density fire counter

#define PIXLAG (uint16_T) 10 // also defined in Outputs
if ( (direction[0]==1 && encoder0[0] <
im_edge_enc_counts[0]+im_width_enc_counts[0]) ||
    (direction[0]==0 && encoder0[0] > im_edge_enc_counts[0]) &&
    xD[1] < width[0]+PIXLAG ) {
    xD[0]++;
    if(xD[0] == Np[0]){
        xD[0] = 0;
        xD[2]++;
        if ( xD[2] == maximgdensity[0] ) {
            xD[2] = 0;
            if (xD[1] < width[0] + PIXLAG + 1)
                xD[1]++;
        }
    }
}
else if ( (direction[0]==1 && encoder0[0] >
im_edge_enc_counts[0]+im_width_enc_counts[0]) ||
    (direction[0]==0 && encoder0[0] < im_edge_enc_counts[0]) ) {
    xD[0] = 0;
    xD[1] = 0;
    xD[2] = 0;
}

```

A.3.2.2.6 DiscreteFire Subsystem

The DiscreteFire ability of the model is used in materials testing, board validation, and the calibrate command to individually address specific nozzles on the cartridges.

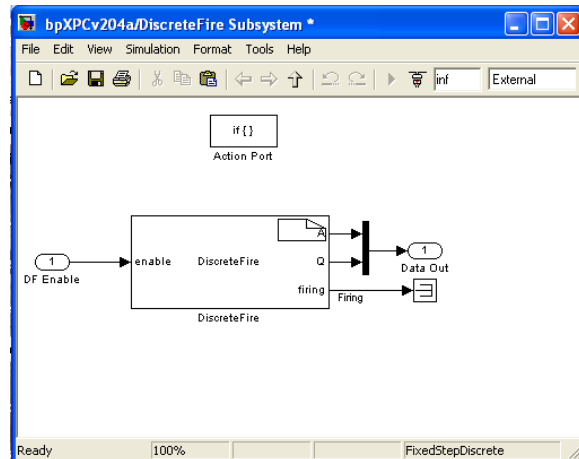
A.3.2.2.6.1 Input ports/Output ports/Parameters

Input Ports

- 1) enable – once the DiscreteFire Subsystem is enabled by the Logical OR block, the DF Enable sends an enable signal to enable the Outputs code.

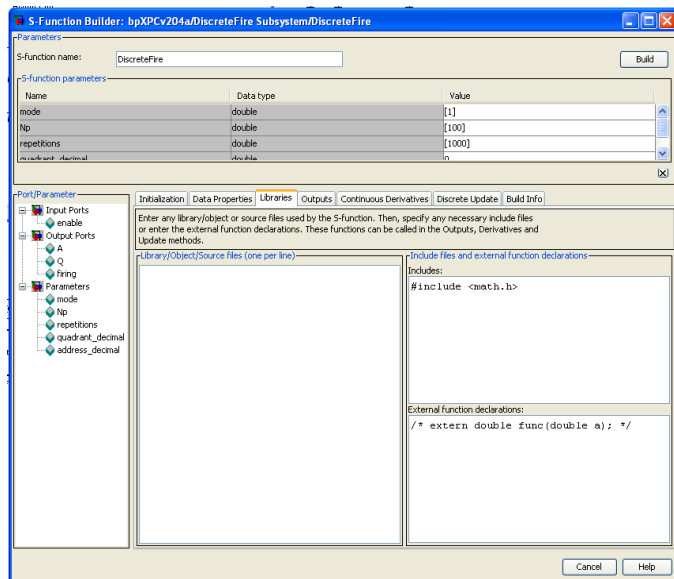
Output Ports

- 1) A – the address of the nozzle which is commanded to fire
- 2) Q – the quadrant of the nozzle which is commanded to fire
- 3) firing – status line that is polled by the fireNozzle command



Parameters

- 1) mode – this value is always set to zero, locking the Outputs code into printing the same address with the user specified quadrants
- 2) Np - this value is permanently set to 13 and gets its value from the maximum number of nozzles in Q1 and Q4. It is used in the code in the Discrete Update tab to determine when to move to the next column of pixel values.
- 3) repetitions – user defined value passed by the fireNozzle command to describe how many drops the user wants to fire from the nozzle
- 4) quadrant_decimal – decimal representation of the desired quadrant(s) that the user would like to fire, decoded by the Outputs code to determine the Q output value
- 5) address_decimal - decimal representation of the desired address(es) that the user would like to fire, decoded by the Outputs code to determine the A output value



A.3.2.2.6.2 Outputs Tab (code walkthrough)

```
uint32_T address, quads=quadrant_decimal[0], i;  
Q[0] = Q[1] = Q[2] = Q[3] = 1;
```

```
if (enable[0] == 1) {  
    if (mode[0] == 0) {
```

```

        //if (xD[0] == 0 && xD[1] < repetitions[0]) { //only fires when xD=0, this
occurs every Np sampletimes for 'repetitions' number of times
        if (xD[1] < repetitions[0]) {
            for (i=0; i<4; i++) //shift into Q
                if ((quads>>i) & 0x01) //shift nozzle[0] into Q
                    Q[i] = 0;
            address = address_decimal[0]; //put nozzle[1] address into A ( shifted below)
        }
        else if (mode[0] == 1) { %this if statement is never entered
            if (xD[0] < 13) { //this continuously fires
                Q[0] = Q[1] = Q[2] = Q[3] = 0;
                address = xD[0];
            }
        }
    }

A[0] = (address) & 1; // decode address lines from counter
A[1] = (address>>1) & 0x01;
A[2] = (address>>2) & 0x01;
A[3] = (address>>3) & 0x01;

if (enable[0] && xD[1] < repetitions[0])
    firing[0] = 1;
else
    firing[0] = 0;

```

A.3.2.2.6.3 Discrete Update Tab (code walkthrough)

```

if (enable[0] == 1) {
    if (!mode[0]) {
        xD[0]++; %xD[0] is never used in the mode[0]==0 section of Outputs
        if (xD[1] <= repetitions[0]) { %xD[0] never increments while true
            xD[1]++;
            xD[0]=0;
        }
    }
    if (mode[0]) { %this 'if' statement is never entered
        if (xD[0] == Np[0]) {
            xD[0]=0;
        }
        else {
            xD[0]++;
        }
    }
}
else {
    xD[0] = 0;
    xD[1] = 0;
}

```

A.3.3 Function Dependency Diagrams

This section presents two major functions, `initBioPrinter` and `print`, and demonstrates how they rely on the other functions in the bioprinting operating system. These were made by taking each function as it was encountered and looking at its dependent functions. This was continued until base level Anaheim Automation (AA) or MatLab commands were reached. In the AA commands, custom messages are sent to the PCL601 motor controllers. The structure for these commands can be found in the Anaheim Automation manual located in Riggs SB3.

Since some baser functions are called by multiple other functions, if the diagram for that function has already been explained a call to the previous explanation will be provided.

A.3.3.1 *FUNCTION: initBioPrinter*

- I. initBioPrinter
 - a. initializeStage()
 - i. initializeAxis
 1. checkAxisID
 2. AA_InitializeAxis
 - a. AA_SetAcceleration
 - b. AA_SetBaseSpeed
 - c. AA_SetMaxSpeed
 - d. AA_MotorCurrent
 - e. AA_SetDirection
 3. AA_EncoderAutoCorrect
 - a. AA_Verify
 - ii. stageHome
 1. homeAxis
 - a. AA_Home
 - b. waitWhileAxisMoving
 - i. checkAxisID
 - ii. AA_WaitWhileBusy
 2. waitWhileAxisMoving (see I.a.ii.1.b)
 - b. resetEncoders
 - i. load
 - c. initTarget
 - i. checkModel
 1. waitWhileAxisMoving (see I.a.ii.1.b)
 2. buildModel
 - a. rtwbuild
 3. reloadModel
 - a. unload
 - b. load
 4. setPrintMode
 - a. setparam
 - b. getparamid
 - ii. setSampleTime
 1. setparam
 2. getparamid
 - iii. printNoMovement
 1. checkModel (see I.c.i)
 2. setSampleTime (see I.c.ii)
 3. setPrintMode (see I.c.i.4)
 4. loadImageSwath
 - a. fliplr
 - b. reshape
 - c. setSampleTime (see I.c.ii)
 - d. setparam
 - e. getparamid
 5. setPrintTrigger
 - a. convertPixelsToEncCounts
 - i. checkAxisID
 - b. convertMMToEncCounts
 - i. checkAxisID
 - ii. convertMMToSteps
 1. checkAxisID
 - iii. convertStepsToEncCounts
 1. checkAxisID

- c. setparam
 - d. getparamid
 - iv. flushNozzle
 - 1. loadCalibFromStruct
 - 2. print (see **FUNCTION: print**)
 - v. stageHome (see I.a.ii)
- d. LucamCameraOpen
- e. LucamIsConnected
- f. LucamDisplayPropertyPage
- g. LucamCameraClose

A.3.3.2 *FUNCTION: print*

- II. print
 - a. checkModel
 - i. waitWhileAxisMoving
 - 1. checkAxisID
 - 2. AA_WaitWhileBusy
 - ii. buildModel
 - 1. rtwbuild
 - iii. reloadModel
 - 1. unload
 - 2. load
 - iv. setPrintMode
 - 1. setparam
 - 2. getparamid
 - b. setSampleTime
 - i. setparam
 - ii. getparamid
 - c. setPrintMode
 - i. setparam
 - ii. getparamid
 - d. maxImageDensity
 - i. imageDensity
 - e. convertPixelsToMM
 - i. checkAxisID
 - ii. convertPixelsToEncCounts
 - 1. checkAxisID
 - iii. convertEncCountsToMM
 - 1. checkAxisID
 - 2. convertEncCountsToSteps
 - a. checkAxisID
 - 3. convertStepsToMM
 - a. checkAxisID
 - f. convertStepsToMM
 - i. checkAxisID
 - g. imageDensity
 - h. convertMMtoPixels
 - i. checkAxisID
 - ii. convertMMToEncCounts
 - 1. checkAxisID
 - 2. convertMMToSteps
 - a. checkAxisID
 - 3. convertStepsToEncCounts
 - a. checkAxisID
 - iii. convertEncCountsToPixels
 - 1. checkAxisID
 - i. setPrintTrigger
 - i. convertPixelsToEncCounts

- 1. checkAxisID
 - ii. convertMMToEncCounts (see II.h.ii)
 - iii. setparam
 - iv. getparamid
 - j. setFirePulseParameters
 - i. getparam
 - ii. getparamid
 - iii. floor
 - k. writeLogfile
 - i. strcat
 - l. setparam
 - m. getparamid
 - n. setAxisAcceleration
 - i. checkAxisID
 - ii. convertMMToSteps (see II.h.ii.2)
 - iii. AA_SetAcceleration
 - 1. AA_Verify
 - a. AA_DispatchError
 - b. AA_ClearMessages
 - c. fgetl
 - iv. convertStepsToMM (see II.f)
 - o. setAxisBaseSpeed
 - i. checkAxisID
 - ii. convertMMToSteps (see II.h.ii.2)
 - iii. AA_SetBaseSpeed
 - 1. findCmdSpeed
 - a. checkAxisID
 - b. polyfit
 - c. polyval
 - iv. convertStepsToMM (see I.f)
 - p. setAxisSpeed
 - i. checkAxisID
 - ii. findCmdSpeed (see II.o.iii.1)
 - iii. convertMMToSteps (see II.h.ii.2)
 - iv. AA_SetMaxSpeed
 - 1. AA_Verify (see II.n.iii.1)
 - v. convertStepsToMM (see II.f)
 - q. getPosition
 - i. checkAxisID
 - ii. getEncoderCounts
 - 1. checkAxisID
 - 2. getsignal
 - 3. getsignalidsfromlabel
 - iii. convertEncCountsToMM (see II.e.iii)
 - r. moveAxis
 - i. checkAxisID
 - ii. setAxisSpeed (see I I.p)
 - iii. convertMMToSteps (see I I.h.ii.2)
 - iv. AA_MoveRelative
 - 1. AA_SetDirection
 - a. AA_Verify (see II.n.iii.1)
 - 2. AA_SetNumberSteps
 - a. AA_Verify (see II.n.iii.1)
 - 3. AA_MotorCurrent
 - a. AA_HardStop
 - i. AA_Transmit
 - b. AA_DispatchError
 - i. AA_ClearMessages
 - 1. fgetl

- c. AA_Verify (see II.n.iii.1)
 - 4. AA_Go
 - a. AA_Transmit
 - s. waitWhileAxisMoving (see II.a.i)
 - t. setBacklashPosition
 - i. moveAxisRelative
 - 1. checkAxisID
 - 2. getPosition (see II.q)
 - 3. covertMMToSteps (see II.h.ii.2)
 - 4. AA_MoveRelative (see II.r.iv)
 - ii. waitWhileAxisMoving (see II.a.i)
 - u. displayImages
 - i. figure
 - ii. exist
 - v. printImageSwath
 - i. loadImageSwath
 - 1. fliplr
 - 2. reshape
 - 3. setSampleTime
 - a. setparam
 - b. setparamid
 - 4. setparam
 - 5. getparamid
 - ii. setPrintMode
 - 1. setparam
 - 2. getparamid
 - iii. waitWhileAxisMoving (see II.a.i)
 - iv. moveAxisRelative (see II.t.i)
 - v. getsignal
 - vi. getsignalidsfromlabel
 - vii. WaitWhilePrinting
 - 1. Getsignal
 - 2. getsignalidsfromlabel
 - w. moveAxisRelative (see II.t.i)
 - x. enableAxis
 - i. checkAxisID
 - ii. AA_MotorCurrent (see II.r.iv.3)

A.3.4 *Print fxn code walk through*

The goal of the print function is to take in an ‘x y’ location, set of images for each cartridge, the offset between the cartridges, and a log file if applicable. With the current state of the printer, the backlash is large enough that we cannot utilize the full functionality of this command as written. The backlash in the X axis prevents the user from putting in a set of images that is taller than 50 pixels because the second pass of the image would be offset from the first pass. The backlash in the Y axis prevents the user from putting in a set of images using multiple images because the images would not line up vertically as the Y axis moved back and forth to account for the offsets of the various cartridges.

The print command is used in current scripts to print single cell type images less than 50 rows tall. Multiple cell-type experiments with images less than 50 rows tall are created by performing additional prints for each cell-type, with the print location offset by the proper calibration offset based on which cartridge is printing.

```

function print(x, y, images, calibration, logfile)
%%%%%%%%%%%%%%%%%%%%%%%%%%%%%%%%%%%%%%%%%%%%%%%%%%%%%%%%%%%%%%%%%%%%%%%%
% 'print' - prints a two dimensional image
%
% x - 'x' position to print the image in mm
%
% y - 'y' position to print the image in mm
%
% images - Struct house images:
%   data_in.img0->image for cart0
%   data_in.img1->image for cart1
%   data_in.img2->image for cart2
%   data_in.img3->image for cart3
% These are expected to be grayscale images with values between 0 and the
% maximum density
%
% calibration - Struct to house cartridge errors:
%   calibration.cart1.x->cart1 x calibration relative to cart0 in mm
%   calibration.cart1.y->cart1 y calibration relative to cart0 in mm
%   calibration.cart2.x->cart2 x calibration relative to cart0 in mm
%   calibration.cart2.y->cart2 y calibration relative to cart0 in mm
%   calibration.cart3.x->cart3 x calibration relative to cart0 in mm
%   calibration.cart3.y->cart3 y calibration relative to cart0 in mm
%
% pulswidth_in - time in microseconds of the pulse length used to fire
%   the nozzle (typical values b/w 2 and 2)
%
% logfile - name of log experiment data is save to
%
% Np - A drop can be printed from the same nozzle every Np sample
%   periods, this is no longer a modifiable parameter
%
% White pixels in the input image (value 1 or greater) are printed in ink
%
%%%%%%%%%%%%%%%%%%%%%%%%%%%%%%%%%%%%%%%%%%%%%%%%%%%%%%%%%%%%%%%%%%%%%%%%

%need access to BioPrinter Struct
global BioPrinter;
%need acces to the xpc object
tg=xpc;

%open a new figure to draw items in. Prevent polluting other GUI's/Plots
h = figure('Name', 'Print Output', 'NumberTitle', 'off');

%period to advance col count should be min. should be const when Ts is defined. Remove.
printer.period = 13; % this value will never change, see section 1.3.2.2.5
%make sure correct model is loaded and is running
checkModel(BioPrinter.Target.sim_model);
setSampleTime(BioPrinter.Target.execution_speed);
setPrintMode('NoPrint');
%flushPrintSwaths(); %flush contents of printswaths

%Find image properties - density and dimensions
img_density = double(maxImageDensity(images));
if(~img_density)
    warning('Image is blank, no media will be printed')
end

%assume all images are the same dimensions, this was checked in imJustify
imageHeight = size(images.img0,1);
imageWidth = size(images.img0,2);
imageHeightMM = convertPixelsToMM('y', imageHeight);
imageWidthMM = convertPixelsToMM('x', imageWidth);

fill_pattern_length=32;
printer.acceleration = BioPrinter.Stage.Axis0.max_acceleration_mm;
if(img_density >= 0 && img_density < BioPrinter.Target.max_density)

```

```

    printer.printSpeed = convertStepsToMM('x', 84.7 / BioPrinter.Stage.Axis0.um_per_ustep
/ printer.period / BioPrinter.Target.execution_speed / BioPrinter.Target.max_density);
    density = BioPrinter.Target.max_density;
    fill_pattern = [BioPrinter.Target.fill_pattern zeros(1, fill_pattern_length-
size(BioPrinter.Target.fill_pattern,2))];
    stage_delay = 0;
elseif(img_density > 0)
    printer.printSpeed = convertStepsToMM('x', 84.7 / BioPrinter.Stage.Axis0.um_per_ustep
/ printer.period / BioPrinter.Target.execution_speed / img_density);
    warning('Maximum image density exceeds limits, print speed is being slowed down. Max
density is %d, requested density is %d.', BioPrinter.Target.max_density, img_density)
    density = img_density;
    fill_pattern = [1:1:img_density zeros(1, fill_pattern_length-img_density)];
    warning('To accommodate large density uniform fill pattern is being used')
    stage_delay = 1;
end
printer.accelerationDistance = (printer.printSpeed^2 / printer.acceleration);

%find the print length, images which are blank are not counted. The largest
%calibration offset in the 'x' direction needs to be recovered for the
%furthest valid cartridge
imgdensity(1) = double(imageDensity(images.img0));
imgdensity(2) = double(imageDensity(images.img1));
imgdensity(3) = double(imageDensity(images.img2));
imgdensity(4) = double(imageDensity(images.img3));
ind_imgs = find(imgdensity ~=0);
ind_blanks = find(imgdensity ==0);

original_calibration = calibration;
%make the blank images start 'printing' when the first void image begins
%printing. caltemp_x = [0 calibration.cart1.x calibration.cart2.x calibration.cart3.x];
caltemp_y = 0 calibration.cart1.y calibration.cart2.y calibration.cart3.y];
lowest_cal_x= caltemp_x(ind_imgs(1));
lowest_cal_y= caltemp_y(ind_imgs(1));
caltemp_x(:) = caltemp_x(:) - lowest_cal_x;
caltemp_y(:) = caltemp_y(:) - lowest_cal_y;

for i=1:numel(ind_blanks)
    caltemp_x(ind_blanks(i)) = caltemp_x(ind_imgs(1));
    caltemp_y(ind_blanks(i)) = caltemp_y(ind_imgs(1));
end

calibration.cart1.x = caltemp_x(2);
calibration.cart2.x = caltemp_x(3);
calibration.cart3.x = caltemp_x(4);
calibration.cart1.y = caltemp_y(2);
calibration.cart2.y = caltemp_y(3);
calibration.cart3.y = caltemp_y(4);

min_cal_x = min(caltemp_x(find(caltemp_x~=0)));
max_cal_y = max(caltemp_y);
min_time_move_x = min_cal_x / printer.printSpeed;
max_time_move_y = max_cal_y / BioPrinter.Stage.Axis1.max_speed_mm;
t_tot = min_time_move_x + max_time_move_y + .1;
maxw_fine_corr_mm = t_tot * printer.printSpeed;
maxw_fine_corr_pixels = convertMMToPixels('x', maxw_fine_corr_mm);

%need the length of the largest calibration since will need to move that
%much in addition to the length of the image and accel distance
cal_length=0;
if(ind_imgs(end)>1)
    cal_length = eval(sprintf('calibration.cart%d.x', ind_imgs(end)-1));
end
printer.length = convertPixelsToMM('x', imageWidth-1+10) + cal_length;

%Set edges of image in PrintSwaths for triggering during printing
setPrintTrigger(calibration, imageWidth, x);

```

```

%Set up PWM for use with printing
setFirePulseParameters(BioPrinter.Target.pulse_length, 1);

%If logging
if(exist('logfile', 'var'))
    writeLogfile(logfile, BioPrinter, img_density, density, x, y, original_calibration,
stage_delay, images, imageHeight, imageWidth);
end

%Send the image density to the PrintSwath blocks
tg.setparam(tg.getparamid('PrintSwath0 Subsystem/PrintSwath0', 'P5'),
density);%img_density);
tg.setparam(tg.getparamid('PrintSwath1 Subsystem/PrintSwath1', 'P5'),
density);%img_density);
tg.setparam(tg.getparamid('PrintSwath2 Subsystem/PrintSwath2', 'P5'),
density);%img_density);
tg.setparam(tg.getparamid('PrintSwath3 Subsystem/PrintSwath3', 'P5'),
density);%img_density);

%Send the fill pattern to the PrintSwath blocks
tg.setparam(tg.getparamid('PrintSwath0 Subsystem/PrintSwath0', 'P8'), fill_pattern);
tg.setparam(tg.getparamid('PrintSwath1 Subsystem/PrintSwath1', 'P8'), fill_pattern);
tg.setparam(tg.getparamid('PrintSwath2 Subsystem/PrintSwath2', 'P8'), fill_pattern);
tg.setparam(tg.getparamid('PrintSwath3 Subsystem/PrintSwath3', 'P8'), fill_pattern);

% Set up the stages for printing
setAxisAcceleration('x', BioPrinter.Stage.Axis0.max_acceleration_mm); % Set the
acceleration
setAxisBaseSpeed('x', BioPrinter.Stage.Axis0.base_speed_mm); % Set the base
speed
setAxisSpeed('x', BioPrinter.Stage.Axis0.max_speed_mm); % Set the maximum
speed
setAxisSpeed('y', BioPrinter.Stage.Axis1.max_speed_mm); % make y axis move
fast

%Make sure image isn't too large to be printed and the requested position
%won't try to make the stage move out of bounds
if(imageWidth > BioPrinter.Target.swath_length)
    error('The image is too wide to print, the image is %d pixels wide while the maximum
size is %d', imageWidth, BioPrinter.Target.swath_length)

elseif(getPosition('x') < (x + 0.5*printer.length) && x - printer.accelerationDistance <
0)
    adjustment = printer.accelerationDistance - x;
    error('The requested position would require the stage to move out of bounds, adjust
"x" by %.3f millimeters', adjustment)

elseif(getPosition('x') > (x + 0.5*printer.length) && x + imageWidthMM +
printer.accelerationDistance > BioPrinter.Stage.Axis0.size)
    adjustment = x - imageWidthMM - printer.accelerationDistance;
    error('The requested position would require the stage to move out of bounds, adjust
"x" by %.3f millimeters', adjustment)

elseif(imageHeightMM > BioPrinter.Stage.Axis1.size)
    error('The image is too tall to print, the image is %d pixels high while the maximum
size is %d', imageHeight, BioPrinter.Stage.Axis1.size)

elseif( (imageHeightMM + y) > BioPrinter.Stage.Axis1.size)
    adjustment = (imageHeightMM + y) - BioPrinter.Stage.Axis1.size;
    error('The requested position would require the stage to move out of bounds, adjust
"y" by %.3f millimeters', adjustment)
end

%Get stage in position to print, picks the closest side to cut down on
%stage movements and time
if(getPosition('x') < (x + 0.5*printer.length) )

```

```

        moveAxis('x', (x-printer.accelerationDistance) );
        start_mov = 0;
    else
        moveAxis('x', (x+printer.length+printer.accelerationDistance) );
        start_mov = 1;
    end
end
moveAxis('y',y);

%allow stage to reach start position
waitWhileAxisMoving('x');
pause(.1)
waitWhileAxisMoving('y');

%this is really only effective moving in the +x direction and for images
%that are less than 50 rows tall
setBacklashPosition;

setAxisSpeed('x', printer.printSpeed)% Set the printing speed

%Start sending swaths to the printer
for ln=1:ceil(imageHeight/50), %prints 50 row swaths at a time until entire image is
printed

    % these are the row numbers to be printed next
    imrows = (50*(ln-1)+1) : ( min(50*ln,imageHeight));

    % this is the data to be printed in this pass
    imSwath.img0 = images.img0( imrows, : );
    imSwath.img1 = images.img1( imrows, : );
    imSwath.img2 = images.img2( imrows, : );
    imSwath.img3 = images.img3( imrows, : );

    %Display what is being printed
    temp.img0=images.img0(1:imrows(end),:);
    temp.img1=images.img1(1:imrows(end),:);
    temp.img2=images.img2(1:imrows(end),:);
    temp.img3=images.img3(1:imrows(end),:);
    displayImages(temp, 'usehandle', h);

    % direction: 0 = stage moves in +mm, 1 = stage moves in -mm)
    % each line should be opposite direction, but it doesn't matter
    % which direction you start with. Both options are here.
    if(start_mov)
        direction = mod(ln,2); % start printing right to left (stage moves -x), this is
the old school default
    else %image is on the typical close edge
        direction = mod(ln+1,2); % start printing left to right (stage moves +x)
    end

    printImageSwath(printer, imSwath, direction, calibration, maxw_fine_corr_pixels); %
2*direction-1 converts [0,1] into [-1,1]

    %If there is more to print move the 'y' axis to get in position
    if(ceil(imageHeight/50)- ln > 0)
        moveAxisRelative('y', -convertPixelsToMM('y', 50)); % Axis 1 moves 50 pixels every
time
    end
end %end for loop

%flushPrintSwaths();
setPrintMode('NoPrint'); % Make sure no more printing will happen
waitWhileAxisMoving('x');
waitWhileAxisMoving('y');
setAxisSpeed('x', BioPrinter.Stage.Axis0.max_speed_mm);% Set the x axis back to maximum
speed
enableAxis('x',0);

```

```

enableAxis('y',0);
% turn off current to motors after printing. This may cause system to
% be off by 1/2 when starting up again (since motor won't be held at
% microstep, but it should save the motors). Also, this doesn't really
% matter any more since position is determined from encoder count instead
% of some value saved to the 'axis' struct for AA, AA is proven to loose
% steps making the value in the struct useless as error accrues

%%%%%%%%%%%%%%%%%%%%%%%%%%%%%%%%%%%%%%%%%%%%%%%%%%%%%%%%%%%%%%%%%%%%%%%%
% End of print
%%%%%%%%%%%%%%%%%%%%%%%%%%%%%%%%%%%%%%%%%%%%%%%%%%%%%%%%%%%%%%%%%%%%%%%%

end %end main function

function printImageSwath( printer, imSwath, direction, calibration, maxw_fine_corr_pixels
)
%%%%%%%%%%%%%%%%%%%%%%%%%%%%%%%%%%%%%%%%%%%%%%%%%%%%%%%%%%%%%%%%%%%%%%%%
% printSwath moves the stage the appropriate distance to print the current
% swath (50 horizontal lines) of the image
% printer - the printer structure defined above
% direction - direction to move stage
%           0 for left (-x), 1 for right (+x)
%%%%%%%%%%%%%%%%%%%%%%%%%%%%%%%%%%%%%%%%%%%%%%%%%%%%%%%%%%%%%%%%%%%%%%%%

%Need access to xpc object for retrieving 'print' signals
tg=xpc;

% Load image data into PrintSwath on target
loadImageSwath(imSwath, direction, printer.period);
setPrintMode('Print')
% Make sure motion has stopped
waitWhileAxisMoving('x'); % make sure there is not motion from previous printed line
if (printer.length < convertPixelsToMM('x', 50)) % only wait for axis 1 to stop if the
image is very, very narrow
    waitWhileAxisMoving('y');
end

distance = (printer.length + 2 * printer.accelerationDistance);

accel_time = printer.printSpeed / printer.acceleration;
print_time = printer.length/printer.printSpeed + 2*accel_time;
%travel_time = ( distance - printer.accelerationDistance) / printer.printSpeed;
%print_time = accel_time + travel_time;

if (direction == 1) % move right (+x)
    moveAxisRelative('x', -distance );
elseif (direction == 0) % move left (-x)
    moveAxisRelative('x', +distance );
else
    error('direction != 0 in function printSwath')
end

%If the image in <= max image size for correction of 'y' offset then use
%the 'y' access to correct. Otherwise assume user has used imJustify to
%correct offset, imJustify will only correct to the closest 84.7um.
cal_vector_x = [0 calibration.cart1.x calibration.cart2.x calibration.cart3.x];
cal_vector_y = [0 calibration.cart1.y calibration.cart2.y calibration.cart3.y];

ind=find(cal_vector_x ~= 0);
if(numel(ind)>0 && size(imSwath.img0,2) <= maxw_fine_corr_pixels) % Fine correction can
be done
    warning(sprintf('Image size is less than %d pixels (~%dmm), calibration in "y" axis
is being corrected using "y" stage movement', size(imSwath.img0,2),
convertPixelsToMM('x',size(imSwath.img0,2))))
    %set things up for the loop
    if(direction==0)

```

```

        range = ind(1):1:ind(end);
        last = cal_vector_y(ind(end));
    else
        range = ind(end)-1:-1:ind(1)-1;
        last=0;
        moveAxisRelative('y', cal_vector_y(ind(end)))
    end

    %Correct in 'y' after each cartridge is done printing
    for i=range
        %wait for cartridge done printing before moving in 'y'
        flag = tg.getsignal(tg.getsignalidsfromlabel(sprintf('Printing%d',i-
2*~direction)));
        while(flag==1)
            pause(.01); %don't poll signal too fast      MEP 2010Aug12 pause(.15);
            flag = tg.getsignal(tg.getsignalidsfromlabel(sprintf('Printing%d',i-
2*~direction)));
        end
        %negate last movement (since relative to cart0) and then correct
        %for current cartridge printing
        movement = -cal_vector_y(i-(-1)^direction) + cal_vector_y(i);
        moveAxisRelative('y', movement);
    end

    %make sure last cartridge is done printing
    WaitWhilePrinting();
    %get back to where the stage was orginally, o.w. the relative movement
    %will be wrong to move the stage down 50 'pixels'
    moveAxisRelative('y', -last);
    waitWhileAxisMoving('y');
else %assume image corrected to within 84.7um, just do a timed wait before returning
    pause(print_time);
    WaitWhilePrinting();
end

pause(.01);
setPrintMode('NoPrint')
end

function WaitWhilePrinting()
%%%%%%%%%%%%%%%%%%%%%%%%%%%%%%%%%%%%%%%%%%%%%%%%%%%%%%%%%%%%%%%%%%%%%%%%
%
%%%%%%%%%%%%%%%%%%%%%%%%%%%%%%%%%%%%%%%%%%%%%%%%%%%%%%%%%%%%%%%%%%%%%%%%

tg=xpc;
flag0 = tg.getsignal(tg.getsignalidsfromlabel('Printing0'));
flag1 = tg.getsignal(tg.getsignalidsfromlabel('Printing1'));
flag2 = tg.getsignal(tg.getsignalidsfromlabel('Printing2'));
flag3 = tg.getsignal(tg.getsignalidsfromlabel('Printing3'));

while (flag0 == 1 || flag1 == 1 || flag2 == 1 || flag3 == 1)
    pause(0.25);
    flag0 = tg.getsignal(tg.getsignalidsfromlabel('Printing0'));
    flag1 = tg.getsignal(tg.getsignalidsfromlabel('Printing1'));
    flag2 = tg.getsignal(tg.getsignalidsfromlabel('Printing2'));
    flag3 = tg.getsignal(tg.getsignalidsfromlabel('Printing3'));
end

if (flag0 ~=0 || flag1 ~=0 || flag2 ~=0 || flag3 ~=0)
    disp('Model is not running');
end

end

```


A.3.5 Cell Counting Algorithm

After counting the samples from the first experiment by hand in the cell settling studies (section 4.2.1.2), an algorithm implemented in MatLab was used to analyze the cell count in the samples for slides from the second and third preliminary experiments. Each individual sample on all slides was imaged using a fluorescent microscope. Converting the samples images to grayscale and applying a threshold resulted in insignificant data loss due to the high contrast present in the fluorescent sample images. Since the cells vary slightly in size and tend to group together, an average cell area could not be found that would yield an accurate cell count. Therefore, a training set of (8 ~ 10) images was used to find a more accurate average cell area using images with few clumped cells. MatLab numbers non-zero regions in binary images and calculates various statistics about them using the **regionprops** command. Using the **area** and **eccentricity** attributes provided by **regionprops**, all contiguous regions in a thresholded training set image with appreciable area and low eccentricity, or “high roundness”, were assumed to be single cells. These areas were averaged to find an average cell pixel area. A second set of (8 ~ 10) validation images containing low numbers of ungrouped cells, medium numbers of grouped and ungrouped cells, and large number of grouped cells was then used to verify the final algorithm. This second set of images was manually counted beforehand to verify the accuracy of the algorithm’s predicted cell count. The validation set was also thresholded and numbered using the values from the training set, after which each area was run through a series of **if** statements:

- 1) **If** the eccentricity is higher than a certain value and the area less than three times the average cell size, increment the **cell_count** variable.
- 2) **Elseif** the area of the region was smaller than the average cell size, increment the **cell_count** variable.
- 3) **Else** divide the area of the region by the average cell size plus a small correction factor and increment the **cell_count** variable by the quotient

The performance of the algorithm was assessed by sum the square of the difference between the predicted count and the manual count, also known as sum of the square of the error (SSE). The algorithm was modified until the predicted count was within 2-3% of the actual for over 85% of the images.

A.4 Bioprinter Operational notes

A.4.1 Applying the BFI to bioprinted patterned co-cultures

Located in \\GSCLUSTER_GS15_POOL\ECE\ECEBio\BioPrinting\Experiment Protocols\, the document titled 'IBIOE_SOP_010 Measuring Sample Fidelity with the BFI.doc' outlines the steps required to analyze a patterned co-culture image utilizing the patterns used to create the co-culture. The protocol guides the user in how to turn the pattern into a mask image, overlay it onto the patterned co-culture image, and how to generate the BFI number from that masked image..

A.4.2 New Cartridge modification for bioprinting

Located in \\GSCLUSTER_GS15_POOL\ECE\ECEBio\BioPrinting\Experiment Protocols\, the document titled 'IBIOE_SOP_007 HP26A Cartridge Modification for Bioprinting.doc' outlines the steps required to modify a new-in-box HP26A print cartridge so that it can be used to print cell solutions with the bioprinter.

A.4.3 EtOH Cleaning

Located in \\GSCLUSTER_GS15_POOL\ECE\ECEBio\BioPrinting\Experiment Protocols\, the document is titled 'IBIOE_SOP_009 EtOH Cleaning for HP26A Cartridges.doc', outlines the steps required to clean a HP26A print cartridge so that it can be used to print cell solutions with the bioprinter.

A.4.4 Cartridge validation

Located in \\GSCLUSTER_GS15_POOL\ECE\ECEBio\BioPrinting\Experiment Protocols\, the document is titled 'IBIOE_SOP_008 Verifying HP26A Cartridge Functionality.doc', outlines the steps required to clean a HP26A print cartridge so that it can be used to print cell solutions with the bioprinter.

A.4.5 Hardware/Software Anomaly Reporting

Located in \\GSCLUSTER_GS15_POOL\ECE\ECEBio\BioPrinting\Bug Tracking\, the document is titled 'Bug Report.docx', and it outlines previous hardware and software issues encountered while working with the bioprinter.

A.4.6 Hardware/Consumables Logs

Located in \\GSCLUSTER_GS15_POOL\ECE\ECEBio\BioPrinting\Hardware\, the document is titled 'Driver Board Deployment Log.xlsx', and it shows the location and status of all cartridge driver boards.

Located in \\GSCLUSTER_GS15_POOL\ECE\ECEBio\BioPrinting\, the document is titled 'Cartridge Log.xls', and it shows number of uses and functionality of current cartridges.

A.4.7 Setting up/Running an experiment

This section is written to outline the major points of experiment preparation and execution. It is assumed that the experiment will be performed by two people, an operator (who sits at the computer and controls MatLab), and a researcher (this person typically handles the cell work and is in charge of handling the cell related parts of the procedure). These roles do not have to be adhered to strictly and are provided mostly to ease in the separation of duties over the course of the experiment.

The best preparation for an experiment comes in the form of a detailed experiment plan. It is important that both people in the experiment are aware of the different requirements over the duration of the experiment. One the easiest ways to define these requirements is while writing the experiment script (and creating the experiment pattern). Ideally, both parties want to collaborate on how the script is going to perform. If necessary, the script should be tested to ensure locations, image densities, etc are correct.

The following experiment preparation steps should be divided. The most time intensive and long term preparation step is culturing cells. Whether that involves bringing cells out of cryogenic stasis (IBIOE_SOP_006) or starting a few extra flasks of cells (IBIOE_SOP_003), someone must ensure that

enough cells will be available for the creation of the cell solution at the specified concentration on the day of the experiment. Silicone masks also need to be made (IBIOE_SOP_001 & 002) at least the day before to allow for gelation/preparation of the collagen substrates. To prep the bioprinter, all the required cartridges must be cleaned and validated the day before the experiment. If the required number of functioning cartridges cannot be found, new cartridges will have to be opened and cleaned (IBIOE_SOP_007,008, & 009). Testing to ensure the stage camera is properly positioned may need to be done. The quickest way to check correct position of the microscope station is by moving the stage to the values stored in the `BioPrinter` struct, `BioPrinter.Calibration.camera_ref_abs`, and making sure the bolt is in the approximate center of the camera field of view.

On the day of the experiment, the tagging and preparation of the cell solution (IBIOE_SOP_004) will take a few hours. It never hurts to set aside and pre-label polystyrene Petri dishes for the printed slides. When the cells have been properly tagged and counted, they should be kept on ice until the beginning of the experiment. If the timing is right, the experiment should begin 30 minutes later. The bioprinter should be initialized using `initBioPrinter` and the prepared cartridges set out. If both users have completed their tasks, everything should be ready to go.

To start the experiment, the cells should be removed from ice and vortexed for a few seconds to evenly distribute them throughout the solution. A small amount, usually between 50 to 75 μL of solution is removed and combined with the same amount of HBSS containing 0.53 mM EDTA in a microvial and titrated. While the cartridge is being loaded with cell solution, the clean glass microscope slide needs to be taped down to the sample platform's calibration slide location on top of an opaque background (black spray painted slide). A slip of scrap paper needs to be inserted on the right hand side of the platform to catch evacuated cells. Once the cartridge and calibration slide are in place, the calibration procedure may begin. During the calibration procedure, after each cartridge has deposited their reference drop and the platform has moved them underneath the Microscope station, be sure to check the zoom setting on the lens is set to 2.0x. When the image preview comes up on the screen, adjust the focus to the top of the drops (move Fine knob CCW), this should give better drop imaging. Since each cartridge printed a column of

drops, the user can select the row that contains drops with cells from all cartridges. Once selection has been made and the cartridges have been calibrated to each other, the calibration slide may be removed and the experiment slide inserted in its place. The experiment script can then be executed, with printed samples placed in the prelabeled petri dishes. Depending on the experiment requirements, after the first three or four slides have been printed, more cell solution can be loaded into other clean cartridges and the process repeated.

After the experiment, the samples should be imaged and incubated as desired and the bioprinter shutdown. Make sure to clean the used cartridges as soon as possible to prevent debris from sitting in the printhead, making it harder to clean in the future.

REFERENCES

- [1] A. Khademhosseini, R. Langer, J. Borenstein and J.P. Vacanti, "Microscale technologies for tissue engineering and biology," *Proc.Natl.Acad.Sci.U.S.A.*, vol. 103, no.8, pp. 2480-2487, Feb 21, 2006.
- [2] N.R. Schiele, D.T. Corr, Y. Huang, N.A. Raof, Y. Xie and D.B. Chrisey, "Laser-based direct-write techniques for cell printing," *Biofabrication*, vol. 2, no.3, pp. 032001, Sep, 2010.
- [3] H. Kaji, G. Camci-Unal, R. Langer and A. Khademhosseini, "Engineering systems for the generation of patterned co-cultures for controlling cell-cell interactions," *Biochim.Biophys.Acta*, Jul 23, 2010.
- [4] S.N. Bhatia, U.J. Balis, M.L. Yarmush and M. Toner, "Probing heterotypic cell interactions: hepatocyte function in microfabricated co-cultures," *J.Biomater.Sci.Polym.Ed.*, vol. 9, no.11, pp. 1137-1160, 1998.
- [5] J. Tien, C.M. Nelson and C.S. Chen, "Fabrication of aligned microstructures with a single elastomeric stamp," *Proc.Natl.Acad.Sci.U.S.A.*, vol. 99, no.4, pp. 1758-1762, Feb 19, 2002.
- [6] Y. Tsuda, A. Kikuchi, M. Yamato, A. Nakao, Y. Sakurai, M. Umezu and T. Okano, "The use of patterned dual thermoresponsive surfaces for the collective recovery as co-cultured cell sheets," *Biomaterials*, vol. 26, no.14, pp. 1885-1893, May, 2005.
- [7] D.G. Barrett and M.N. Yousaf, "Rapid patterning of cells and cell co-cultures on surfaces with spatial and temporal control through centrifugation," *Angew.Chem.Int.Ed Engl.*, vol. 46, no.39, pp. 7437-7439, 2007.
- [8] D.T. Chiu, N.L. Jeon, S. Huang, R.S. Kane, C.J. Wargo, I.S. Choi, D.E. Ingber and G.M. Whitesides, "Patterned deposition of cells and proteins onto surfaces by using three-dimensional microfluidic systems," *Proc.Natl.Acad.Sci.U.S.A.*, vol. 97, no.6, pp. 2408-2413, Mar 14, 2000.
- [9] R.S. Kane, S. Takayama, E. Ostuni, D.E. Ingber and G.M. Whitesides, "Patterning proteins and cells using soft lithography," *Biomaterials*, vol. 20, no.23-24, pp. 2363-2376, Dec, 1999.
- [10] M. Suzuki, T. Yasukawa, H. Shiku and T. Matsue, "Negative dielectrophoretic patterning with different cell types," *Biosens.Bioelectron.*, vol. 24, no.4, pp. 1049-1053, Dec 1, 2008.
- [11] E.E. Hui and S.N. Bhatia, "Micromechanical control of cell-cell interactions," *Proc.Natl.Acad.Sci.U.S.A.*, vol. 104, no.14, pp. 5722-5726, Apr 3, 2007.
- [12] F. Guillemot, V. Mironov and M. Nakamura, "Bioprinting is coming of age: Report from the International Conference on Bioprinting and Biofabrication in Bordeaux (3B'09)," *Biofabrication*, vol. 2, no.1, pp. 010201, Mar, 2010.
- [13] K. Francis and B.O. Palsson, "Effective intercellular communication distances are determined by the relative time constants for cyto/chemokine secretion and diffusion," *Proc.Natl.Acad.Sci.U.S.A.*, vol. 94, no.23, pp. 12258-12262, Nov 11, 1997.
- [14] S.Y. Shvartsman, H.S. Wiley and D.A. Lauffenburger, "Epidermal growth factor receptor signaling in tissues," *Control Systems Magazine, IEEE*, vol. 24, no.4, pp. 53-61, 2004.

- [15] P.K. Wu and B.R. Ringeisen, "Development of human umbilical vein endothelial cell (HUVEC) and human umbilical vein smooth muscle cell (HUVSMC) branch/stem structures on hydrogel layers via biological laser printing (BioLP)," *Biofabrication*, vol. 2, no.1, pp. 014111, Mar, 2010.
- [16] C.A. Boulanger, D.L. Mack, B.W. Booth and G.H. Smith, "Interaction with the mammary microenvironment redirects spermatogenic cell fate in vivo," *Proc.Natl.Acad.Sci.U.S.A.*, vol. 104, no.10, pp. 3871-3876, Mar 6, 2007.
- [17] E.J. McCave, C.A. Cass, K.J. Burg and B.W. Booth, "The normal microenvironment directs mammary gland development," *J.Mammary Gland Biol.Neoplasia*, vol. 15, no.3, pp. 291-299, Sep, 2010.
- [18] T. Goldmann and J.S. Gonzalez, "DNA-printing: utilization of a standard inkjet printer for the transfer of nucleic acids to solid supports," *J.Biochem.Biophys.Methods*, vol. 42, no.3, pp. 105-110, Mar 16, 2000.
- [19] W.C. Wilson Jr and T. Boland, "Cell and organ printing 1: protein and cell printers," *Anat.Rec.A.Discov.Mol.Cell.Evol.Biol.*, vol. 272, no.2, pp. 491-496, Jun, 2003.
- [20] W.A. Buskirk, D.E. Hackleman, S.T. Hall, P.H. Kanarek, R.N. Low, K.E. Trueba and R.R. {d. Poll}, "Development of a high-resolution thermal inkjet printhead," *Hewlett Packard Journal: Technical Information from the Laboratories of Hewlett Packard Company*, vol. 39, no.5, pp. 55-61, oct, 1988.
- [21] X. Cui and T. Boland, "Human microvasculature fabrication using thermal inkjet printing technology," *Biomaterials*, vol. 30, no.31, pp. 6221-6227, Oct, 2009.
- [22] T. Xu, C.A. Gregory, P. Molnar, X. Cui, S. Jalota, S.B. Bhaduri and T. Boland, "Viability and electrophysiology of neural cell structures generated by the inkjet printing method," *Biomaterials*, vol. 27, no.19, pp. 3580-3588, Jul, 2006.
- [23] T. Xu, C. Baicu, M. Aho, M. Zile and T. Boland, "Fabrication and characterization of bio-engineered cardiac pseudo tissues," *Biofabrication*, vol. 1, no.3, pp. 035001, Sep, 2009.
- [24] X. Cui, D. Dean, Z.M. Ruggeri and T. Boland, "Cell damage evaluation of thermal inkjet printed Chinese hamster ovary cells," *Biotechnol.Bioeng.*, vol. 106, no.6, pp. 963-969, Aug 15, 2010.
- [25] T. Xu, J. Jin, C. Gregory, J.J. Hickman and T. Boland, "Inkjet printing of viable mammalian cells," *Biomaterials*, vol. 26, no.1, pp. 93-99, Jan, 2005.
- [26] C.A. Parzel, M.E. Pepper, T. Burg, R.E. Groff and K.J. Burg, "EDTA enhances high-throughput two-dimensional bioprinting by inhibiting salt scaling and cell aggregation at the nozzle surface," *J.Tissue Eng.Regen.Med.*, vol. 3, no.4, pp. 260-268, Jun, 2009.
- [27] M.E. Pepper, C.A. Parzel, T. Burg, T. Boland, K.J. Burg and R.E. Groff, "Design and implementation of a two-dimensional inkjet bioprinter," *Conf.Proc.IEEE Eng.Med.Biol.Soc.*, vol. 2009, pp. 6001-6005, 2009.
- [28] P.G. Campbell, E.D. Miller, G.W. Fisher, L.M. Walker and L.E. Weiss, "Engineered spatial patterns of FGF-2 immobilized on fibrin direct cell organization," *Biomaterials*, vol. 26, no.33, pp. 6762-6770, Nov, 2005.
- [29] L.E. Weiss, L. Shultz and E. Milller, "Inkjet Deposition System with Computer Vision-based Calibration for Targeting Accuracy," Carnegie Mellon University, Carnegie Mellon University, Rep. CMU-RI-TR-06-15, pp. 1-13, 2006.

- [30] T. Boland, V. Mironov, A. Gutowska, E.A. Roth and R.R. Markwald, "Cell and organ printing 2: fusion of cell aggregates in three-dimensional gels," *Anat.Rec.A.Discov.Mol.Cell.Evol.Biol.*, vol. 272, no.2, pp. 497-502, Jun, 2003.
- [31] L. Pardo, W.C. Wilson and T. Boland, "Characterization of Patterned Self-Assembled Monolayers and Protein Arrays Generated by the Ink-Jet Method," *Langmuir*, vol. 19, no.5, pp. 1462-1466, 03/01, 2003.
- [32] G.M. Cooper, E.D. Miller, G.E. Decesare, A. Usas, E.L. Lensie, M.R. Bykowski, J. Huard, L.E. Weiss, J.E. Losee and P.G. Campbell, "Inkjet-based biopatterning of bone morphogenetic protein-2 to spatially control calvarial bone formation," *Tissue Eng.Part A.*, vol. 16, no.5, pp. 1749-1759, May, 2010.
- [33] E.D. Miller, G.W. Fisher, L.E. Weiss, L.M. Walker and P.G. Campbell, "Dose-dependent cell growth in response to concentration modulated patterns of FGF-2 printed on fibrin," *Biomaterials*, vol. 27, no.10, pp. 2213-2221, Apr, 2006.
- [34] E.D. Miller, J.A. Phillippi, G.W. Fisher, P.G. Campbell, L.M. Walker and L.E. Weiss, "Inkjet printing of growth factor concentration gradients and combinatorial arrays immobilized on biologically-relevant substrates," *Comb.Chem.High Throughput Screen.*, vol. 12, no.6, pp. 604-618, Jul, 2009.
- [35] J.A. Phillippi, E. Miller, L. Weiss, J. Huard, A. Waggoner and P. Campbell, "Microenvironments engineered by inkjet bioprinting spatially direct adult stem cells toward muscle- and bone-like subpopulations," *Stem Cells*, vol. 26, no.1, pp. 127-134, Jan, 2008.
- [36] R.E. Saunders, B. Derby, J.E. Gough and N. Reis, "Ink-Jet Printing of Human Cells," *Mat.Res.Soc.Symp.Proc.*, vol. EXS-1, pp. 95-98, 2004.
- [37] R.E. Saunders, J.E. Gough and B. Derby, "Delivery of human fibroblast cells by piezoelectric drop-on-demand inkjet printing," *Biomaterials*, vol. 29, no.2, pp. 193-203, Jan, 2008.
- [38] C. Henmi, M. Nakamura, Y. Nishiyama, K. Yamaguchi and S. Mochizuki, "Development of an effective three dimensional fabrication technique using inkjet technology for tissue model sample," in Proc. 6th World Congress on Alternatives & Animal Use in the Life Sciences, pp. 689-692, 2008.
- [39] M. Nakamura, Y. Nishiyama, C. Henmi, S. Iwanaga, H. Nakagawa, K. Yamaguchi, K. Akita, S. Mochizuki and K. Takiura, "Ink Jet Three-Dimensional Digital Fabrication for Biological Tissue Manufacturing: Analysis of Alginate Microgel Beads Produced by Ink Jet Droplets for Three Dimensional Tissue Fabrication," *J Imaging Sci Technol*, vol. 52, no.6, pp. 060201, November/December 2008, 2008.
- [40] Y. Nishiyama, M. Nakamura, C. Henmi, K. Yamaguchi, S. Mochizuki, H. Nakagawa and K. Takiura, "Development of a three-dimensional bioprinter: construction of cell supporting structures using hydrogel and state-of-the-art inkjet technology," *J.Biomech.Eng.*, vol. 131, no.3, pp. 035001, Mar, 2009.
- [41] Y. Nishiyama, M. Nakamura, C. Henmi, K. Yamaguchi, S. Mochizuki, H. Nakagawa and K. Takiura, "Fabrication of 3D Cell Supporting Structures With Multi-Materials Using the Bio-Printer," *ASME Conf.Proc.*, vol. 2007, no.42908, pp. 97-102, January 1, 2007, 2007.
- [42] S. Khalil, J. Nam and W. Sun, "Multi-nozzle deposition for construction of 3d biopolymer tissue scaffolds," *Rapid Prototyping Journal*, vol. 11, pp. 9-17, 2005.
- [43] W. Lee, J. Pinckney, V. Lee, J.H. Lee, K. Fischer, S. Polio, J.K. Park and S.S. Yoo, "Three-dimensional bioprinting of rat embryonic neural cells," *Neuroreport*, vol. 20, no.8, pp. 798-803, May 27, 2009.

- [44] R. Chang, J. Nam and W. Sun, "Effects of dispensing pressure and nozzle diameter on cell survival from solid freeform fabrication-based direct cell writing," *Tissue Eng.Part A.*, vol. 14, no.1, pp. 41-48, Jan, 2008.
- [45] S. Khalil and W. Sun, "Biopolymer deposition for freeform fabrication of hydrogel tissue constructs," *Materials Science and Engineering: C*, vol. 27, no.3, pp. 469-478, 4, 2007.
- [46] R. Chang, J. Nam and W. Sun, "Direct cell writing of 3D microorganism for in vitro pharmacokinetic model," *Tissue Eng.Part C.Methods*, vol. 14, no.2, pp. 157-166, Jun, 2008.
- [47] S. Khalil and W. Sun, "Bioprinting endothelial cells with alginate for 3D tissue constructs," *J.Biomech.Eng.*, vol. 131, no.11, pp. 111002, Nov, 2009.
- [48] B.R. Ringeisen, D.B. Chrisey, A. Pique, H.D. Young, J. Jones-Meehan, R. Modi, M. Bucaro and B.J. Spargo, "Generation of mesoscopic patterns of viable *Escherichia coli* by ambient laser transfer," *Biomaterials*, vol. 23, no.1, pp. 161-166, Jan, 2002.
- [49] D.B. Chrisey, A. Pique, R.A. McGill, J.S. Horwitz, B.R. Ringeisen, D.M. Bubb and P.K. Wu, "Laser deposition of polymer and biomaterial films," *Chem.Rev.*, vol. 103, no.2, pp. 553-576, Feb, 2003.
- [50] B.R. Ringeisen, P.K. Wu, H. Kim, A. Pique, R.Y. Auyeung, H.D. Young, D.B. Chrisey and D.B. Krizman, "Picoliter-scale protein microarrays by laser direct write," *Biotechnol.Prog.*, vol. 18, no.5, pp. 1126-1129, Sep-Oct, 2002.
- [51] J.A. Barron, B.R. Ringeisen, H. Kim, B.J. Spargo and D.B. Chrisey, "Application of laser printing to mammalian cells," *Thin Solid Films*, vol. 453-454, pp. 383-387, 4/1, 2004.
- [52] P.K. Wu, B.R. Ringeisen, J. Callahan, M. Brooks, D.M. Bubb, H.D. Wu, A. Piqué, B. Spargo, R.A. McGill and D.B. Chrisey, "The deposition, structure, pattern deposition, and activity of biomaterial thin-films by matrix-assisted pulsed-laser evaporation (MAPLE) and MAPLE direct write," *Thin Solid Films*, vol. 398-399, pp. 607-614, 11, 2001.
- [53] J.A. Barron, D.B. Krizman and B.R. Ringeisen, "Laser printing of single cells: statistical analysis, cell viability, and stress," *Ann.Biomed.Eng.*, vol. 33, no.2, pp. 121-130, Feb, 2005.
- [54] T.M. Patz, A. Doraiswamy, R.J. Narayan, W. He, Y. Zhong, R. Bellamkonda, R. Modi and D.B. Chrisey, "Three-dimensional direct writing of B35 neuronal cells," *J.Biomed.Mater.Res.B.Appl.Biomater.*, vol. 78, no.1, pp. 124-130, Jul, 2006.
- [55] B. Guillotin, A. Souquet, S. Catros, M. Duocastella, B. Pippenger, S. Bellance, R. Bareille, M. Remy, L. Bordenave, J. Amedee and F. Guillemot, "Laser assisted bioprinting of engineered tissue with high cell density and microscale organization," *Biomaterials*, vol. 31, no.28, pp. 7250-7256, Oct, 2010.
- [56] J.A. Barron, P. Wu, H.D. Ladouceur and B.R. Ringeisen, "Biological laser printing: a novel technique for creating heterogeneous 3-dimensional cell patterns," *Biomed.Microdevices*, vol. 6, no.2, pp. 139-147, Jun, 2004.
- [57] B.R. Ringeisen, H. Kim, J.A. Barron, D.B. Krizman, D.B. Chrisey, S. Jackman, R.Y. Auyeung and B.J. Spargo, "Laser printing of pluripotent embryonal carcinoma cells," *Tissue Eng.*, vol. 10, no.3-4, pp. 483-491, Mar-Apr, 2004.

- [58] A. Doraiswamy, R.J. Narayan, M.L. Harris, S.B. Qadri, R. Modi and D.B. Chrisey, "Laser microfabrication of hydroxyapatite-osteoblast-like cell composites," *J.Biomed.Mater.Res.A.*, vol. 80, no.3, pp. 635-643, Mar 1, 2007.
- [59] Y. Lin, Y. Huang and C. D.B., "Droplet formation in matrix-assisted pulsed-laser evaporation direct writing of glycerol-water solution," *J.Appl.Phys.*, vol. 105, no.9, pp. 093111, may, 2009.
- [60] F. Guillemot, A. Souquet, S. Catros, B. Guillotin, J. Lopez, M. Faucon, B. Pippenger, R. Bareille, M. Remy, S. Bellance, P. Chabassier, J.C. Fricain and J. Amedee, "High-throughput laser printing of cells and biomaterials for tissue engineering," *Acta Biomater.*, vol. 6, no.7, pp. 2494-2500, Jul, 2010.
- [61] F. Guillemot, A. Souquet, S. Catros and B. Guillotin, "Laser-assisted cell printing: principle, physical parameters versus cell fate and perspectives in tissue engineering," *Nanomedicine (Lond)*, vol. 5, no.3, pp. 507-515, Apr, 2010.
- [62] C. Mezel, A. Souquet, L. Hallo and F. Guillemot, "Bioprinting by laser-induced forward transfer for tissue engineering applications: jet formation modeling," *Biofabrication*, vol. 2, no.1, pp. 014103, Mar, 2010.
- [63] S. Moon, S.K. Hasan, Y.S. Song, F. Xu, H.O. Keles, F. Manzur, S. Mikkilineni, J.W. Hong, J. Nagatomi, E. Haeggstrom, A. Khademhosseini and U. Demirci, "Layer by layer three-dimensional tissue epitaxy by cell-laden hydrogel droplets," *Tissue Eng.Part C.Methods*, vol. 16, no.1, pp. 157-166, Feb, 2010.
- [64] T. Xu, S. Petridou, E.H. Lee, E.A. Roth, N.R. Vyavahare, J.J. Hickman and T. Boland, "Construction of high-density bacterial colony arrays and patterns by the ink-jet method," *Biotechnol.Bioeng.*, vol. 85, no.1, pp. 29-33, Jan 5, 2004.
- [65] M. Nakamura, A. Kobayashi, F. Takagi, A. Watanabe, Y. Hiruma, K. Ohuchi, Y. Iwasaki, M. Horie, I. Morita and S. Takatani, "Biocompatible inkjet printing technique for designed seeding of individual living cells," *Tissue Eng.*, vol. 11, no.11-12, pp. 1658-1666, Nov-Dec, 2005.
- [66] W. Lee, J.C. Debasitis, V.K. Lee, J.H. Lee, K. Fischer, K. Edminster, J.K. Park and S.S. Yoo, "Multi-layered culture of human skin fibroblasts and keratinocytes through three-dimensional freeform fabrication," *Biomaterials*, vol. 30, no.8, pp. 1587-1595, Mar, 2009.
- [67] K.J. Burg and T. Boland, "Minimally invasive tissue engineering composites and cell printing," *IEEE Eng.Med.Biol.Mag.*, vol. 22, no.5, pp. 84-91, Sep-Oct, 2003.
- [68] T. Boland, X. Tao, B.J. Damon, B. Manley, P. Kesari, S. Jalota and S. Bhaduri, "Drop-on-demand printing of cells and materials for designer tissue constructs," *Materials Science and Engineering C*, vol. 27, no.3, pp. 372-376, 2007.
- [69] J.P. Mattimore, R.E. Groff, T. Burg and M.E. Pepper, "A general purpose driver board for the HP26 ink-jet cartridge with applications to bioprinting," in Proceedings of the IEEE SoutheastCon 2010, pp. 510-513, 2010.
- [70] D.J. May, M.D. Lund, T.B. Pritchard and C.W. Nichols, "Data to dots in the HP DeskJet Printer," *Hewlett Packard Journal: Technical Information from the Laboratories of Hewlett Packard Company*, vol. 39, no.5, pp. 76-80, oct, 1988.

- [71] R.B. Vernon, M.D. Gooden, S.L. Lara and T.N. Wight, "Microgrooved fibrillar collagen membranes as scaffolds for cell support and alignment," *Biomaterials*, vol. 26, no.16, pp. 3131-3140, Jun, 2005.
- [72] D.E. Ingber, "Cellular basis of mechanotransduction," *Biol.Bull.*, vol. 194, no.3, pp. 323-5; discussion 325-7, Jun, 1998.
- [73] S. Parsa, M. Gupta, F. Loizeau and K.C. Cheung, "Effects of surfactant and gentle agitation on inkjet dispensing of living cells," *Biofabrication*, vol. 2, no.2, pp. 025003, Jun, 2010.
- [74] E.C. Anderson, D.F. Petersen and R.A. Tobey, "Density invariance of cultured Chinese hamster cells with stage of the mitotic cycle," *Biophys.J.*, vol. 10, no.7, pp. 630-645, Jul, 1970.
- [75] Z. Wang and J.M. Belovich, "A simple apparatus for measuring cell settling velocity," *Biotechnol.Prog.*, vol. 26, no.5, pp. 1361-1366, Sep, 2010.
- [76] N.A. Madigan, C.R.S. Hagan, H. Zhang and L.A. Coury, "Effects of sonication on electrode surfaces and metal particles," *Ultrason.Sonochem.*, vol. 3, no.3, pp. S239-S247, 11, 1996.
- [77] J.P. Harmon and J.A. Widder, "Integrating the printhead into the HP DeskJet Printer," *Hewlett Packard Journal: Technical Information from the Laboratories of Hewlett Packard Company*, vol. 39, no.5, pp. 62-66, oct, 1988.
- [78] K. Mitzner, *Complete PCB Design Using OrCAD and Layout*, Burlington, MA: Elsevier, 2007, pp. 123-125,139,147,151.
- [79] M.I. Montrose, *EMC and the Printed Circuit Board*, New York: Wiley-Interscience, 1998, pp. 136-138, 144-154.
- [80] J. Fan, J. Drewniak, J. Knighten, N. Smith, A. Orlandi, T. Van Doren, T. Hubing and R. DuBroff, "Quantifying SMT Decoupling Capacitor Placement in DC Power-Bus Design for Multilayer PCBs," *IEEE Trans on EMC*, vol. 43, no.4, pp. 588-599, November, 2001.
- [81] T. Hubing, T. Van Doren, F. Sha, J. Drewniak and M. Wilhelm, "An Experimental Investigation of 4-Layer Printed Circuit Board Decoupling," in *Proc.1995 IEEE Int Symposium on EMC*, pp. 308-312, 1995.